Charles University

Faculty of Science

Study programme: Biology

Branch of study: Immunology

Bc. Martina Fejtková

Cell signaling aberrations in primary immunodeficiencies

Odchylky v buněčné signalizaci u primárních imunodeficitů

Diploma thesis

Supervisor: **RNDr. Veronika Kanderová, Ph.D.**

Prague, 2018

Prohlášení

Prohlašuji, že jsem závěrečnou práci zpracovala samostatně a že jsem uvedla všechny použité informační zdroje a literaturu. Tato práce ani její podstatná část nebyla předložena k získání jiného nebo stejného akademického titulu.

Praha, 30.4.2018

Podpis:

Acknowledgement

I wish to sincerely thank my supervisor, RNDr. Veronika Kanderová, Ph.D., for her guidance, encouragement, priceless advice and patience. I also wish to express my gratitude to doc. MUDr. Tomáš Kalina, Ph.D. and doc. MUDr. Ondřej Hrušák, Ph.D. for providing me an opportunity to do my research and diploma thesis in laboratories of Childhood Leukaemia Investigation Prague (CLIP) at the 2nd Faculty of Medicine, Charles University. I also thank to all clinitians, especially MUDr. Markéta Bloomfield for proofreading, specialists and lab workers who participated in the projects and who helped me and gave me advice. Lastly, I have to thank my family and the closest friends for a great psychological support and patience.

This work was supported by grants obtained from the Ministry of Health of the Czech Republic no. 15-28541A, and a grant obtained from the Grant Agency of the Czech Republic no. P302/12/G101. Infrastructure was supported by the Ministry of Education, Youth and Sports NPU I LO1604 and institutional support obtained from University Hospital Motol 00064203.

Abstract

Primary immunodeficiencies (PID) are genetic disorders characterized by increased susceptibility to infections and various degrees of immune dysregulation. With the expansion of massive parallel sequencing, an increasing number of defects in immune-related genes is being identified in PID. However, the biological impact of the found mutations is often unknown. It is necessary to devise methods to clarify their causality for disease development, which may also aid therapeutic decisions.

One of the novel discoveries are gain-of-function mutations in *STAT1* gene, resulting in chronic mucocutaneous candidiasis. Candidiasis may be ameliorated with antimycotics or with targeted JAK-STAT inhibitor, ruxolitinib. For our patient with a novel mutation in *STAT1*, we developed a simple test for the detection of phospho-STAT molecules in peripheral blood lymphocytes. The test confirmed the gain-of-function character of the identified mutation and was used to monitor ruxolitinib treatment efficacy. In the second patient, who presented with lymphadenopathy and immunodeficiency, the as yet undescribed mutation in *CASP8* was found. We proved its loss-of-function property expressed as reduced caspase-8 and caspase-3 cleavage, impaired cellular apoptosis, and decreased NFκB-related signaling. The third patient who suffered from pulmonary fibrosis and vasculitis carries a remarkable mutation in Src-family kinase *HCK*. We found a mutated HCK protein in the patient's cells and proved its activation character, detected as hyperphosphorylation of HCK, increased expression of adhesion molecules, and enhanced release of cytokines IL-1β and TNFα.

In conclusion, we established correlations between novel *STAT1*, *CASP8*, and *HCK* mutations and altered cellular functions by using a serie of functional tests.

Abstrakt

Primární imunodeficience (PID) jsou charakterizovány zvýšenou náchylností k infekcím a různě závažnými imunologickými poruchami. S rozvojem masivně paralelního sekvenování je ve skupině PID identifikováno stále více poruch v genech asociovaných s imunitním systémem. Biologická podstata mnoha nalezených mutací je ale často neznámá. Je proto nezbytné vyvíjet metodické nástroje, které pomohou objasnit kauzalitu daných mutací a mohou pomoci nalézt optimální terapii.

Jedněmi z nově objevených mutací jsou aktivační, tzv. gain-of-function, mutace v genu pro STAT1 způsobující chronickou mukokutánní kandidózu. Kandidózu mohou zmírňovat antimykotika nebo cílený JAK-STAT inhibitor, ruxolitinib. Pro našeho pacienta s nově nalezenou mutací ve *STAT1* jsme vyvinuli jednoduchý test pro detekci fosforylace STAT molekul v lymfocytech plné periferní krve. Tímto testem jsme potvrdili aktivační charakter dané mutace a použili jej i pro monitorování cílené léčby ruxolitinibem. U druhého pacienta, který trpí lymfadenopatií a imunodeficitem, byla identifikována dosud nepopsaná mutace v genu pro kaspázu-8. Prokázali jsme inhibiční, tzv. loss-of-function character dané mutace projevující se sníženým štěpením samotné kaspázy-8 i jejího substrátu kaspázy-3, poruchou v buněčné apoptóze a sníženou signalizací NFκB. U třetí pacientky, která trpí závažnou plicní fibózou a vaskulitidou, byla identifikována velmi neobvyklá mutace v Src kináze HCK. Mutovaný protein HCK jsme v buňkách pacientky nalezli a potvrdili i jeho aktivační character projevující se hyperfosforylací samotné HCK, zvýšenou expresí adhezivních molekul a zvýšenou produkcí cytokinů IL-1β a TNFα v buňkách nesoucích mutovanou HCK.

Souhnně lze konstatovat, že jsem v mé diplomové práci objevila mnoho funkčních souvislostí mezi nově nalezenými mutacemi ve *STAT1*, *CASP8* a *HCK* a poruchami buněčného chování.

Keywords:

Primary immunodeficiency, PID, STAT1, Caspase-8, HCK, gain-of-function, loss-of-function, signaling, apoptosis

Klíčová slova:

Primární imunodeficit, PID, STAT1, kaspáza-8, HCK, signalizace, apoptóza

Contents

Abbreviations

ADA - adenosine deaminase
AIRE - autoimmune regulator
AKT - protein kinase B
ALPS - autoimmune lymphoproliferative syndrome
APECED - autoimmune polyendocrinopathy-candidiasis-ectodermal dystrophy
B-ALL - B-cell acute lymphoblastic leukemia
BCG - Bacillus Calmette–Guérin
BCR - B-cell receptor
BSA - bovine serum albumin
BTK - Bruton Tyrosin Kinase
CCR7 - C-C chemokine receptor type 7
PARP - Poly (ADP-ribose) polymerase
bp - base pair
Tyr - Tyrosine
Ser - serine
PI3K - Phosphatidylinositol-4,5-bisphosphate 3-kinase
Src - Proto-oncogene Tyrosine-protein Kinase Src
T-cells - T-lymphocytes
B-cells - B-lymphocytes
phospho - phosphorylation
WB - western blot
MTOR - mammalian target of rapamycin (mTOR)
TGF - transforming growth factor β
MOPS - 3-(N-morpholino)propanesulfonic acid) buffer
MES - 2-(N-morpholino)ethanesulfonic acid buffer
GPCR - G-protein coupled receptor
CARD - caspase recruitment domain
CASP - caspase
CD - cluster of differentiation
CMC - chronic mucocutaneous candidasis
CXCL - chemokine with C-X-C motif
DED - death effector domain
ELISA - Enzyme-Linked ImmunoSorbent Assay
FADD - Fas-associated protein with death domain
Fas - Fas receptor
FasL - Fas ligand
FBS - fetal bovine serum
FcR - Fc binding receptor
FSC-A - forward scatter - Area
FSC-H - forward scatter - Height
GAM - goat anti-mouse antibody
GAR - goat anti-rabbit antibody
G-CSF - granulocyte colony stimulating factor
GOF - gain-of-function
GPCR - G-protein coupled receptor
HCK - hematopoietic cell kinase
HEPES - 4-(2-hydroxyethyl)-1-piperazineethanesulfonic acid
HLA - human leukocyte antigen
HLA-DR - type of human leukocyte antigen
HSCT - hematopoietic stem cell transplant

ID - immunodeficiency
IFN - interferon
IL - interleukin
IS - immune system
IVIG – intravenous immunoglobulin
JAK - Janus kinase
LOF - loss-of-function
LPS - lipopolysaccharide
MALT - mucosa-associated lymphoid tissue
MAPK - mitogen-activated protein kinases
M-CSF - macrophage colony-stimulating factor
MEK1/2 - dual-specificity protein kinase
MFI - median fluorescence intensity
NADPH - Nicotinamide adenine dinucleotide phosphate
NFκB - nuclear factor kappa B
MPS - massive parallel sequencing
PAMP - pathogen associated molecular pattern
PBMC - peripheral blood mononuclear cell
PBS - Phosphate Buffered Saline
PHA - phytohaemagglutinin
PID - primary immunodeficiency
PRR - pattern recognition receptor
RCF - relative centrifugal force
ROS - reactive oxygen species
RPMI - Roswell Park Memorial Institute (culture medium)
RT - room temperature
SCID - severe combined immunodeficiency
SDS-PAGE - SDS Protein Acrylamide Gel Electrophoresis
SFK - Src Family Kinase
SH - Src-homology domain
SSC-A - side scatter - Area
SSC-H - side scatter - Height
STAT - Signal Transducer and Activator of Transcription
T-ALL - T-cell acute lymphoblastic leukemia
Tbet - T-box transcription factor
TCR - T-cell receptor
Th - helper T-cell
TLR - Toll-like receptor
TNF - tumor necrosis factor
TNFR - tumor necrosis factor receptor
TRADD - tumor necrosis factor receptor type 1-associated DEATH domain protein
TREC - T-cell receptor excision circle
Treg - regulatory T-cell
WAS - Wiskott-Aldrich syndrome
WBC - white blood cells
ZVAD - Z-VAD-FMK (carbobenzoxy-valyl-alanyl-aspartyl-[O-methyl]-fluoromethylketone)

Fluorochromes:

Alexa Fluor 647

Alexa Fluor 700

APC - Allophycocyanin

APC-Alexa Fluor 750-Allophycocyanin-Alexa Fluor 750

APC-Cy7 - Allophycocyanin-Cyanine 7

APC-H7 - Allophycocyanin-H7

BV421 - Brilliant Violet 421

BV510 - Brilliant Violet 510

BV605 - Brilliant Violet 605

DAPI - 4',6-diamidin-2-phenylindol

Dy647 - Dyomics 647

ECD - Phycoerythrin-Texas Red

FITC - Fluorescein Isothiocyanate

PB - Pacific Blue

PE - Phycoerythrin

PE-Cy7 - Phycoerythrin-Cyanine 7

PerCP-Cy5.5 - Peridinin-chlorophyll-protein-Cyanine 5.5

PO - Pacific Orange

All flow cytometry-based fuctional experiments were measured on LSR II flow cytometer with FACSDiva™ acquiring software if not written differently. Analysis was performed using FlowJo® 9.9.6 Mac version software.

1. Introduction

Primary immunodeficiencies (PID) is a group of hereditary disorders of the immune system where one or more components are altered or oven missing. These disorders can be simply divided into milder forms, in which the patients are only more vulnerable to pathogens, and severe forms which can be lethal without bone marrow transplantation and replacement of nonfunctional immune cells. Recently, more than 300 types of PID have been described (*1*). Deficiency can be found in the different parts of the immune system, in complement, phagocytic cells, T-lymphocytes, B-lymphocytes. Alternatively, it can be a combination of several types (*2*). For the most severe form of PID, severe combined immunodeficiency (SCID), a newborn screening has been developed to spot the disease in time, since vaccination could be lethal to these infants and immediate hematopoietic stem cell transplantation (HSCT) is required. The screening is based on the detection of T-cell receptor (TCR) excision circles (TREC) (*3*). The less severe forms are often manifested by recurrent infections and failure to thrive. It is crucial to distinguish PID from other diseases, to prevent damage to health or patient death. Clinicians should follow 10 well-known warning signs of PID and, in a suspicious case, transfer the patient to a specialized hospital to proceed with detailed laboratory examination. Examination generally includes hematology (white blood cell differential) and immunology (immunoglobulins, complement, and autoantibodies in serum, and detailed immunophenotype of lymphocytes, including naïve and mature forms). The third essential examination is molecular genetics. PID arise as a result of mutation in the genes which are important for the proper function of immune cells. Progress in molecular genetic technologies has definitively assisted in localizing the responsible gene in many PIDs. Recently, with the development of massive parallel sequencing (MPS) and its introduction in clinical laboratories, a vast quantity of novel genomic abnormalities in patients with PID is being discovered (*4*). However, their functional consequences at the cellular level are usually not known. The fourth important examination, a functional testing of the affected cells, is therefore needed to be implemented. Functional tests are on the edge of clinics and research, therefore must be well planned, accurately realized, properly interpreted and provided only by an experienced laboratory. In CLIP laboratories at the Department of Pediatric Hematology and Oncology at the 2nd Faculty of Medicine, Charles University, we provide complete genetic testing (using MPS followed by Sanger sequencing), and a detailed immunophenotyping (using multicolor flow cytometry), complemented with sets of functional tests both for PID and immune system malignancies. We identify the affected genes, proteins and cellular subpopulations, and test the functional properties of novel mutations. A full spectrum of laboratory examinations is crucial for a proper treatment decision.

2. Aims

The main aim of my diploma thesis was to functionally characterize human PIDs with novel yet undescribed mutations in Signal transducer and activator of transcription 1 *(STAT1)*, Caspase-8 (*CASP8)*, and Tyrosine-protein kinase HCK *(HCK)* at a cellular level, in terms of changed immunophenotype, *in vitro* proliferation, apoptosis, intracellular signaling, and cytokine production. The experiments were performed on both primary cells and cell lines, in particular by the use of multicolor flow cytometry, immunoprecipitation, western blotting, and ELISA.

3. A basic description of the human immune system

The immune system (IS) is composed of specialized organs, tissues, and cells. The main lymphatic organs and tissues are the bone marrow and thymus, where the multiplication and differentiation from hematopoietic stem cell into lymphoid and myeloid progenitors and further into more specialized cells takes place (Fig. 1). Immune cells belong to the non-specific (innate) or antigen-specific (adaptive) part of immunity. Innate immunity consists of a cellular (e.g. NK cells, phagocytic cells) and a humoral (e.g. complement) part. Adaptive immunity is also composed of a cellular (e.g. T-lymphocytes, B-lymphocytes) and a humoral part (e.g. immunoglobulins (Ig) secreted from plasmablasts).

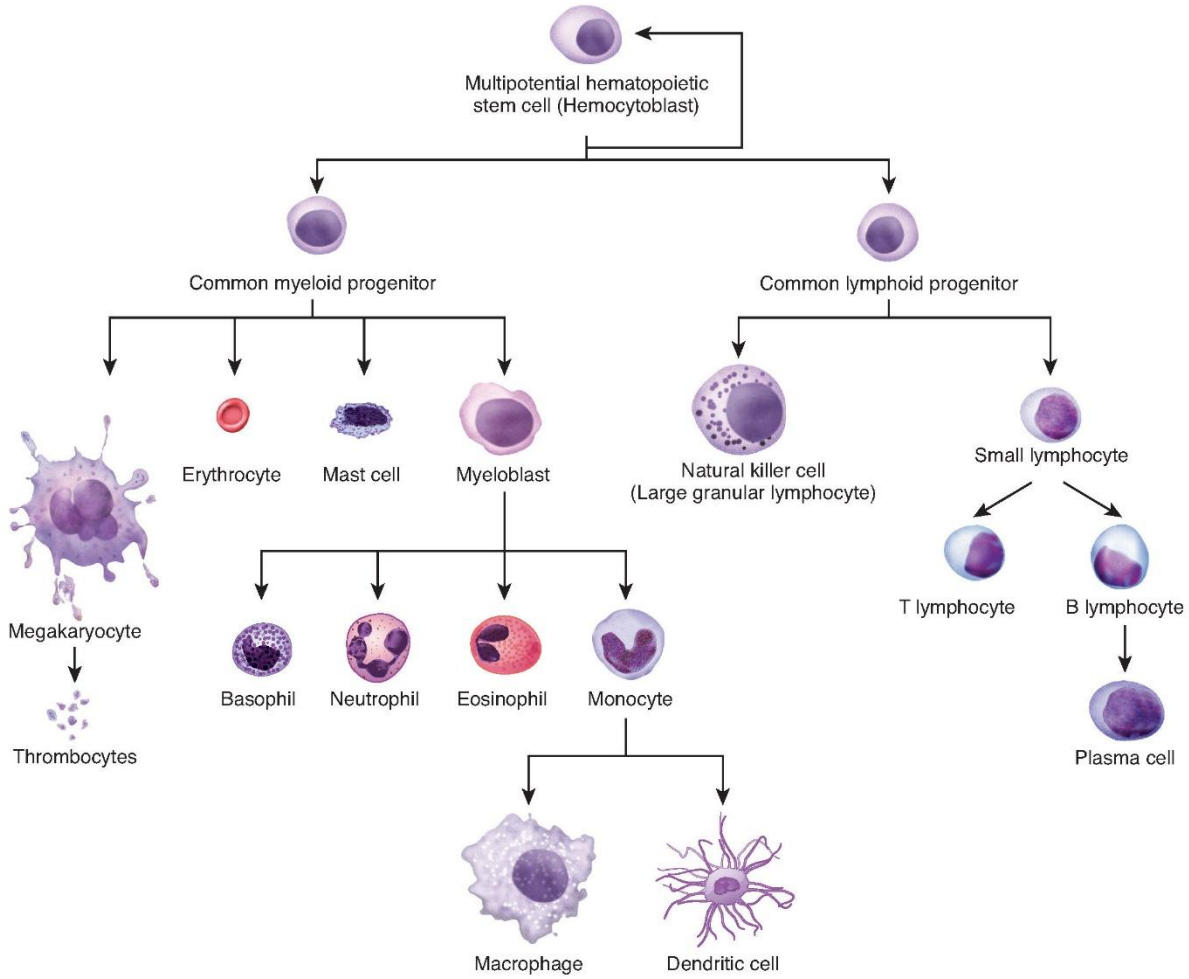

Fig. 1. Simplified scheme of human hematopoiesis. The two main lineages, myeloid and lymphoid, are generated from the hematopoietic stem cell. In a myeloid lineage, we find mainly innate immune cells: granulocytes (basophils, neutrophils, and eosinophils) and antigen presenting cells (monocytes, macrophages, and dendritic cells). In a lymphoid lineage, we find mainly adaptive immune cells (T- and B-lymphocytes) and natural killer (NK) cells. The diagram was obtained from Wikimedia Commons (available at *commons.wikimedia.org/w/index.php?curid=30131219*).

4. Immunodeficiency

Immunodeficiency (ID) is a complex defect of the immune system. Immunodeficiencies are characterized by an impairment of the immune response, resulting mainly in poor or no response to infection or vaccination. The first encounter with a patient's state of health is usually by a pediatrician, immunologist, dermatologist, or a respiratory system specialist who, in the case of suspected ID, recommends specialized examinations. The intrinsic defects in the immune system (gene mutations) cause primary immunodeficiencies (PID). Extrinsic factors affecting the immune system (e.g. viruses, malnutrition, disrupted gut flora, breached integumentary barriers etc.) can cause secondary immunodeficiencies, which are acquired during a lifetime. Patients with ID are generally vulnerable to opportunistic infections, which do not cause disease in a healthy person who has a functioning immune system. Moreover, they have a higher risk of developing a cancer (*5*).

4.1. Primary immunodeficiency

Primary immunodeficiency (PID), recently called "inborn error of immunity", develops mostly in the background of a genetic defect, mutation in genes which are important for the proper functioning of the immune system. Impaired immune response is usually captured in infancy or later childhood. In the case of milder forms, it can be diagnosed after a delay. A PID first discovered was X-linked agammaglobulinemia, caused by B-cell maturation defect (*6*). To date, many different PIDs have been discovered, each of them manifested by different severity and consequences due to impairment of various immune components.

4.1.1. Classification of PIDs

Briefly, PID group can be divided based on the missing/altered immune components to:

i) immunodeficiencies affecting cellular and humoral immunity,
ii) combined immunodeficiencies with associated or syndromic features,
iii) predominantly antibody deficiencies,
iii) diseases of immune dysregulation,
iv) congenital defects of phagocyte numbers or function,
v) defects in intrinsic and innate immunity,
vi) autoinflammatory disorders,
vii) complement deficiencies, and
vii) phenocopies of inborn errors of immunity.

Every year, the Inborn Errors of Immunity Committee (IEI) provides an up-to-date classification of all PIDs (*5*).

4.1.1.1. Immunodeficiencies affecting cellular and humoral immunity

T-lymphocytes and often B-lymphocytes are impaired or decreased in number in this subgroup. The main representative is severe combined immunodeficiency (SCID), with T-cells (T-B+ SCID) or both T-cells and B-cells missing (T-B- SCID). SCID patients present with a very serious condition emerging soon after birth. Patients suffer from severe viral and intracellular infections and do not react to vaccination. If it is not treated in time, SCID patients do not survive past 1 year of age (*7*, *8*).

4.1.1.2. Combined immunodeficiencies with associated or syndromic features

These deficiencies are recognizable by distinct clinical or immunological features. The representatives are Wiskott-Aldrich syndrome with low antibody response to polysaccharides, accompanied by congenital thrombocytopenia with small platelets (*9*), or ataxia-teleangiectasia with a decrease in T-cells, accompanied by DNA repair defects and increased radiosensitivity (*10*).

4.1.1.3. Predominantly antibody deficiencies

Antibody deficiencies can occur from a slight decrease in immunoglobulins to complete depletion of B-cells. These PIDs are the most common. The main symptoms are chronic inflammation and repeated bacterial infections. Due to obtained IgG from the mother's milk, these deficiencies are revealed only at approximately the first year of life. The representative is X-linked agammaglobulinemia caused by mutated Bruton Tyrosine Kinase (BTK). BTK is essential for B-cell development. Patients suffer from low B-cell levels and decreased Igs. Agammaglobulinemia is successfully treated with intravenous Igs (*6*, *11*).

4.1.1.4. Diseases of immune dysregulation

Autoimmunities (immune reactions to own cells, tissues and organs causing e.g. autoimmune cytopenias) are often associated with PID. An example is autoimmune lymphoproliferative syndrome (ALPS). ALPS is based on deficiency of FAS, FASL, or caspase-10 resulting in impaired apoptosis. The main symptoms are lymphadenopathy, splenomegaly, and diverse autoimmune cytopenias; anemia or thrombocytopenia (*12*).

4.1.1.5. Congenital defects of phagocyte numbers or function

Patients with defects of phagocytic cells often suffer from skin infections, systemic infections, and bacterial or fungal diseases. The representative of this group is chronic granulomatous disease (CGD). It is manifested by impaired generation of reactive oxygen species and superoxide due to mutation in nicotinamide adenine dinucleotide phosphate-oxidase (NADPH oxidase). The phagocytes are not effective in immune responses and recurrent infections occur (*13*, *14*).

4.1.1.6. Defects in intrinsic and innate immunity

The antiviral intrinsic immunity blocks the spread of the virus. The representative of this PID subgroup may be STAT1 deficiency. Upon interaction with Janus kinases (JAK), STAT proteins transmit a signal to the nucleus and promote interferon (IFN) response, mediating the antiviral state of the cell (for further details please see page 14). STAT1 deficiency is manifested by impaired STAT1-dependent IFNγ responses and severe viral and mycobacterial infections (*15*).

4.1.1.7. Autoinflammatory disorders

Immune response has to be regulated to protect the organism but to avoid abnormal inflammation. In autoinflammatory disorders, the innate immune system is not regulated properly, leading to its overactivation. Representative of this subgroup is the stimulator of interferon genes (STING)-associated vasculopathy. Mutation in STING leads to autoinflammatory disease due to abnormal interferon transcription (*16*).

4.1.1.8. Complement disorders

Complement is a set of over 30 soluble and membrane proteins of the innate immunity. Many parts of the complement system can function inadequately or be missing. The representative is e.g. C1 inhibitor deficiency. C1 inhibitor can inhibit C1 complex of the classic pathway of complement. In the case of deficiency, auto-activation of the complement system occurs, leading to hereditary angioedema (*17*).

4.1.1.9. Phenocopies of inborn errors of immunity

A phenocopy is the expression for a genetically normal patient with a phenotype that mimics a genetic disorder. The representative is chronic mucocutaneous candidiasis (CMC) associated with autoimmune polyendocrinopathy-candidiasis-ectodermal dystrophy (APECED).

In APECED, autoantibodies against IL-17A or IL-17F are secreted, which allow for the development of CMC. For further details, please see page 17 (*18*, *19*).

4.1.2. Genetic background of primary immunodeficiency

A majority of PIDs are caused by gene defects or mutations. Moreover, gene transcription or post-translational modifications can also be altered. Gene mutation is defined as a permanent change in the DNA. PIDs are mostly caused by germline mutations; they are inherited as the mutation is present in the parent's germ cell. *De novo* mutations sometimes occur as well. Gene defects can be smaller (a change in one base pair) or bigger (ranging from a gene segment to a bigger part of chromosome affecting multiple genes). When a transcription of aberrant gene into mRNA is productive and a protein is subsequently translated, it can possess changed functions. Mutations in PIDs are generally divided into two groups: loss-of-function (LOF) or deficiency, where the protein is not translated or is dysfunctional (*20*), or gain-of-function (GOF) where the protein gains stronger or additive functions (*21*).

4.1.2.1. Loss-of-function mutations

LOF or simply "deficiency" denotes **inactivating or weakening**. The gene product (protein) has a weak or no function. The recessive variants can be amorphic, causing a total loss of function, or partially recessive, retaining partial function. Many LOF mutations have been described to date. To delineate some of the newest : homozygous LOF mutation in breast cancer 1 (*BRCA1*), causing Fanconi anemia-like phenotype, impaired growth, bone marrow failure, and high inclination to tumors (*22*); LOF mutation in autoimmune regulator (*AIRE*), causing impaired immune tolerance caused by low expression of autoantigens in thymus (*23*), or LOF mutation in *JAK1*, connected with immune evasion of tumors (*24*).

4.1.2.2. Gain-of-function mutations

GOF or activating mutation is the exact opposite of LOF, causing an alteration in the DNA that leads to **enhanced or empowered function** of a given protein. A frequent scenario is also a suppression of function of another protein or pathway due to stronger preference of the mutated protein. GOF mutations are mostly dominant and, when the mutated allele is transcribed, heterozygous carriers are affected. Apart from *STAT1* GOF mutation, which is one of our interests, many GOF mutations have recently been discovered, e.g. Caspase recruitment domain-containing protein 11 (CARD11), a scaffold protein expressed mainly in lymphoid cell line, which binds B-cell lymphoma 10 (BCL10) and Mucosa-associated lymphoid tissue

translocation gene 1 (MALT1) and which forms a complex that activates NFκB signaling. GOF mutation in CARD11 leads to abnormal B-cell proliferation (*25*). Another interesting example is GOF mutation in STAT3, causing hyper-IgE syndrome (*26, 27*).

4.1.3. Treatment of primary immunodeficiencies

Many approaches to treating PIDs are used. It is crucial to determine the type of PID, which cellular subsets are affected and if the patient is in a condition to undergo the treatment without complications. Antibody treatment to supplement the deficiency of nonfunctional immune cells represents one of the oldest techniques. Since 1952, when Bruton's Agammaglobulinemia was discovered, scientists realized the value of immunoglobulin replacement and the prevention of infections in these patients (*6*). Antimicrobial treatment to avoid infections is also very common. HSCT is a revolutionary treatment, which is lifesaving in severe forms such as SCID (*28*). However, in STAT1 GOF patients, the overall survival after HSCT was reported as being only 40% (*29*), indicating the diverse success rate of HSCT in different types of PID. Gene therapy is also being tested. Lentiviral and retroviral systems have been reported in many successful experiments in X-SCID, adenosine deaminase (ADA)-SCID, or Wiskott-Aldrich syndrome (*9, 30, 31*). Small molecular inhibitors are also possible treatments in PID, such as rapamycin (mammalian target of rapamycin (MTOR) inhibitor, frequently used in ALPS (*32*), or PI3K inhibitors which are tested in clinical studies in Activated PI3K delta syndrome (*33, 34*).

4.2. Secondary immunodeficiency

Secondary or acquired immunodeficiency is a defect of the immune system which is caused by several extrinsic factors, excluding genetic defects. The majority of all secondary immunodeficiencies is caused by malnutrition. Among other factors, viruses (HIV) or cancers are also identified. Tumor cells can affect the immune system in a complex way; by suppression of cytotoxic cells by the tumor microenvironment or by production of cytokines which can even completely eliminate some immune cell subpopulations (*35*). Furthermore, chemotherapy or irradiation can also affect several parts of the immune system and eradicate a huge number of healthy cells (*36*). A summary of the diverse factors influencing the immune system in secondary immunodeficiencies is depicted in Table 1.

Table 1. The main causes of secondary immunodeficiencies.

Name	Main effect on the immune system
HIV infection	CD4+ T-lymphocytes depletion
Malnutrition	Inhibition of lymphocyte development
Chemotherapy and irradiation	Bone marrow (lymphocyte precursors) damage
Cancer	Suppression or eradication of immune cell subpopulations or metastases in a bone marrow
Splenectomy	Decreased phagocytosis

5. PID testing procedure

5.1. Anamnesis and laboratory testing

The suspicion of PID emerges in childhood when a patient fails to thrive. The child can suffer numerous infections, repeated pneumonias, inflammation, candidiasis, meningitis, or viral infections. Problems of lymphatic tissue are very common; lymphoid organs (lymph nodes, spleen) may be enlarged or absent. Another warning sign is disproportionate reaction to vaccination with a live vaccine when a patient develops a rash, granuloma, or tuberculosis (e.g. after Bacillus Calmette–Guérin (BCG) vaccination) (*37*). Clinicians must be aware of the list of 10 warning signs (Fig. 2) that depicts the possible attributes of a suspected immunodeficient patient, in order to refer him or her to a specialist.

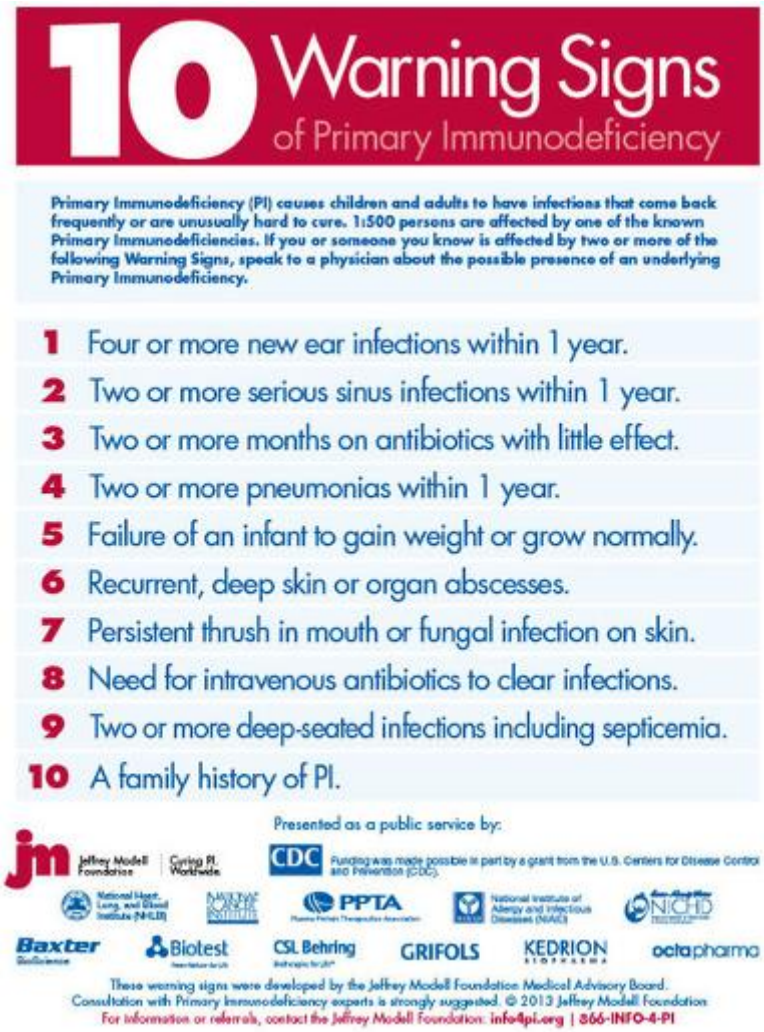

Fig. 2. Ten Warning Signs of Primary Immunodeficiency (Jeffrey Modell Foundation; *info4pi.org/library/educational-materials/10-warning-signs*).

One of the first tests to spot PID is a complete blood count and differential. It can show thrombocytopenia, lymphopenia, neutropenia, anemia, as well as leukocytosis or lymphocytosis. Another screening test is flow cytometry-based immunophenotyping. It can easily characterize leukocyte subpopulations in detail. Surface molecules can be quickly detected, using antibodies directly conjugated with fluorochromes.

In general, flow cytometers consist of 3 main parts (Fig. 3): fluidics (1), optics (2), and electronics (3). **Fluidics** take care of the transport of the cells (cytometers can generally measure particles from 0.2 to 150 µm); the sample is carried by sheath fluid and transported to lasers. **Optics** consist of prisms and lenses which lead the laser beam into the sample. The laser beams cause excitation of the antibody-conjugated fluorochromes on the cells. Emission spectra of the fluorochrome is subsequently captured by mirrors and detectors. Finally, **electronics** convert the light signal into digital signal for further processing and analysis using specialized software.

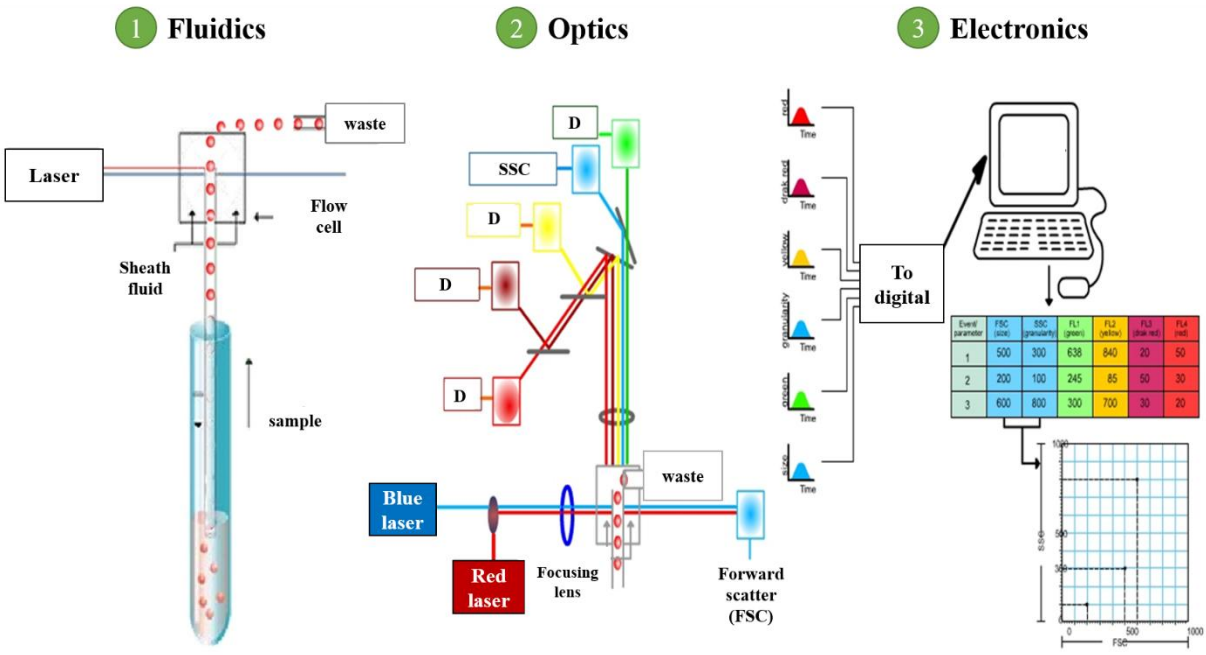

Fig. 3. Simplified scheme of flow cytometry. (1) Fluidics transports the sample in the sheath fluid toward lasers, the laser meets the cells in the flow cell. **(2)** In **optics**, lasers generate the light signals and detectors (D) detect them. FSC = forward scatter light, SSC = side scatter light. **(3) Electronics** converts the light signal to digital signal and prepare the data for further computational analysis. (The scheme was adapted from the website Obfuscata, Flow cytometry analysis, available at *obfuscata.com/flow-cytometry-analysis-4791.html*).

Apart from molecules defining specific subpopulations (e.g. CD19 for B-cells or CD3 for T-cells), other markers characterizing the differentiation status (e.g. CD45RA and C-C chemokine receptor type 7 (CCR7) for naïve T-cells) or cell activation (e.g. CD69, CD25, or HLA-DR) are also successfully used.

Functional leukocyte testing is also very important. Apart from present or missing markers, it is necessary to determine whether immune cells are competent to perform their function correctly (*38*, *39*). Among the functional tests which are usually routinely performed in immunology laboratories, we include cytokine and immunoglobulin production (or their

presence in serum), phagocytosis (*40*), proliferation of cells after mitogen stimulation (*41*), or NK cell degranulation (*42*).

5.2. PID screening procedure in CLIP laboratories

In the CLIP-cytometry laboratory, special PID tubes developed by EuroFlow consortium (EuroFlow, available at *euroflow.org/usr/pub/pub.php*) are routinely processed from the patients' peripheral blood if clinically suspected of PID. Four distinct antibody panels are used: PID Screening tube containing markers of naïve and mature lymphocytes, which is suitable for primary screening; Pre-GC tube suitable for B-cell subpopulations; Eff-Mem tube for T-cell subpopulations, and finally SCID-RTE tube for detection of the most naïve T-cells, known as recent thymic migrants (RTE). The antibody combination in each tube is shown in Table 2. Since these tests have not yet been published, the fluorochromes are not revealed.

Table 2. Combination of markers which are tested using PID Screening tube, Pre-GC tube, Eff-Mem tube, and SCID-RTE tube. Pre-GC = pre-germinal center, Eff-Mem = effector (Eff) memory (Mem), SCID-RTE = recent thymic emigrants (RTE) and severe combined immunodeficiency (SCID).

PID Screening tube

Epitope	CD27	CD45RA	CD8 + IgD	CD16 + CD56	CD4 + IgM	CD19 + TCRγδ	CD3	CD45

Pre-GC tube for B-cell subpopulations

Epitope	CD27	CD45RA	CD8	CD5	IgD	CD19	CD21	CD24

Eff-Mem tube for T-cell subpopulations

Epitope	CD27	CD45RA	CD8	CCR7	CD28	TCRγδ	CD3	CD8

SCID-RTE for recent thymic emigrants (RTE) and T-cells activation (HLA-DR)

Epitope	CD27	CD45RA	CD8	CD31	HLA-DR	TCRγδ	CD3	CD8

The reference values obtained from Piatosa et al. and Schatorjé et al. for each of the detected subpopulations are used to assess the alterations in the patients‘ samples (*43*, *44*).

When needed, especially when severe forms of PID (SCID) are suspected, a screening of T-cell receptor (TCR) excision circles (TREC) is undertaken in the CLIP-genomics laboratory. TRECs are small parts of episomal DNA, formed when naïve T-cells rearrange V, D, and J segments of TCR (Fig. 4). TRECs are used as markers for RTE and naïve cells. The number of TRECs precisely refers to the RTE count. This test was first applied by Douek et al. in 1998. In critical cases, massive parallel sequencing of DNA from peripheral blood or buccal smear is also indicated and undertaken in the CLIP-genomics laboratory.

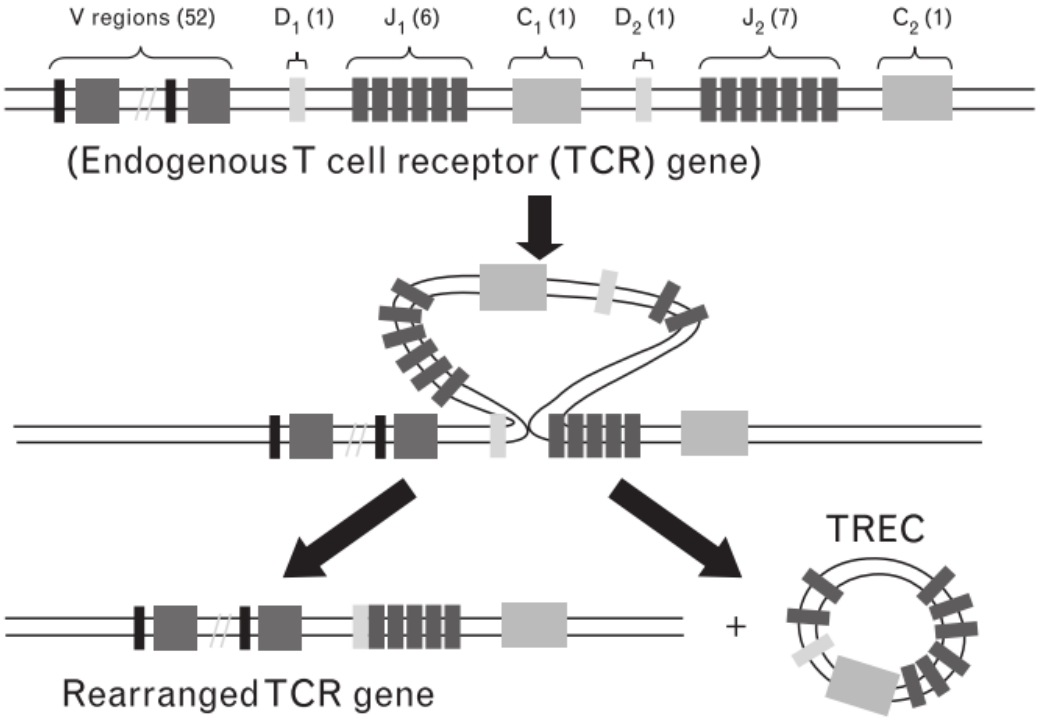

Fig. 4. Process of TREC formation during the V, D, J segments rearrangement in naïve T-cells (*46*).

6. Patient no. 1 with heterozygous STAT1 mutation

6.1. Abstract

In the 12-year-old male patient, a novel heterozygous mutation in gene encoding Signal transducer and activator of transcription 1 (STAT1) protein, c.617T>C, L206P was identified. We aimed to prove the functional status of this mutation. We tested activation (phosphorylation on Tyrosine 701) of STAT1 protein in the patient's and controls' peripheral blood cells (PBMC) upon stimulation with interferons (IFNα and IFNγ) using both western blotting and single-cell phospho-flow cytometry. We found hyperphosphorylation of STAT1 in the patient's cells. Moreover, we tested a small molecular inhibitor of JAK/STAT signaling, ruxolitinib, in the patient's cells *ex vivo* and proved its efficacy. Finally, we developed a single-tube whole-blood test which was used for ruxolitinib treatment monitoring.

6.2. Introduction to STAT1 topic

6.2.1. STAT family of proteins

There have been seven STAT proteins described to date: STAT1, 2, 3, 4, 5a, 5b, and 6. These proteins function as signal transducers and transcription factors which regulate differentiation, migration, proliferation or apoptosis of immune cells (*47*). They transmit the outside-in signals via STAT phosphorylation and stable dimerization to both homo- and heterodimers. Signaling begins on a cell membrane. Cytokine or growth factor binds to its receptor and induces its dimerization. JAK kinases, which thereby come in close proximity, phosphorylate each other to enhance their activities and subsequently phosphorylate the receptor. STAT molecules are bound to the receptors via their Src Homology 2 (SH2) domains and are phosphorylated by JAK kinases. Activated STAT molecules can subsequently dimerize, translocate to the nucleus and bind to DNA as transcription factors (*48–50*). STAT proteins have various functions: **STAT1** is activated by both type I IFN (IFNα) and type II IFN (IFNγ), or by interleukin-27 (IL-27), and promotes Th1 polarization (*51*, *52*). **STAT2** protein responds to type I IFN, forms a multimeric transcription factor IFNα-stimulated gene factor 3 (ISGF3) containing STAT2, STAT1, and p48 and activates the transcription of IFN-stimulated genes, driving the antiviral state (*53–55*). Surprisingly, STAT2 deficiency was not connected with higher susceptibility to viral infections in humans (*56*). **STAT3** activation can be triggered by IFNs, or IL-5 and IL-6 and it is involved in anti-apoptotic signaling, resulting in enhanced T-cell proliferation (*57*), and in Th17-immune response polarization (*58*). **STAT4** is activated by IL-12 and is needed for Th1 differentiation from naïve T-cells and for IFNγ production (*59*, *60*). The

STAT5 family includes two proteins, STAT5a and STAT5b, which are encoded by separate genes. The amino acid composition of STAT5a and STAT5b is almost the same. STAT5 regulates proliferation, differentiation and apoptosis of hematopoietic cells (*61*), and is also involved in T-regulatory cell development (*62*). STAT5b deficiency in humans leads to impaired response to growth hormone and to short stature (*63*). STAT5 has been also observed hyperphosphorylated in cancer cells, where it promotes proliferation (*64*). **STAT6** is activated by IL-4, and is essential for Th2 differentiation and for immunoglobulin class switching to IgE (*65*, *66*).

6.2.2. *STAT1* gene position and STAT1 protein scheme

STAT1 protein is encoded by *STAT1* gene positioned on chromosome 2 (Fig. 5).

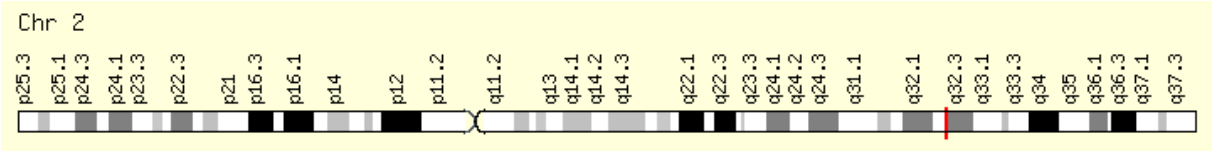

Fig. 5. *STAT1* gene localization. Gene can be found on chromosome 2 in position 32.2. (GeneCards, *http://www.genecards.org/cgi-bin/carddisp.pl?gene=STAT1*).

STAT1 belongs to the STAT family of proteins. STAT proteins generally consist of several conserved structural motifs, including N-terminal domain (important for dimerization of STATs (*67*), a coiled-coil domain (necessary for both STAT1 transport into the nucleus and STAT1 nuclear dephosphorylation (*68*), a DNA-binding domain (providing a bond with DNA (*69*)), a linker domain (important for formation of transcriptional complex (*70*), and an SH2 domain which has the ability to recognize the phospho-Tyrosine residues, mediates dimerization and is required for transport into the nucleus (*71*). The last two domains of STAT1 are a tail segment domain (TS), containing activation Tyrosine (Tyr701 in STAT1) (*72*) and a transactivator domain (TA) which regulates specific gene transcription (*73*) (Fig. 6).

Fig. 6. STAT1 protein scheme. STAT1 protein has seven main domains. Adapted from Depner et al., 2016 and Kawata, 2011 (*75-76*). Aminoacid positions are indicated by numbers.

6.2.3. STAT1 protein function

Two alternatively spliced transcripts of STAT1 have been described, resulting in two isoforms of the protein, STAT1a and STAT1b. Isoform a has a full length of 91 kDa; isoform b is shorter, terminates at the C-terminus and has 84 kDa. Both isoforms can be phosphorylated on Tyr701, translocate to nucleus, and bind to DNA (*76*). The STAT1 pathway transmits IFN signals required for numerous immune functions, e.g. antiviral functions slowing or blocking virus dissemination (*77*). Type I IFNs (IFNα and β) induce oligomerization of STAT1/STAT2/p48 to IFN-stimulated response elements (ISRE), whereas type II IFNs (IFNγ) induce formation of STAT1 homodimers and their recruitment to Interferon-gamma-activated sequence (GAS) promoter element (*76*).

In humans, two major types of STAT1-associated primary immunodeficiencies have been described to date: „STAT1 deficiency“ and „gain-of-function STAT1 mutations“. **STAT1 deficiency** is characterized by impaired cellular responses to IFNs, mediating severe viral and mycobacterial infections (*15*, *78*). Chapgier et al. also reported severe disseminated bacillus Calmette-Guérin (BCG) infection (*79*). **Gain-of-function STAT1 mutations** are characterized by both viral and bacterial infections, autoimmune and inflammatory conditions and, in all cases, chronic mucocutaneous candidiasis (CMC). CMC symptoms are presented as white fungal cover on the mucosa (oral or/and genital) and skin, stomatitis, bronchitis and sometimes infections of the gastrointestinal tract (*75*, *80–82*). Several GOF mutations in *STAT1* have been described in both coiled-coil domain and DNA-binding domain (Fig. 7).

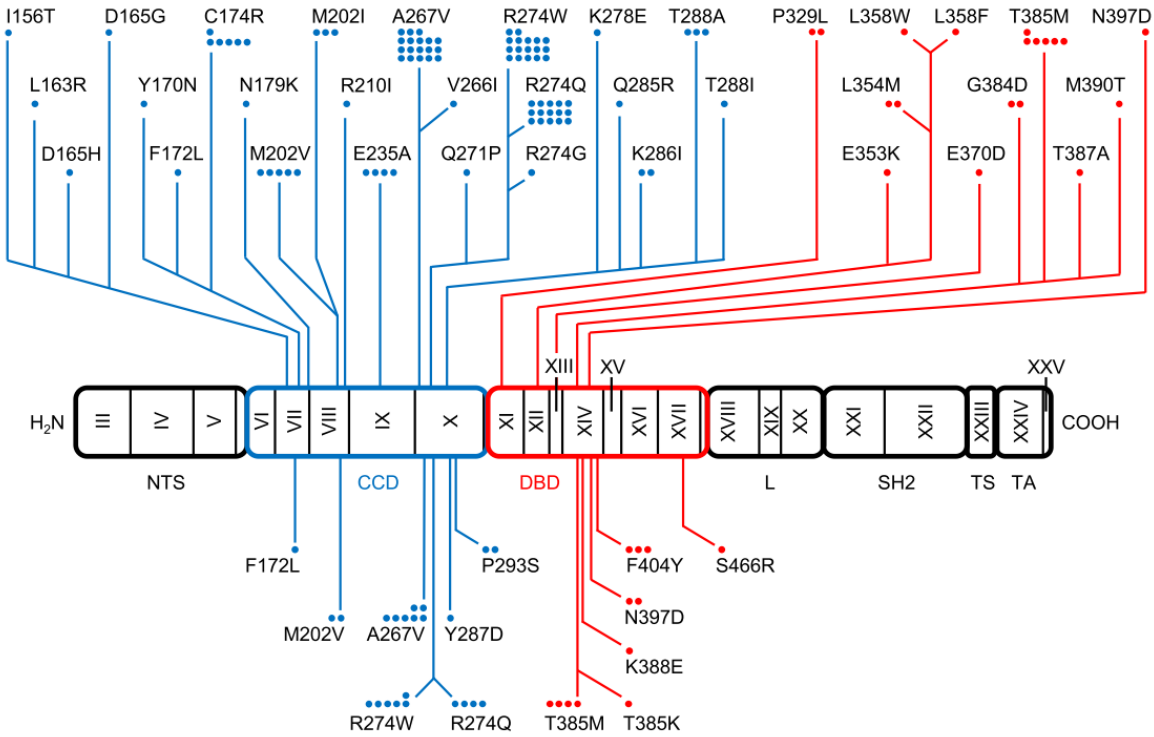

Fig. 7. Reported GOF mutations in STAT1 as described in Depner et al., 2016 (*76*). Roman numbers indicate encoding exons. Coiled-coil mutations are shown in blue; DNA-binding domain mutations are shown in red. Dots indicate the numbers of identified patients with a particular mutation.

The patients with GOF STAT1 are treated mainly with azole antimycotics. In serious cases, HSCT seems to be the treatment option. However, the overall survival after HSCT is only 40 %, as reported by Leiding et al. (*29*). In the study by Toubiana et al., a small molecular inhibitor of JAK/STAT signal transmission, ruxolitinib, was suggested and administered to patients and a satisfactory clinical improvement was found (*80*).

6.2.4. How is hyperactive STAT1 involved in the fight against Candida?

Fig. 8 clearly depicts how the combat against fungal pathogens is continuing. NADPH oxidase plays the major role. This protein is responsible for microtubule-associated protein 1A/1B-light chain 3A (LC3)-associated phagocytosis along with reactive oxygen species (ROS) production, which are necessary in antifungal defense. Another important signaling is mediated by pathogen-associated molecular patterns (PAMPs), fungal cell wall components. Upon binding of PAMPs to pattern recognition receptors (PRRs), dectins, a downstream signaling activates CARD9, which forms a complex with BCL-10 and MALT1. This initiates NFκB response and cytokine production (IL-1β, IL-6, IL-23, or TGFβ). The third important players are STAT1 and STAT3 molecules. Proinflammatory cytokines signalize through STAT3. STAT3 induces RORγt

transcription and naïve T-cells start to differentiate into Th17 lineage. IL-17A, IL-17F, and IL-22, the key adaptive cytokines in host defense against fungi are produced, mediating pro-inflammatory responses (NFκB activation and neutrophil recruitment). Hyperactive STAT1 impairs STAT3-mediated signaling and abolishes Th17 differentiation, thereby decreasing antifungal defense (*83*).

As indicated in Fig. 8, also patients with CARD9 deficiency (*84*) or STAT3 deficiency (*85*) may suffer from CMC. Interestingly, patients with autoimmune regulator (AIRE) defect, called autoimmune polyendocrinopathy-candidiasis-ectodermal dystrophy (APECED), produce high levels of neutralizing antibodies against IL-17A, IL-17F or/and IL-22, thus attenuating antifungal response as well (*86*).

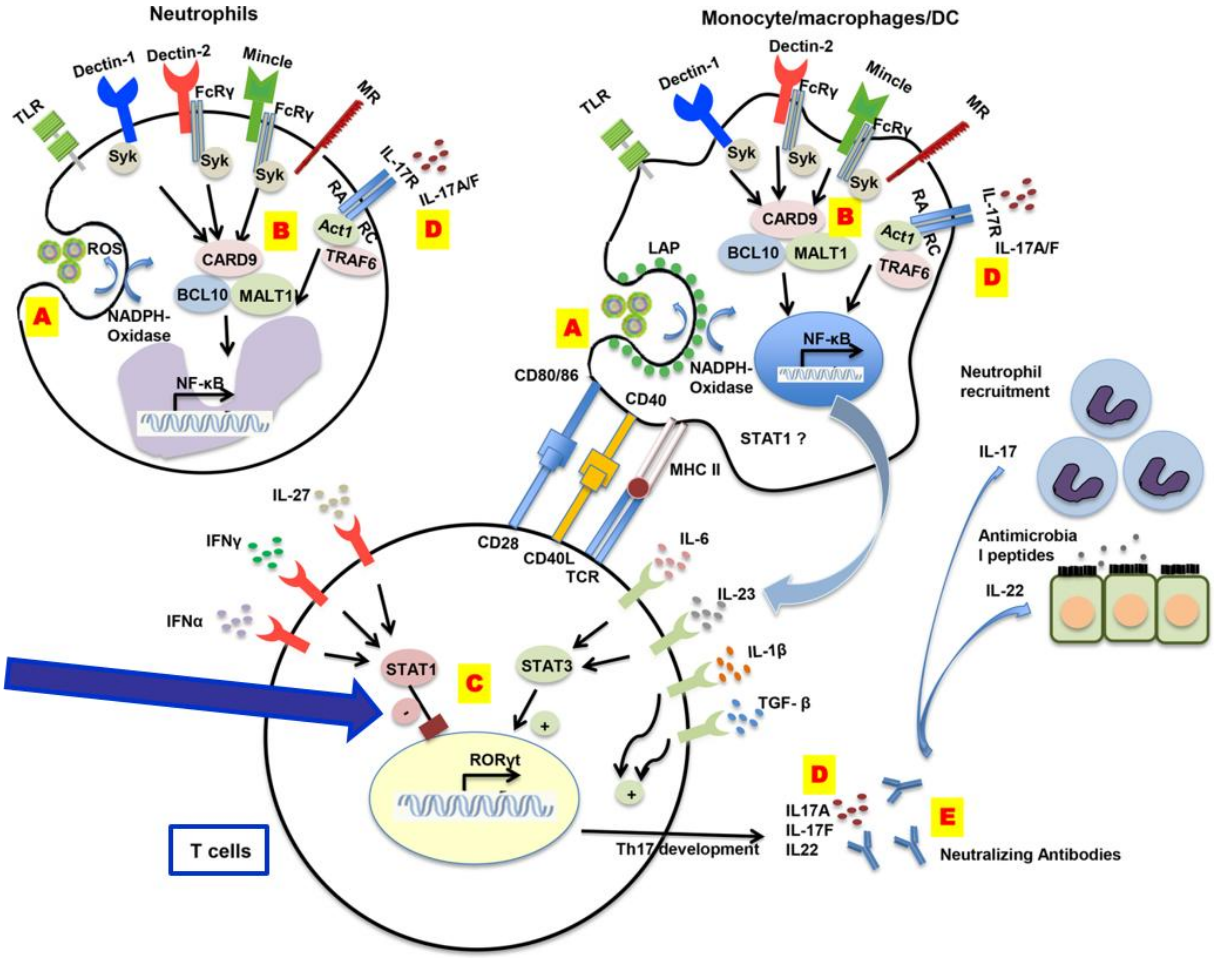

Fig. 8. Signaling pathways in neutrophils, monocytes and macrophages, and in T-cells to induce a proper antifungal defense. A) NADHP oxidase activity, B) CARD9 signaling, C) STAT1/STAT3 balance, D) IL-17 and IL-22 activity, E) neutralizing antibodies against IL-17 and IL-22. The arrow indicates hyperactive STAT1 in T-cells (*83*).

6.3. Clinical case

The patient suffered from chronic mucocutaneous candidiasis (CMC). This disease is caused by *Candida* species, mainly *Candida albicans* and affects skin, nails and mucosae and can cause hypothyroidism (*87*). Early after birth at the age of 2 months the patient firstly suffered with the oral candida infection. During the first year of life, middle-ear infections, mild pneumonia and staphylococcal infection were also reported. Later, onychomycosis appeared. Azole treatment was prescribed, however, candidiasis worsened over time and spread. Patient developed T-cell lymphopenia and Th17 and Treg deficiency (detected at the Department of Immunology, University Hospital Motol). In B-cells, memory B-cell lymphopenia (as described in Results section) and low IgG2, IgG4, and IgM levels were also found. At the age of 12 years, a novel *STAT1* gene mutation was identified. It was yet undescribed substitutional mutation in a coiled-coil domain in position 206 (c.617T>C, L206P), where leucine was replaced by proline.

6.4. Material and methods

6.4.1. Immunophenotyping

Immunophenotyping was routinely performed in CLIP-cytometry laboratory. The following antibody-conjugates were used: CD27-BV421, IgM-BV510, CD5-PE, and IgD-PerCP-Cy5.5 (Biolegend, San Diego, CA), CD19-PE-Cy7 and CD24-APC-Alexa Fluor 750 (Beckman Coulter, Miami, FL), CD38-FITC and CD21-APC (BD Biosciences, San Jose, CA) for B-cells and CD4-BV510, HLA-DR-PerCP-Cy5.5, and CD62L-BV421 (Biolegend), CD3-APC and TCRgd-PE-Cy7 (BD Biosciences), CD8-APC-Alexa Fluor 750 (Beckman Coulter), CD45RO-FITC and CD31-PE (Exbio, Vestec, Czech Republic), and CCR7-PE (Miltenyi Biotec, Bergisch Gladbach, Germany) for T-cells. The samples were acquired on Canto II flow cytometer (BD Biosciences) and the data analysis was performed using FlowJo software (BD Biosciences).

6.4.2. Western blotting

Western blotting was performed on peripheral blood mononuclear cells (PBMC) of the patient and healthy controls. PBMC were separated on Ficoll-Paque (GE Healthcare, Uppsala, Sweden) according to manufacturer's instructions (centrifugation step run in Universal 320 R centrifuge (Hettich, Tuttlingen, Germany) for 20 min at 25°C and 1000 RCF), washed in serum-free RPMI 1640 medium supplemented with L-glutamine, HEPES, and penicillin/streptomycin (Lonza, Basel, Switzerland), and counted on Bürker chamber upon mixing in ratio 1:9 with trypan blue (Sigma Aldrich, St. Louis, MO). PBMC were stimulated with 0.5-1μg/ml IFNγ (R&D Systems, Minneapolis, MN) for 30 minutes at 37°C. Part of PBMC were cultured with 1μM ruxolitinib (Seleckchem, Houston, TX) for 30 min at 37°C prior to IFNγ stimulation.

Activated sodium vanadate was used as a positive control. For activation, 1μl 30% H_2O_2 (Sigma Aldrich) was added to 20 mM sodium vanadate (Na_3VO_4, Sigma Aldrich) and incubated for 5 min at room temperature (RT). Activated sodium vanadate (final concentration 0.1mM) was incubated with PBMC for 10 min at 37°C. All reactions were stopped by washing the cells in ice-cold phosphate buffered saline (PBS) and centrifugation step run in pre-chilled Universal 320 R centrifuge for 5 min at 4°C and 700 RCF. The cell pellet was resuspended in so called tween-lysis buffer (50 mM HEPES, 10 mM $MgCl_2$, 140 mM NaCl, pH 8) supplemented with 0.1% Tween 20, 1% n-dodecyl beta-D-maltoside, 2 mM PMSF, proteinase inhibitor and phosphatase inhibitor coctails (all from Sigma Aldrich), sonicated 4x for 10 s, lysed on ice for 30 min, and centrifuged (5 min, 4°C, 10000 RCF). Supernatants were collected and protein concentration was measured using BCA protein assay kit (Pierce, Thermo Fisher Scientific, Rockford, IL) according to manufacturer's instructions. Briefly, Reagent A containing bicinchoninic acid and Reagent B containing cupric sulfate were mixed in ratio 50:1, and diluted bovine serum albumin (BSA) standards were prepared in 96-well flat bottom plates (final concentrations 200-6.25 μg/ml). The lysates were diluted in the A+B mixture in ratio 1:9, the samples were incubated 30 min at 37°C and the absorbance was measured on VERSAmax Tunable Microplate Reader at 540 nm. The concentrations were analyzed with SoftMaxPro software (Molecular Devices, Sunnyvale, CA). Generally, the concentrations of the lysates were adjusted to 0.5 mg/ml. The samples were diluted with Laemmli reducing sample buffer (Sigma Aldrich) in ratio 1:1 and heated to 98°C for 5 min. Proteins were separated on BOLT 4-12% BisTris plus gels (electrophoresis run for 60 min at 120 V in MOPS buffer, all from Thermo Fisher) and transferred to nitrocellulose membranes (Bio-Rad, Hercules, CA, tranfer run for 90 min at 120 V). Membranes were blocked in 7.5% low-fat bovine milk in PBS supplemented with 0.05% Tween 20 (Sigma Aldrich) at 2-8°C overnight, washed twice in PBS with 0.05% Tween 20 and incubated with primary antibodies against STAT1, phospho-STAT1(Tyr701) (both from Cell Signaling Technologies, Danvers, MA) and beta-actin (Exbio) for 60 min at RT. After washing in PBS with 0.05% Tween 20, the peroxidase-conjugated secondary antibodies (Jackson Immunoresearch, West Grove, PA) were used for 45 min at RT. Finally, after washing in PBS with 0.05% Tween 20, the SuperSignal West Pico Chemiluminescent Substrate (Thermo Fischer) was used for the signal detection on C-DiGit scanner (LI-COR, Lincoln, NE). Signal quantification was performed using Image Studio Digits (LI-COR).

6.4.3. Single-cell phospho-flow cytometry

Detection of phosphorylation of STAT1 molecules was performed in a whole blood of the patient and healthy controls. For stimulation/inhibition 1 μg/ml IFNγ, 0.1 mM activated

sodium vanadate, and 1 μM ruxolitinib were used. Timeline 0, 5, 10, 15 and 30 min at 37°C was tested for IFNγ stimulation. Part of blood samples were cultivated with 1μM ruxolitinib for 30 min at 37°C prior to IFNγ stimulation. The signaling was stopped by fixing the cells in 4% methanol-free formaldehyde (Thermo Fisher) for 10 min at RT. Erythrocytes were lysed using PBS with 0.1% Triton X-100 (Sigma Aldrich) for 15 min at 37°C, and the cells were washed in PBS supplemented with 0.5% BSA (Merck, Darmstadt, Germany, each centrifugation step run for 5 min at RT and 700 RCF). The cells were resuspended in 1 ml ice-cold methanol (Roth, Karsruhe, Germany) and incubated for 30 min on ice. After centrifugation and washing in PBS with 0.5% BSA, the pellets were stained with fluorochrome-conjugates phospho-STAT1(Tyr701)-PE (Cell Signaling Technologies), and CD3-APC and CD45-PB (both from Exbio) for 30 min at RT in the dark. After final wash in PBS (centrifugation 5 min, RT, 700 RCF), the samples were acquired on LSR II flow cytometer and analyzed using FlowJo software. CD19 was detected afterwards, after two additional washes in PBS using CD19-PE-Cy7 (Beckman Coulter) for 15 min at RT.

6.4.4. Ruxolitinib treatment monitoring optimization

For optimal treatment monitoring (to distinguish phosphorylated STAT1/3/5 molecules both in T-cells and B-cells), several fix-perm protocols were tested. Optimization experiment was performed in a whole blood of the healthy control which was stimulated w/wo 1 μg/ml IFNγ for 10 min at 37°C. All samples were fixed with 4% methanol-free formaldehyde for 10 min at RT, permeabilized with 0.1% Triton X-100 in PBS for 15 min at 37°C, and washed in 0.5% BSA in PBS. One part of samples was proceeded directly, one was mixed with 10 % glycerol (Sigma Aldrich) in heat-inactivated fetal bovine serum (FBS, Thermo Fischer) and was frozen overnight or for 8 days at -20°C. The cells were then permeabilized in ice-cold 80% or 90% methanol for 30 min on ice prior and after anti-CD19 staining (15 min of anti-CD19-PE-Cy7 (Beckman Coulter), RT). Finally, the cells were washed in 0.5% BSA in PBS and stained with fluorochrome-conjugates phospho-STAT1 (Tyr701)-Alexa Fluor 647 (BD Biosciences), CD3-PerCP-Cy5.5, and CD45-PB (both from Exbio) for 30 min at RT. After final wash in PBS the cells were measured on LSR II flow cytometer and analyzed using FlowJo software. The whole procedure was repeated also with frozen samples.

6.4.5. Treatment monitoring

In the course of ruxolitinib treatment we used the protocol optimized above. After stimulation of whole blood samples of the patient and healthy control w/wo 1μg/ml IFNγ or IFNα for 10 min at 37°C, the cells were fixed in 4% methanol-free formaldehyde, permeabilized

using 0.1% Triton X-100 in PBS, washed in 0.5% BSA in PBS, and stored in 10% glycerol in FBS overnight at -20°C. The second day, the samples were thawed, stained with anti-CD19-PE-Cy7, and permeabilized in 80% ice-cold methanol. After final wash in 0.5% BSA in PBS, phospho-STAT1 (Tyr701)-Alexa Fluor 647, phospho-STAT3 (Tyr705)-Alexa Fluor 488, and phospho-STAT5 (Tyr694)-PE (all from BD Biosciences) antibodies were used along with CD3-APC, CD45-PB (both from Exbio), and CD19-PE-Cy7 (Beckman Coulter) for 30 min at RT. The samples were measured on LSR II flow cytometer and analyzed using FlowJo software.

6.5. Results

6.5.1. Decreased levels of T-cells and mature B-cells in patient's peripheral blood

The immunophenotyping of peripheral blood lymphocytes was routinely performed in CLIP-cytometry laboratory using EuroFlow PID tubes. When analyzing the PID tubes before inclusion of ruxolitinib we found decreased lymphocytes, decreased CD3+ T-cells (both CD4+ and CD8+), and decreased mature forms of B-cells. Neutrophils were elevated. After ruxolitinib induction, lymphocytes increased to almost reference limits and neutrophils normalized (Table 3).

Table 3. Leukocyte subpopulations in patient's peripheral blood before and after 16 weeks of ruxolitinib treatment. Reference values taken from Piatosa et al., 2010 and Schatorjé et al., 2012 (*43*, *44*)

Subpopulation	Units	Before treatment	On ruxolitinib	Reference value
Lymphocytes	Cells/µl	850	1360	1500-4100
Neutrophils	Cells/µl	9690	5230	1500-5900
CD3+	Cells/µl	621	952	1200-2600
CD3+ CD4+	% from lymphocytes	12	17	20-65
CD3+ CD8+	% from lymphocytes	8,6	13	14-40
Switched memory CD19+ B-cells	% from CD19+	0,7	0,3	8,7-25,6

6.5.2. Hyperactivated patient's STAT1 detected using western blot

The very first test of phospho-STAT1 (Tyr701) was performed on patient's peripheral blood which was collected in the patient's place of residence and transported to our department for more than 6 hours. We found phosphorylation of STAT1 on Tyr701 upon IFNγ and sodium vanadate stimulation but the profile of phospho-STAT1 in the patient's cell was curious. Although the loading control (beta-actin) did not indicate a problem, we found two bands of

phospho-STAT1 in the patient's cell. Moreover, a total STAT1 was not detectable (Fig. 9). We suggested that the apoptosis followed by protein degradation occurred in the sample.

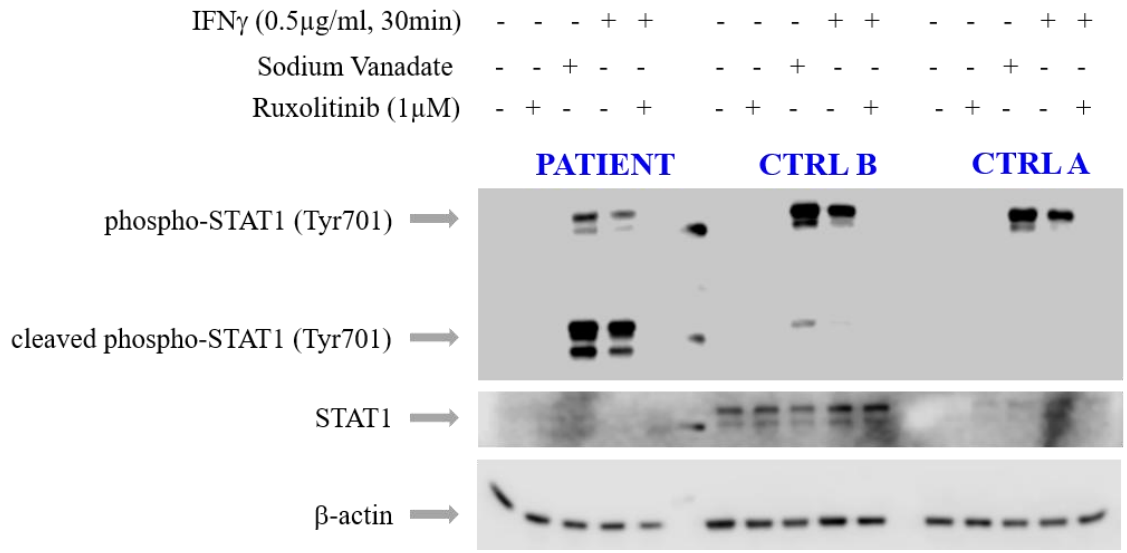

Fig. 9. Western blot #1 from the very first blood samples. STAT1 was cleaved in the patient's cells, therefore two bands of phospho-STAT1 (Tyr701) were substantially visible. Sodium vanadate was used as a positive control for phosphorylation. 1µM ruxolitinib inhibited STAT1 phosphorylation *ex vivo* both in patient's and controls' cells.

The test was therefore repeated on fresh peripheral blood samples which were drawed from patient and healthy controls in Motol University Hospital. Patient's PBMC showed slightly increased total STAT1 expression. Upon IFNγ stimulation we found hyperphosphorylation of STAT1 (Tyr701) in the patient's cells compared to his mother and healthy control B (patients' physician). Additionaly, 1µM ruxolitinib, which inhibits kinase activity of JAK1/2 and subsequently phosphorylation of STAT molecules (*88*), was capable to inhibit STAT1 phosphorylation *ex vivo* both in patient's and controls' cells (Fig. 10). Western blot results were confirmed by single-cell phospho-flow cytometry (see Fig. 12).

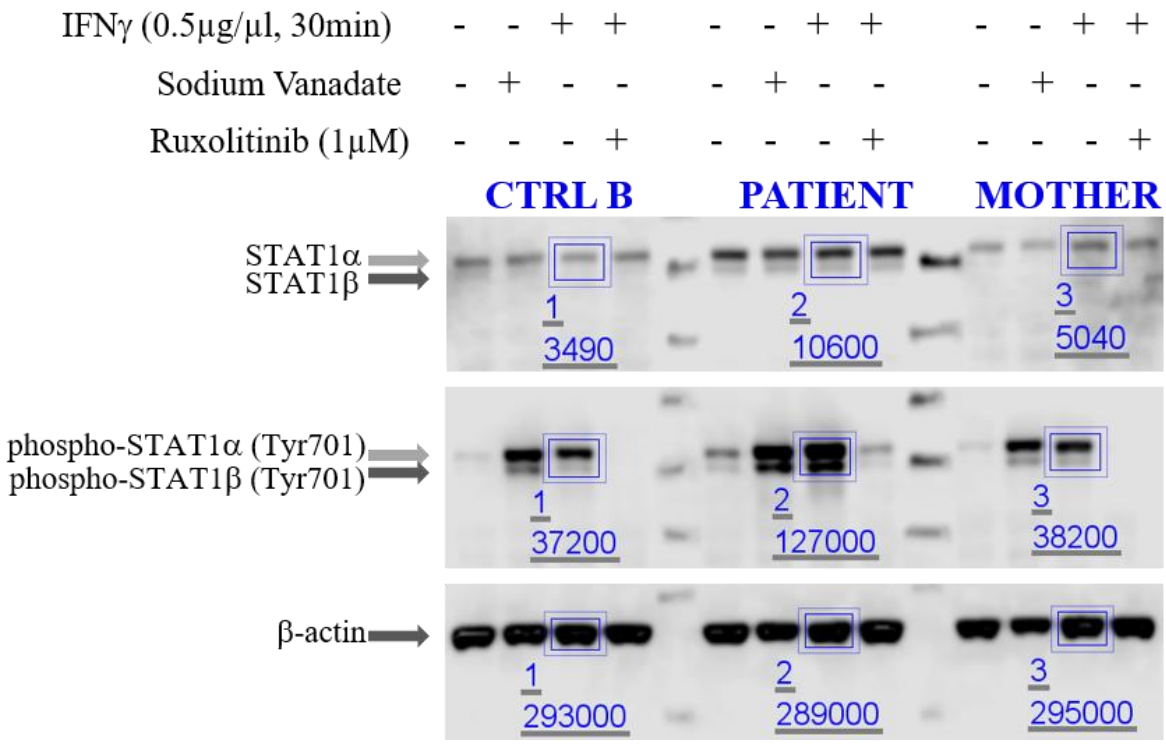

Fig. 10. Western blot #2 from fresh blood samples. Patient's cells showed higher ratio of phosphorylated STAT1 (Tyr701) compared to total STAT1 level. Sodium vanadate was used as a positive control for phosphorylation. 1µM ruxolitinib inhibited STAT1 phosphorylation *ex vivo* both in patient's and controls' cells. Blue numbers indicate a quantification of chemiluminiscence signals.

We had also checked the PBMC of patient and healthy controls by flow cytometry before the 2nd functional western blotting test. PBMC were not much contaminated by granulocytes (Fig. 11).

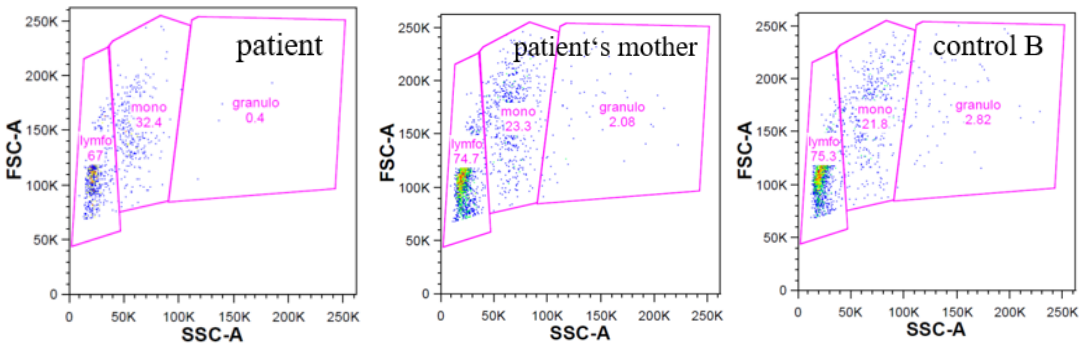

Fig. 11. Lymphocytes, monocytes, and granulocytes in the PMBC of the patient and healthy controls used for western blotting.

6.5.3. Hyperactivated patient's STAT1 detected using single-cell phospho-flow cytometry

Flow cytometry test was performed on PBMC w/wo 0, 5, 10, and 30 minutes of IFNγ stimulation (Fig. 12). We found higher phosphorylation of STAT1 on Tyr701 in patient's CD3+ T-cells and CD19+ B-cells in comparison to healthy control and patient's mother in each of the tested timepoint of IFNγ treatment. 1μM ruxolitinib, as a potential treatment, was able to decrease phospho-STAT1 (Tyr701) levels *ex vivo* in both patient and healthy controls, althought the phosphorylation of STAT1 in the patient's cells remained higher compare to controls (Fig. 12, 13). The *ex vivo* results helped to approve the ruxolitinib treatment.

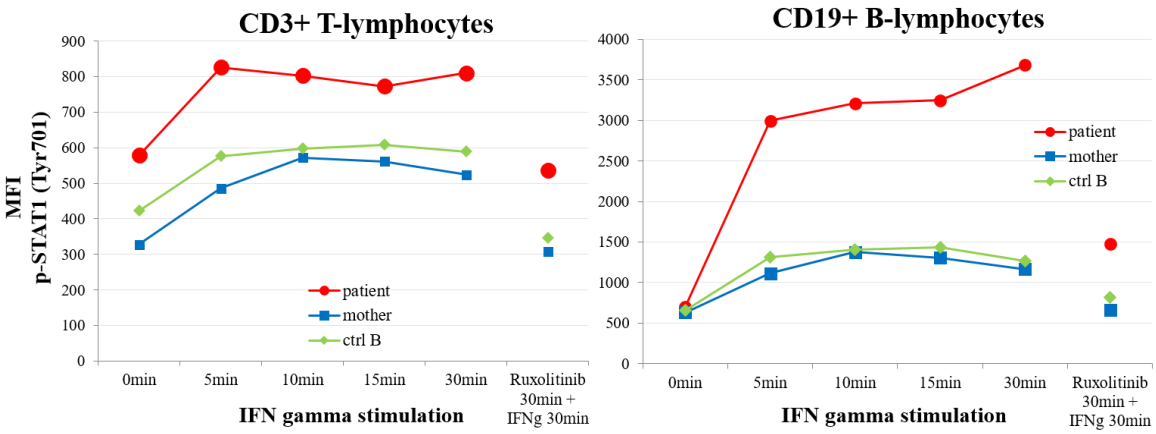

Fig. 12. IFNγ stimulation timeline in T- and B-cells. Patient's cells (red) showed high phospho-STAT1 (Tyr701) in each of the stimulation timepoint both in T-cells and B-cells compared to patient's mother (blue) and independent healthy control (green). 1μM ruxolitinib added to cells 30 min before INFγ stimulation was able to inhibit phosphorylation of STAT1 *ex vivo* albeit rather mildly in the patient's cells. MFI = median intensity fluorescence of phospho-STAT1 (Tyr701)-PE.

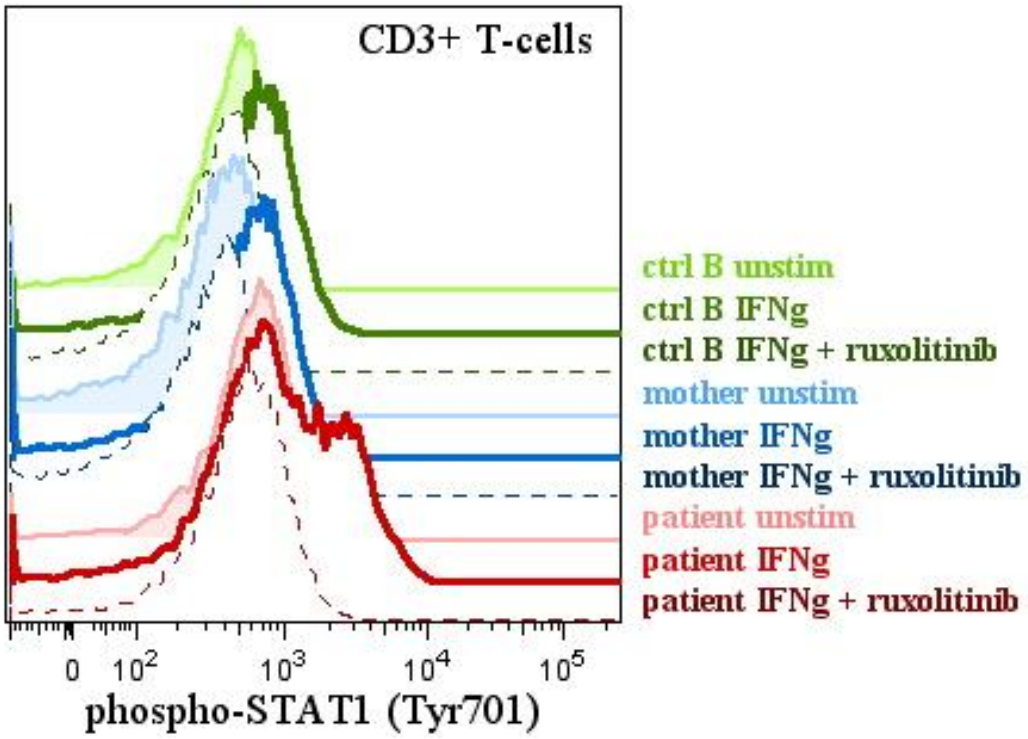

Fig. 13. Phospho-STAT1 (Tyr701) in T-cells. The histograms indicate timepoint 30 min of IFNγ stimulation. Patient's T-cells (red) showed higher phosphorylation of STAT1 compare to patient's mother (blue) and independent healthy control (green). 1μM ruxolitinib inhibited phosphorylation of STAT1 both in patient and healthy controls. Basal phospho-STAT1 (Tyr701) in tinted color, 30 min of IFNγ stimulation in bold, 1μM ruxolitinib inhibition dashed. X-axis shows fluorescence intensity of phospho-STAT1(Tyr701)-PE.

6.5.4. Ruxolitinib treatment monitoring optimization

Optimization of the simple whole-blood protocol for detection of phospho-STAT1, STAT3, and STAT5 in the patient's T-cells and B-cells during ruxolitinib treatment was essential to build an efficient, fast and precise monitoring. Due to long-lasting problems with a detection of CD19 after cell fixation, several possible approaches were tested.

We tested: timepoint of CD19 staining, concentration of methanol used for permeabilization, and an additon of a freezing step between fix and perm. Fig. 12 clearly shows that CD19 could not be detected using appropriate antibody clone directly after methanol permeabilization (not 90% (A) neither 80% methanol (B) was appropriate). CD19 could be detected before methanol permeabilization, but only 80% methanol was suitable (D). We assumed that higher concentration of methanol (C) can degrade fluorochrome PE-Cy7.

Moreover, a freezing of the sample in -20°C in 10% glycerol in FBS clearly decreased autofluorescence in PE-Cy7 channel, thus allowed us to better distinguish CD19+ population (E). Finally, phospho-STAT1 (Tyr701) level was not changed when 80% methanol was used instead of 90% methanol (F) (Fig. 14).

Based on the results, we decided to use following protocol (INF stimulation - formaldehyde - triton X-100 - freezing overnight - thawing - CD19 - 80% methanol - pSTATs, CD3, CD45) for ruxolitinib efficacy monitoring.

A

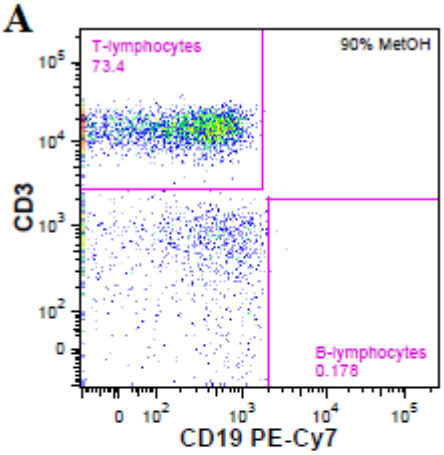

45++
WITHOUT FREEZING, CD19
AFTER 90% METOH

B

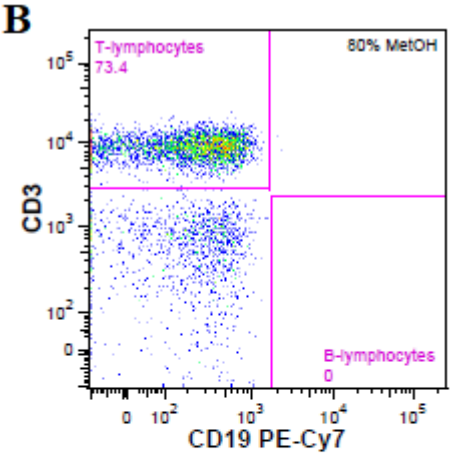

45++
WITHOUT FREEZING, CD19
AFTER 80% METOH

C

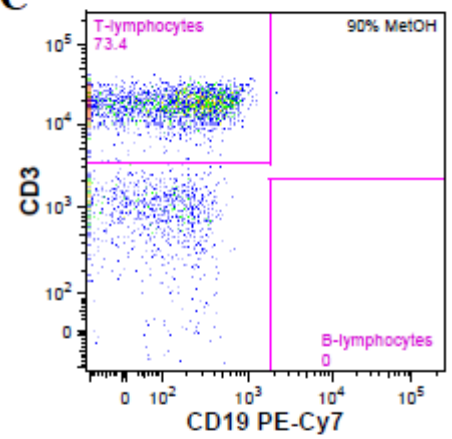

45++
WITHOUT FREEZING, CD19
BEFORE 90% METOH

D

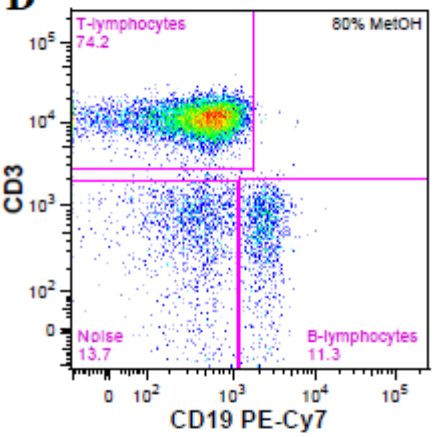

45++
WITHOUT FREEZING, CD19
BEFORE 80% METOH

E

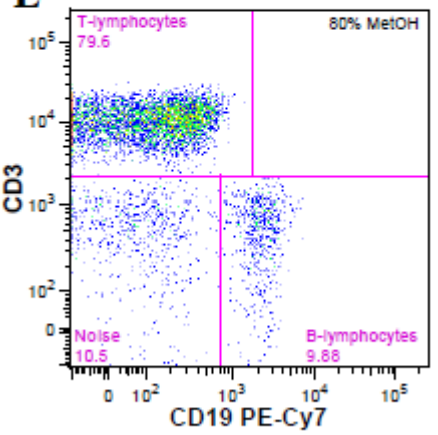

45++
-20°C OVERNIGHT, CD19
BEFORE 80% METOH

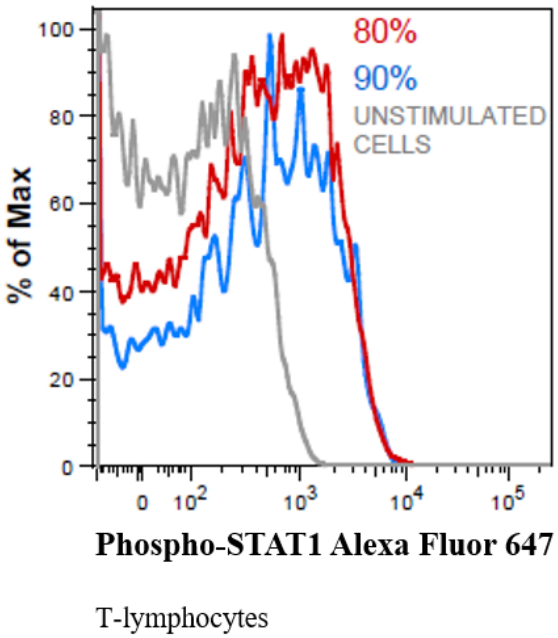

Fig. 14. Optimization of phospho-STAT monitoring protocol. CD19 staining is shown after methanol (METOH) permeabilization (A, B) and before methanol permeabilization (C, D, E). A freezing step (E) decreased background in PE-Cy7 channel allowing better resolution of CD19+ B-cells. Final histogram summarizes the unchanged effect of 80% or 90% methanol permeabilization on phospho-STAT1 (Tyr701) detection.

6.5.5. Quick changes in phosphorylation of STAT molecules during ruxolitinib treatment monitoring

Protocol described above was used in several timepoints during ruxolitinib treatment to monitor its efficacy on phosphorylation of STATs and eliminating Candida infection. The graph (Fig. 13) depicts four major points where the changes were reported by both flow cytometry and in patient's health condition. Point A shows pre-treatment condition, phospho-STAT1 was increased compared to control and Candida infection was visible on skin and mucosae. Afterwards, ruxolitinib was applied, the levels of STATs phosphorylation descended, and patient's Candida retreated (B). After a few weeks, ruxolitinib was unexpectedly withdrawn and changes were immediate. Patient's health condition worsened, Candida infection relapsed, and phospho-STAT1 level increased higher compare to pre-treatment values (C). Finally, ruxolitinib was applied again, patient improved, Candida infection almost receded, and phospho-STATs levels decreased (D) (Fig. 15).

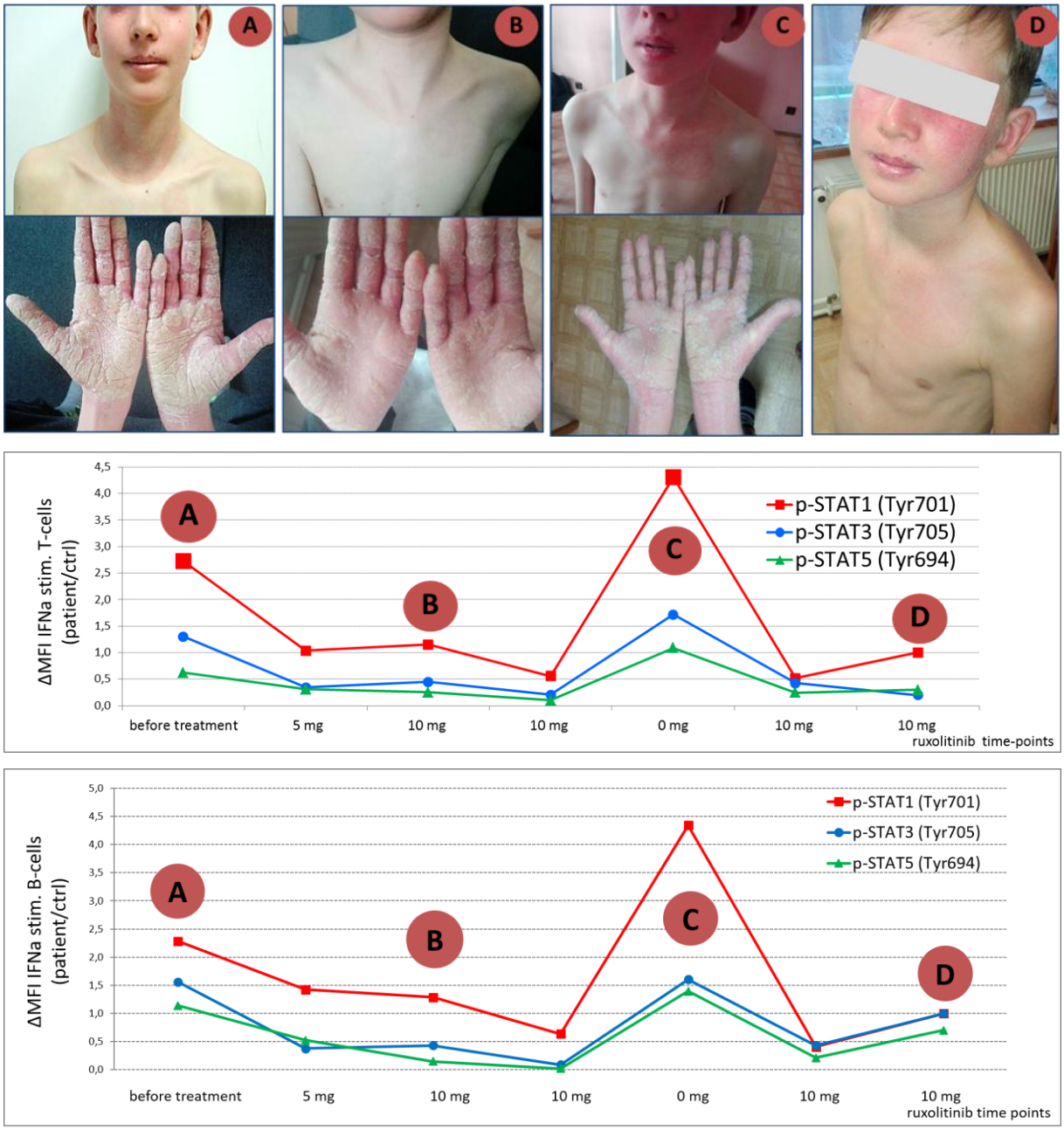

Fig. 15. Monitoring of the patient on ruxolitinib treatment. The photographs show patient's clinical manifestation during ruxolitinib treatment. His health condition and Candida spread correlated with flow cytometry results of the phosphorylation of STAT1, STAT3 and STAT5. X axis shows timepoints on ruxolitinib treatment (mg/m^2/day), Y-axis shows ratio of INFα-induced phospho-STATs in the patient's and healthy control's T-cells and B-cells. The pictures were kindly provided by MUDr. Markéta Bloomfield.

6.6. Discussion

We reported a patient, currently 13-year-old boy, with chronic mucocutaneous candidiasis (CMC). This disease is caused by Candida species when the immune system is unable to develop Th17 polarized immune response. Candida affects skin and mucosae (the lesions are red or grey), moreover infiltrates in lungs and other crucial organs were reported (*21*). Patient's CMC was found to be resistant to all azole antimycotics except of voriconazole. A novel heterozygous mutation (c.617T>C, L206P) was found in a coil-coiled domain of STAT1 in the patient's cells. Since both gain-of-function and loss-of-function mutations were found in the coil-coiled domain (*81*), we could not simply predict the activation status of this novel mutation. As our patient suffered with CMC and presented with low Th17 cells we hypothesized that the novel mutation possess GOF properties.

In the first tests we found that the patient's cells hyperphosphorylated STAT1 protein in reaction to IFNs as verified both by western blotting and a single-cell phospho-flow cytometry. Proteomic experiments had to be performed in a very short time after blood collection. In the first western blotting test, we observed cleavage of STAT1. Since STAT molecules have been reported to be substrate of caspases (*89*) and to be cleaved early in apoptosis (*90*), ongoing apoptosis during a long transport of the blood sample could explain the cleavage phenomenon. Peripheral blood collection was repeated with a fast delivery and we managed to do a successful functional test vizualized by western blotting. When we quantified the ratio of phosphorylated STAT1 (Tyr701) in reaction to IFNγ to total STAT1 level in the patient's cells compared to his mother and unrelated healthy control, this ratio was higher which was later confirmed by a single-cell phospho-flow test. In the phospho-flow test the cells were stimulated with IFNγ in several timepoints to visualize a gradual increase in STAT1 phosphorylation in the patient's cells. Results confirmed GOF property of the new mutation, moreover they indicated delayed STAT1 dephosphorylation. Upon longer IFNγ stimulation (more than 15 min), phosphorylation of STAT1 begun to decrease slightly in the controls but continued to grow in the patient's cells. Actually, a coiled-coil domain of STAT1 has been previously described to be important for signal termination and nuclear dephosphorylation of STAT1 (*68*). However, the test should be extended to 90-120 minutes to demonstrate a lack of STAT1 dephosphorylation in the patient's cells (*91*). Due to limited availability of the patient's peripheral blood samples from the pre-treatment period we did not repeat the timeline and we therefore did not comment on STAT1 dephosphorylation in the manuscript.

Western blotting and phospho-flow cytometry tests also confirmed a possible efficacy of JAK1/2 inhibitor ruxolitinib as a treatment since it was able to inhibit STAT1 phosphorylation *ex*

vivo. Apart from azole anti-fungal treatment other treatment modalities have been described (*80*): JAK 1/2 inhibitor ruxolitinib, granulocyte/macrophage colony-stimulating factor, or HSCT. Since only 40% survival rate was described in GOF STAT1 after HSCT (*29*), and the patient suffered with highly resistant Candida the clinitians decided to use ruxolitinib. Ruxolitinib has been already approved for myelofibrosis (*92*), and has been used successfully in STAT1 GOF oral candidiasis (*88*). To date, our patient is only the sixth patient with GOF STAT1 described in the literature who received ruxolitinib.

Single-cell phospho-flow cytometry protocol for its efficacy monitoring was adapted by Davies et al., 2016 (*94*), and Chow et al., 2005 (*95*), and optimized for detection of phospho-STATs both in T-cells and B-cells in the whole peripheral blood. For each monitoring timepoint only 300μl of peripheral blood was finally needed.

When ruxolitinib was applied, phospho-STAT1 decreased and Candida retreated. After 2 months, treatment was unexpectedly withdrawn and the infection returned. Phosphorylation of STAT1 mirrored the clinical condition, and the phospho-STAT1 level increased to almost twice as much as before treatment. The "ruxolitinib withdrawal syndrome" has been previously reported in patients with myelofibrosis. This phenomenon may be attributed to such a massive increase of pSTAT1 seen in our patient (*95*). Finally, ruxolitinib was applied again, phospho-STATs decreased, and the patient's symptom were once again ameliorated.

The manuscript also deals with Th17 cells changes during treatment which is not a part of this diploma thesis. Ruxolitinib inhibited not only phospho-STAT1 but also phospho-STAT3 which is important for Th17 development. We did not find changes in Th17 cells in the patient. However, the tests were performed on peripheral blood of the patient, and we have to consider that anti-fungal restoration due to ruxolitinib application may happen also in tissues (e.g. by γδT-cells) (*96*, *97*). Moreover, long-term side effects of ruxolitinib treatment have to be carefully monitored since concomittant phospho-STAT5 inhibition and subsequent Treg development restriction (*98*) or impaired growth (*99*) could appear.

6.7. Conclusion

We present a patient with a novel mutation in *STAT1* which we proved to be gain-of-function property using several methods. Ruxolitinib was administered to patient and we monitored its efficacy by single-cell flow cytometry test of phospho-STAT molecules. Protocol for treatment monitoring was optimized and was used to prove the causality of STAT1 mutations in other 4 families. Manuscript "Utility of ruxolitinib in a child with chronic mucocutaneous candidiasis caused by a novel STAT1 gain-of-function mutation" (authors Markéta Bloomfield , Veronika

Kanderová, Zuzana Paračková , Petra Vrabcová, Michael Svatoň , Eva Froňková, Martina Fejtková, Radana Zachová, Michal Rataj, Irena Zentsová, Tomáš Milota, Adam Klocperk, Tomáš Kalina, Anna Šedivá) was submitted to the Journal of Clinical Immunology.

7. Patient no. 2 with homozygous CASP8 mutation

7.1. Abstract

In the 15-year-old male patient a novel mutation in gene encoding caspase-8 protein was identified using MPS. We aimed to prove a functional status of this mutation. We tested Fas-induced apoptosis and proved its impairment in the patient's cells using both western blotting and flow cytometry. Moreover, we tested non-apoptotic signaling of caspase-8 (activation of NFκB and the expression of activation markers CD25, CD69 and proliferation marker Ki-67) upon T-cell receptor (TCR) stimulation that was also found to be weakened in the patient's cells. Using all these tests we confirmed a loss-of-function character of the detected mutation.

7.2. Introduction to caspase-8 topic

7.2.1. *CASP8* gene position and caspase-8 protein scheme

Caspase-8 is encoded by *CASP8* gene positioned on chromosome 2. The precise position of the gene is 2q33.1 and it is 54269 bp long (Fig.16).

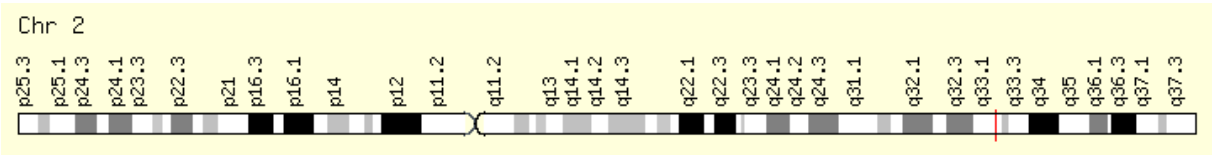

Fig. 16. *CASP8* gene location. Gene is located on the second chromosome in position 2q33.1. (GeneCards, *http://www.genecards.org/cgi-bin/carddisp.pl?gene=CASp8*)

Caspases are intracellular proteases formed as inactive zymogens (procaspases). They generally consist of four main domains; 2 death effector domains (DED), p18 subunit and p10 subunits. A linker part is positioned between these subunits (Fig. 17)

Fig. 8. Procaspase-8 protein scheme. Procaspase-8 consists of two DED domains and p18 and p10 subunits which are connected with a linker. Arrow indicates the position of a novel mutation, red dots represent sites of cleavage. DED = death effector domain. Scheme was adapted from Lavrik and H Krammer, 2009 (*100*).

7.2.2. Caspase-8 protein function

Caspase-8 is an intracellular protease which plays an important role in apoptosis. Upon stimulation via Fas (CD95) or tumor necrosis factor receptors (TNFR-1 or 2) an inactive proenzyme, procaspase-8, is dimerized and autoproteolytically cleaved (cleavage site are indicated as red dots in Fig. 17). Subsequently a highly active heterotetramer is formed. The heterotetramer is composed of two anti-parallel heterodimers each consisting of p18 subunit (18kDa) and p10 subunit (10kDa). Active caspase-8 heterotetramer finally cleaves procaspase-3 which initiates nuclear fragmentation and apoptotic disassembly of the cell (*101*).

Interestingly, caspase-8 participates also in non-apoptotic signaling processes. Upon TCR, Fc-receptor (FcR) or Toll-like receptor (TLR3 and TLR4) or even upon previously mentioned Fas stimulation the signal leads to protein complex including procaspase-8 which is not cleaved in this case and transmits the signal to promote NFκB (Fig. 18, 19) (*102*, *103*).

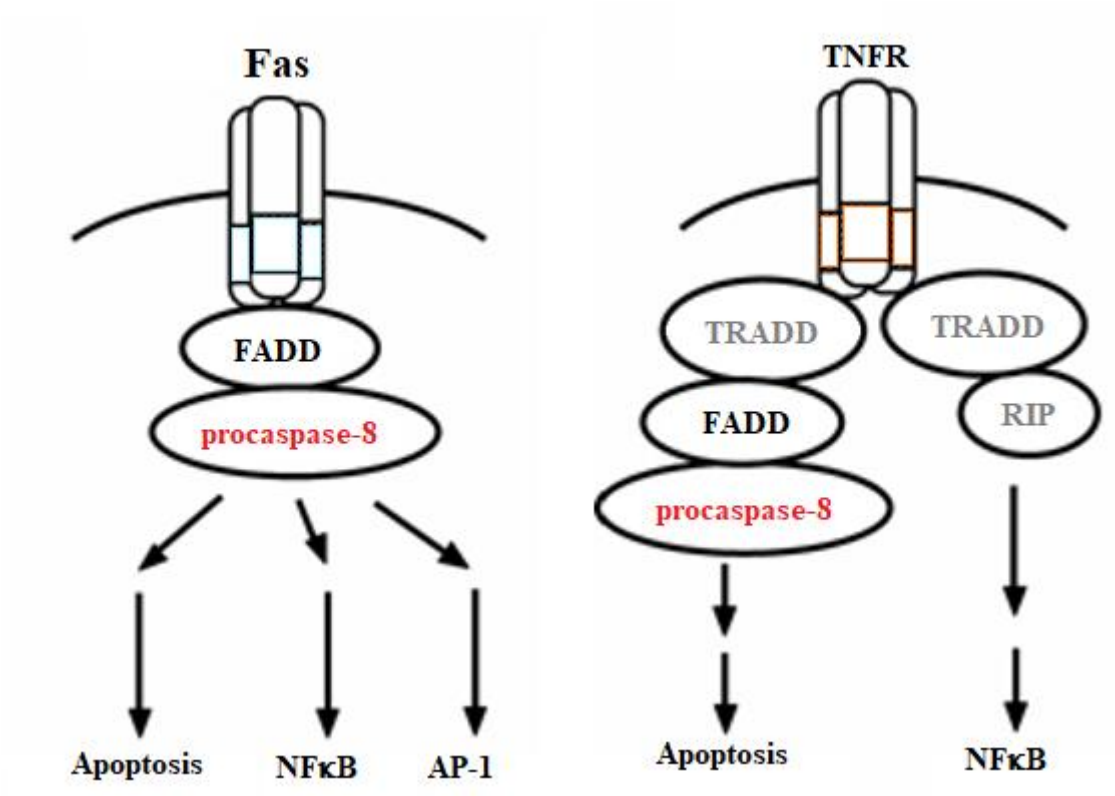

Fig. 18. Signaling pathways mediated via Fas and TNFR. Upon Fas stimulation caspase-8 has been reported in both apoptosis and NFκB activation. Upon TNFR stimulation caspase-8 was not found to be involved in NFκB activation. TRADD = TNFR type 1-associated DEATH domain protein, FADD = Fas-associated protein with DEATH domain, RIP = receptor interacting protein. (The scheme was adapted from Kanazawa University Cancer Research Institute, *http://dimb.w3.kanazawa-u.ac.jp/English/CRI%20reportCDMTD.htm*, Gupta et al., 2006 (*104*) and Su et al., 2005 (*103*)).

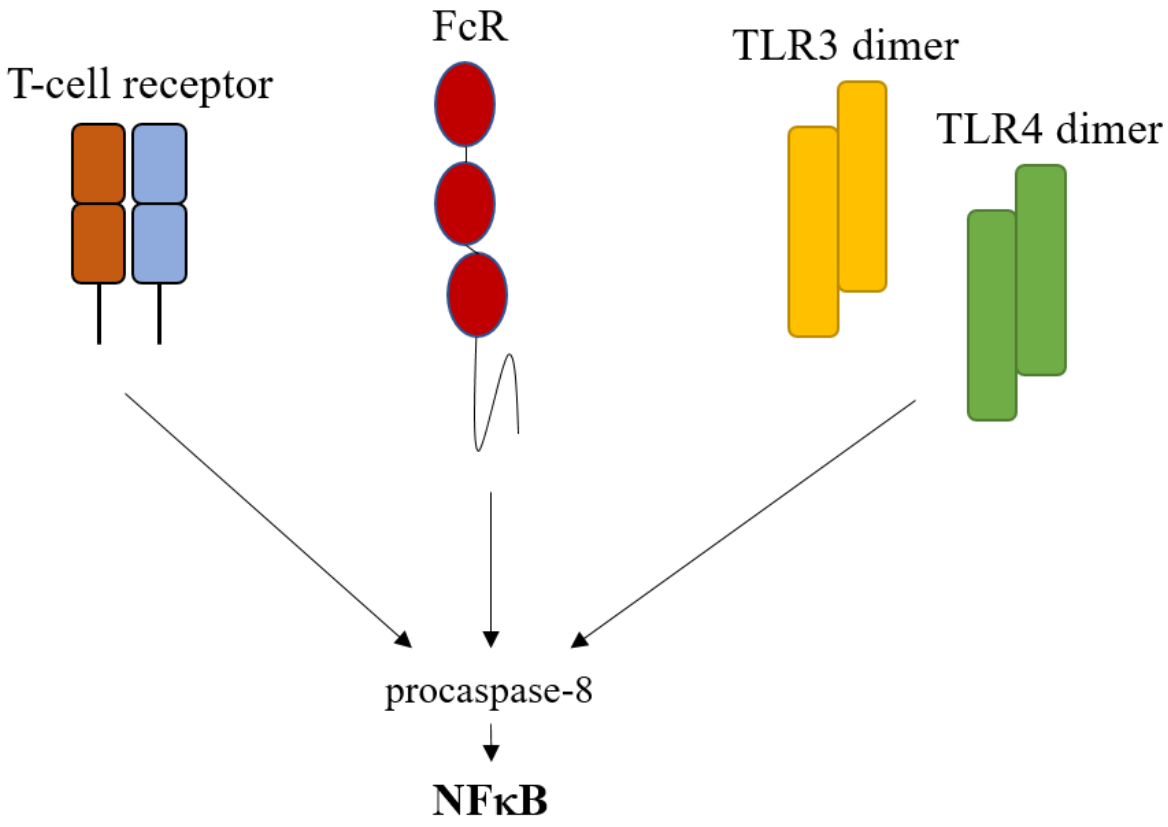

Fig. 19. Non-apoptotic intracellular signaling involving procaspase-8 leading to NFκB activation. (The scheme was adapted from Su et al., 2005 (*103*) and Philip et al., 2016 (*105*))

7.2.3. Known LOF mutations in *CASP8* gene

Only four patients with LOF mutation in *CASP8* have been described in the literature. They carried the same homozygous mutation, c.793C>T, p.R265W, which is positioned in p18 subunit. In the first publication the authors described two siblings, children 11 and 12 years of age who suffered from lymphadenopathy, splenomegaly, and impaired apoptosis induced via Fas. Furthermore, patients presented with immunodeficiency, herpes virus infections, and poor responses to vaccination. The level of procaspase-8 protein was decreased in the patients' cells compared to their relatives, impaired cleavage of caspase-3 and decreased non-apoptotic signaling was also found (*105*). The second publication reported two adult siblings, 41 and 42 years of age. These patients were distant relatives of the originally described family (*105*). They suffered from immune deficiency and lymphadenopathy but also from more severe symptoms such as lymphocytic infiltrates and granulomas in the end-organs (lungs, CNS). Impaired TCR- and TLR-mediated signaling and decreased proliferation of the patients' cell were documented. Both patients died due to post-transplant (patient 1) and neurological and pulmonary (patient 2) complications (*106*).

Interestingly, caspase-8 deficiency in mice causes embryonic lethality; emphesizing the difference between human and mouse (*107*).

7.2.4. Caspase-8 deficiency and autoimmune lymphoproliferative syndrome (ALPS)

Caspase-8 deficiency resembles the clinical syndrome of APLS. In ALPS, a defect in apoptosis which is mediated by mutations in Fas, FasL, or caspase-10 has been described. Patients with ALPS suffer from lymphadenopathy and splenomegaly, similar to patients with caspase-8 deficiency. ALPS patients also suffer from autoimmunity, mainly against blood cells (hemolytic anemia or thrombocytopenia). In contrast, patients with caspase-8 deficiency suffered from immune deficiency; poor response to vaccination, low production of immunoglobulins, severe infections. These symptoms are probably caused by impaired non-apoptotic functions of caspase-8 (*105*, *106*, *108–110*).

7.3. Clinical case

The patient presented from childhood with similar symptoms as reported in Chun et al. in 2002 (*106*), e.g. splenomegaly, lymphadenopathy, failure to thrive, poor response to vaccination, and recurrent severe pulmonary infections. At the age of 13 years, a novel *CASP8* gene mutation was identified. It was a previously undescribed substitutional mutation in a linker domain of procaspase-8 (c.1232C>T, p.P411L), where proline was replaced by leucine.

7.4. Material and methods

7.4.1. Immunophenotyping

Immunophenotyping was routinely performed in CLIP-cytometry laboratory. It was performed using following antibody-conjugates: CD27-BV 421, IgM-BV510, CD5-PE, IgD-PerCP-Cy5.5 (Biolegend)), CD19-PE-Cy7, CD24-APC-Alexa750 (Beckman Coulter), and CD38-FITC, CD21-APC (BD Biosciences)) for B-cells and CD4-BV510, HLA-DR-PerCP-Cy5.5, CD62L-BV421 (Biolegend), CD3-APC, TCRgd-PE-Cy7 (BD Biosciences), CD8-APC-Alexa750 (Beckman Coulter), CD45RO-FITC, CD31-PE (Exbio), and CCR7-PE (Miltenyi Biotec)) for T-cells. The samples were acquired on Canto II flow cytometer and the data analysis was performed using FlowJo software. The gating strategy is shown in the Result section.

7.4.2. Western blotting

The lysates were prepared from patient's and healthy controls' PBMCs. One half of the samples was used immediately for lysate preparation, the second half was stimulated for proliferation. Proliferation was induced by 5 μg/ml phytohemagglutinin (PHA) and 50 ng/ml interleukin-2 (IL-2) in RPMI 1640 medium supplemented with L-glutaminem, HEPES, penicillin/streptomycin (Lonza), and 10% heat-inactivated fetal bovine serum (FBS, Thermo Fisher) in starting concentration 2 million cells per 1 ml. After 3 days, PHA was washed out and the cells were cultivated in RPMI 1640 medium supplemented with L-glutaminem, HEPES, penicillin/streptomycin (Lonza), 10% heat-inactivated FBS (Thermo Fisher), and 50 ng/ml IL-2 for another 9 days. Subsequently, the cells were washed and stimulated w/wo 1 μg/ml anti-Fas antibody (Biolegend), 0,1 μg/ml goat-anti-mouse (GAM) antibody (BD Biosciences) was used to crossling anti-Fas. After 4-5 hours the lysates were prepared using tween lysis buffer as previously described in STAT1 study, protein concentration was measured using BCA kit (Thermo Fisher), and the samples were heated for 5 min and 98°C with sample reducing Laemmli buffer (Sigma Aldrich). Proteins were separated on BOLT 4-12% BisTris plus gels (electrophoresis run for 70 min at 120 V in MES buffer, all from Thermo Fisher) and then transferred to nitrocellulose membranes (Bio-Rad, a tranfer run for 80 min at 110 V). Membranes were blocked in 7.5% low-fat bovine milk in PBS with 0.05% Tween 20 (Sigma Aldrich) at 2-8°C overnight, washed twice in PBS with 0.05% Tween 20 and incubated with primary antibodies anti-caspase-8 (clones D35G2 and 1C12), anti-cleaved caspase-8 (clone Asp391), anti-caspase-3 (clone 8G10), and anti-cleaved-caspase-3 (clone Asp175) (Cell Signaling Technologies) together with peroxidase-conjugated secondary antibodies (Jackson Immunoresearch). The SuperSignal West Pico and Femto Chemiluminescent Substrate (Thermo Fischer) was used for chemiluminiscent signal detection on MINI HD6 scanner (UVITEC, Cambridge, UK).

7.4.3. Apoptosis measured by flow cytometry

Patient's and controls' PBMCs were stimulated for proliferation as described in the above section. The cells were washed and stimulated w/wo 1 μg/ml anti-Fas antibody (Biolegend), 0.1 μg/ml GAM antibody (BD Biosciences) was used to crosslink anti-Fas.

After 24 hours the cells were washed in Annexin V binding buffer (Exbio) and stained with Annexin V-Dy647 and CD45-PO (Exbio), CD27-BV421 (Biolegend), CD45RA-FITC, CD4-PerCP-Cy5.5, and CD8-APC-H7 (BD Biosciences), and CD3-ECD and CCR7-PE (Miltenyi) for 30 min on ice in the dark. The cells were washed once in Annexin V Binding Buffer, measured on LSR II flow cytometer, and analyzed using FlowJo software. The gating

strategy is shown in the Results section. The Mann-Whitney U test was used to assess the significance of the difference between patient's and healthy controls' results. CD95-APC (Biolegend) antibody was used for 15 min at RT to check Fas expression before anti-Fas induction of apoptosis.

After 4 hours the cleaved caspase-3 was also detected using flow cytometry. The cells were fixed in 4% formaldehyde for 10 min in RT, washed in PBS (centrifugation step run 5 min, RT, 700 RCF), and permeabilized using 90% ice-cold methanol for 30 min on ice. After final wash in 0.5% BSA in PBS the cells were stained with antibody-conjugates cleaved-caspase-3-PB and cleaved PARP-PE (Cell Signaling Technologies), CD45-PO, CD3-APC, and CD8-APC-Cy7 (Exbio), CD45RA-FITC and CD4-PerCP-Cy5.5 (BD Biosciences), and CD27-PE-Cy7 (Beckman Coulter) for 30 min at RT in the dark. After final wash in PBS the cells were measured on LSR II flow cytometer and analyzed using FlowJo software. For caspase cleavage activation 5 μg/ml etoposide (Sigma Aldrich) was used instead of anti-Fas, for caspase cleavage inhibition 1 μg/ml pan-caspase inhibitor Z-VAD-FMK (RnD Systems) was used 30 min before anti-Fas.

7.4.4. Single-cell phospho-flow cytometry

Single-cell phospho-flow cytometry for detection of phosho-NFκB p65 (Ser536) was performed in patient's and healthy controls' PBMC. The cells were resuspended in complete RPMI 1640 medium (10% FBS included) in the concentration 1 million cells per 1 ml and stimulated using anti-CD3/CD28 coated beads (Thermo Fisher) according to manufacturer's instructions for 0, 5, 15, and 20 min. Intracellular signaling was stopped by fixing in 4% formaldehyde for 10 min at RT and thecells were permeabilized using 0.1% Triton X-100 for 15 min at 37°C. The cells were washed in 0.5% BSA in PBS and stained using antibody-conjugates anti-phospho-NFκB p65 (Ser536)-Alexa Fluor 647 (Cell Signaling Technologies), CD45-PO, CD8-PB, and CD45RA-FITC (Exbio), and CD3-APC-Cy7 and CD4-PerCP-Cy5.5 (BD Biosciences) for 30 min at RT in the dark. After final wash in PBS (5 min, RT, 700 RCF) the samples were acquired on LSR II flow cytometer and analyzed using FlowJo software.

7.4.5. Activation and proliferation

PBMC of the patient and healthy controls were stimulated with anti-CD3/CD28 beads w/wo 50 ng/ml IL-2 for 3 days to promote activation and proliferation of the cells. The cells were washed in PBS and stained with antibody-conjugates CD45RA-BV510, PD-1-BV605, CD69-PerCP-Cy5.5, and CCR7-APC (Biolegend), CD57-FITC and CD3-APC-H7 (BD Biosciences), CD4-ECD, CD19-PE-Cy7, and CD25-PB (Beckman Coulter), and CD8-Alexa

Fluor 700 (Exbio). After 15 min at RT in the dark, the cells were washed in PBS, fixed in BD FACS Lyse buffer, permeabilized in FACS Perm 2 buffer (both from BD Biosciences) according to manufacturer's instructions, and stained with Ki-67-PE (Exbio) for 30 min at RT. After final wash in PBS the samples were acquired on LSR II flow cytometer and analyzed using FlowJo software.

7.5. Results

7.5.1. Increased activated effector memory T-cells, decreased naïve T-cells, and decreased mature B-cells in the patient's peripheral blood

The immunophenotyping of peripheral blood lymphocytes was performed by CLIP-cytometry laboratory using EuroFlow PID tubes. When analyzing the PID tubes, we found increased and highly activated T-cells (CD8+ prevail over CD4+), with a differentiation shift from naïve to effector memory stages (Table 4). Moreover, we found all mature forms within B-cells to be decreased (Table 5). This was accompanied by low levels of serum IgM and IgA. Figures 20-22 depict the gating strategy of PID tubes as shown in patient's peripheral blood cells.

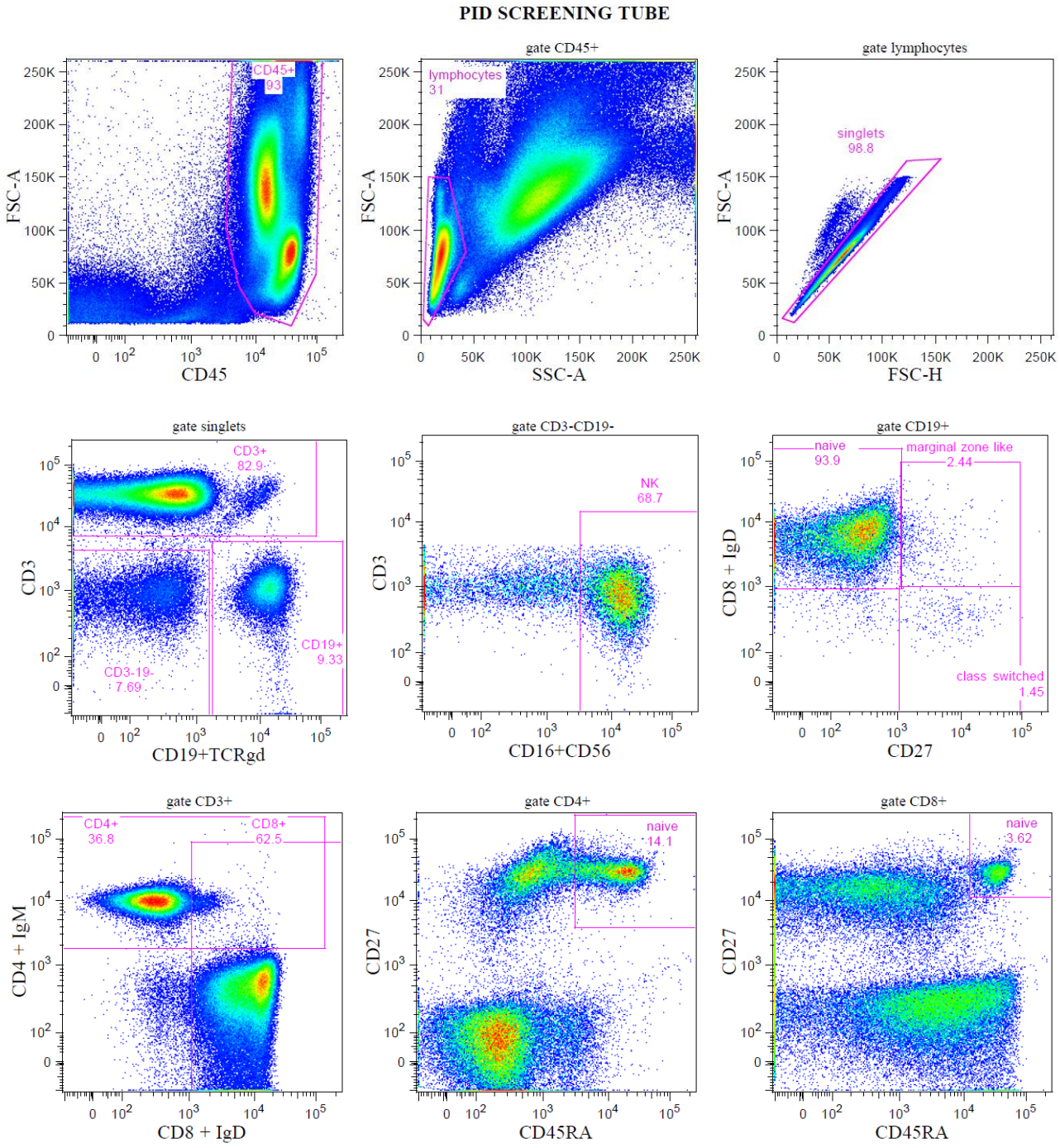

Fig. 20. PID Screening tube gating strategy. CD3+ T-cells (both CD3+4+ and CD3+8+ T-cells including naive CD45RA+CD27+ forms), CD19+ B-cells and CD16+CD56+ NK cells are shown in patient's peripheral blood.

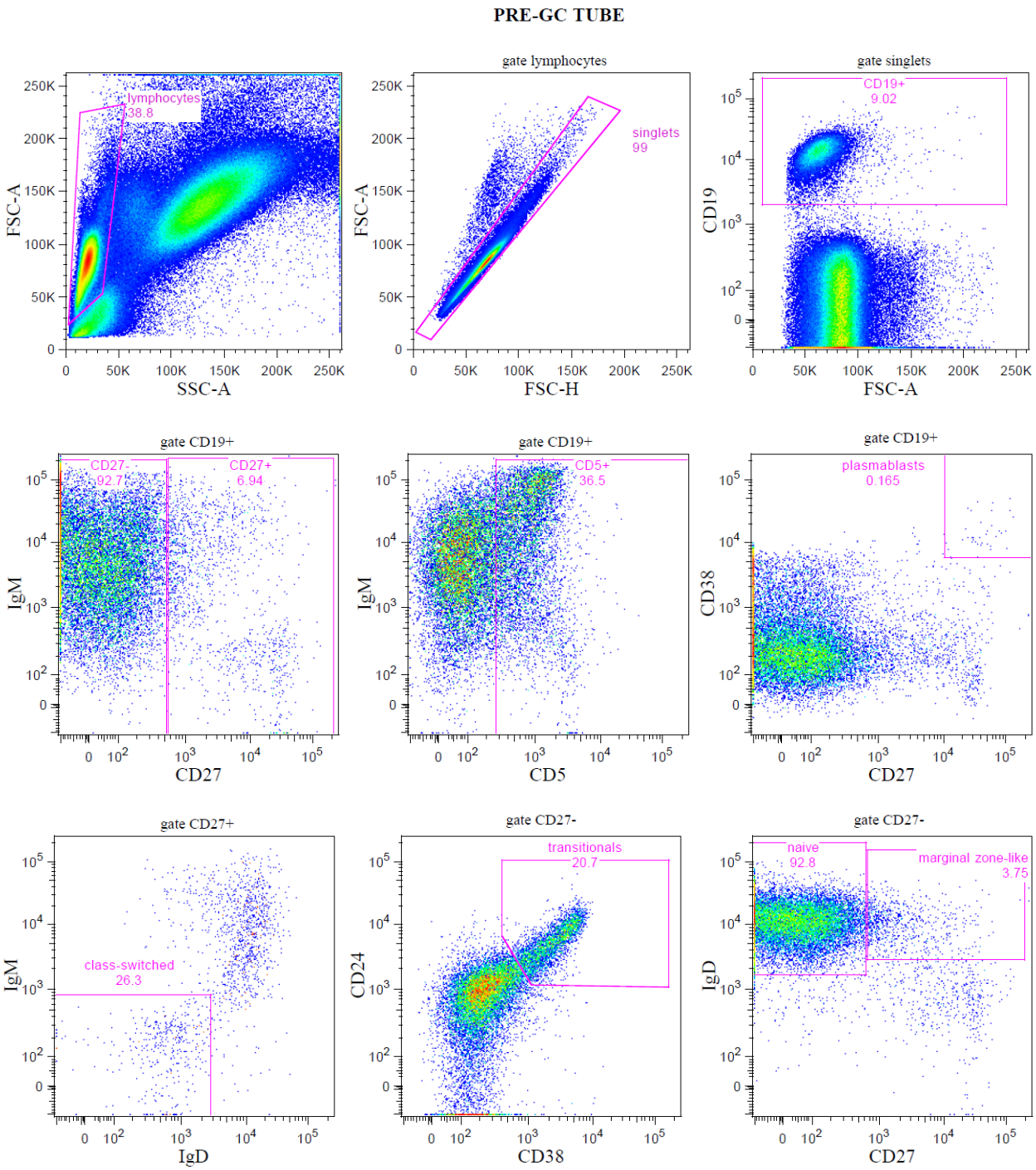

Fig. 21. Pre-GC tube. CD19+ B-cell subpopulations (IgD+CD27- naive, IgD+CD27-CD24++CD38++ transitional, IgD+CD27+ marginal zone-like, IgD-IgM-CD27+ class-switched, and CD27++CD38++ plasmablasts) are shown in patient's peripheral blood.

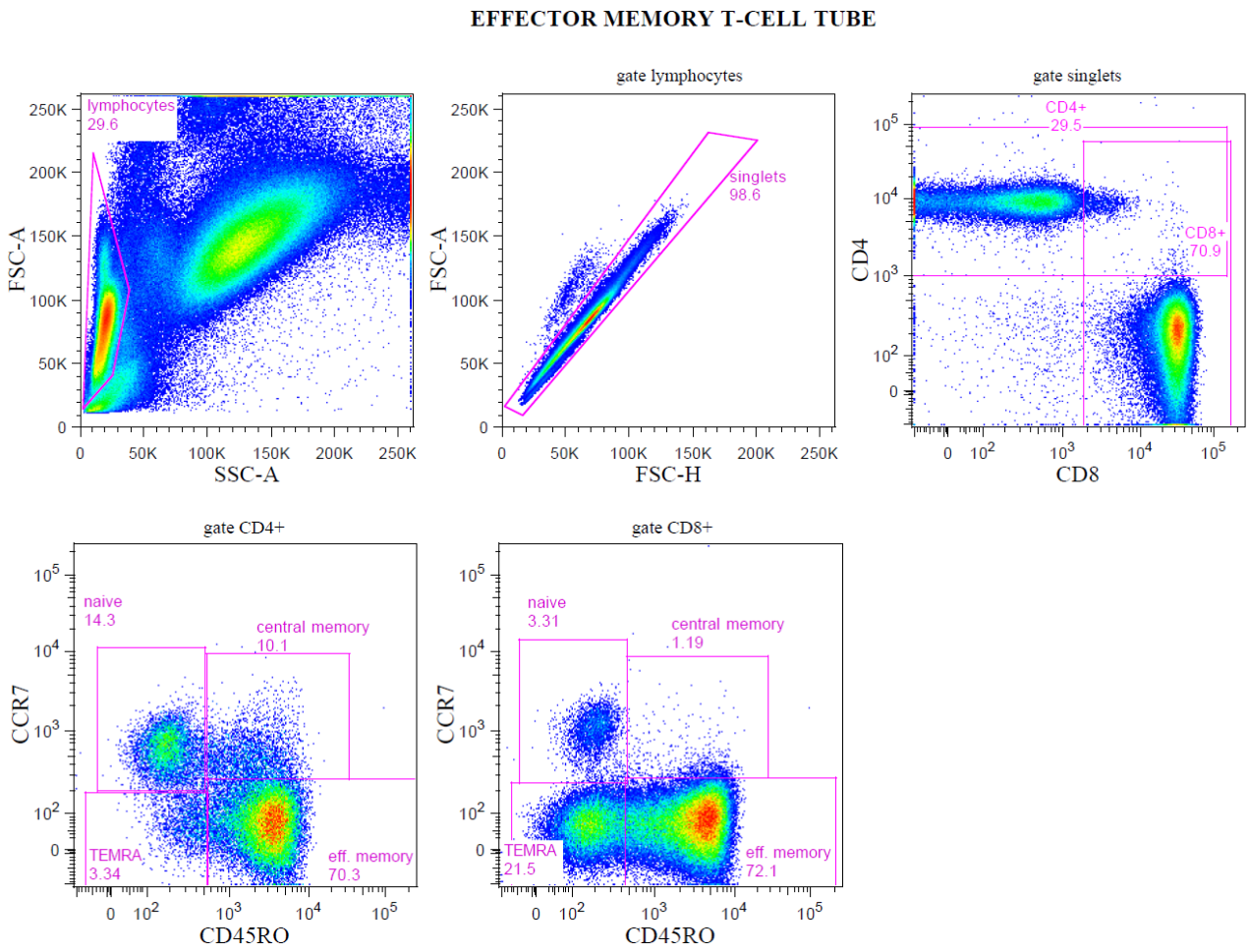

Fig. 22. Eff-Mem T-cells tube. CD3+ T-cell subpopulations (CCR7+CD45RO- naive, CCR7+CD45RO+ central memory, CCR7-CD45RO+ effector memory, and CCR7-CD45RO- terminally differentiated forms) and are shown in patient's peripheral blood.

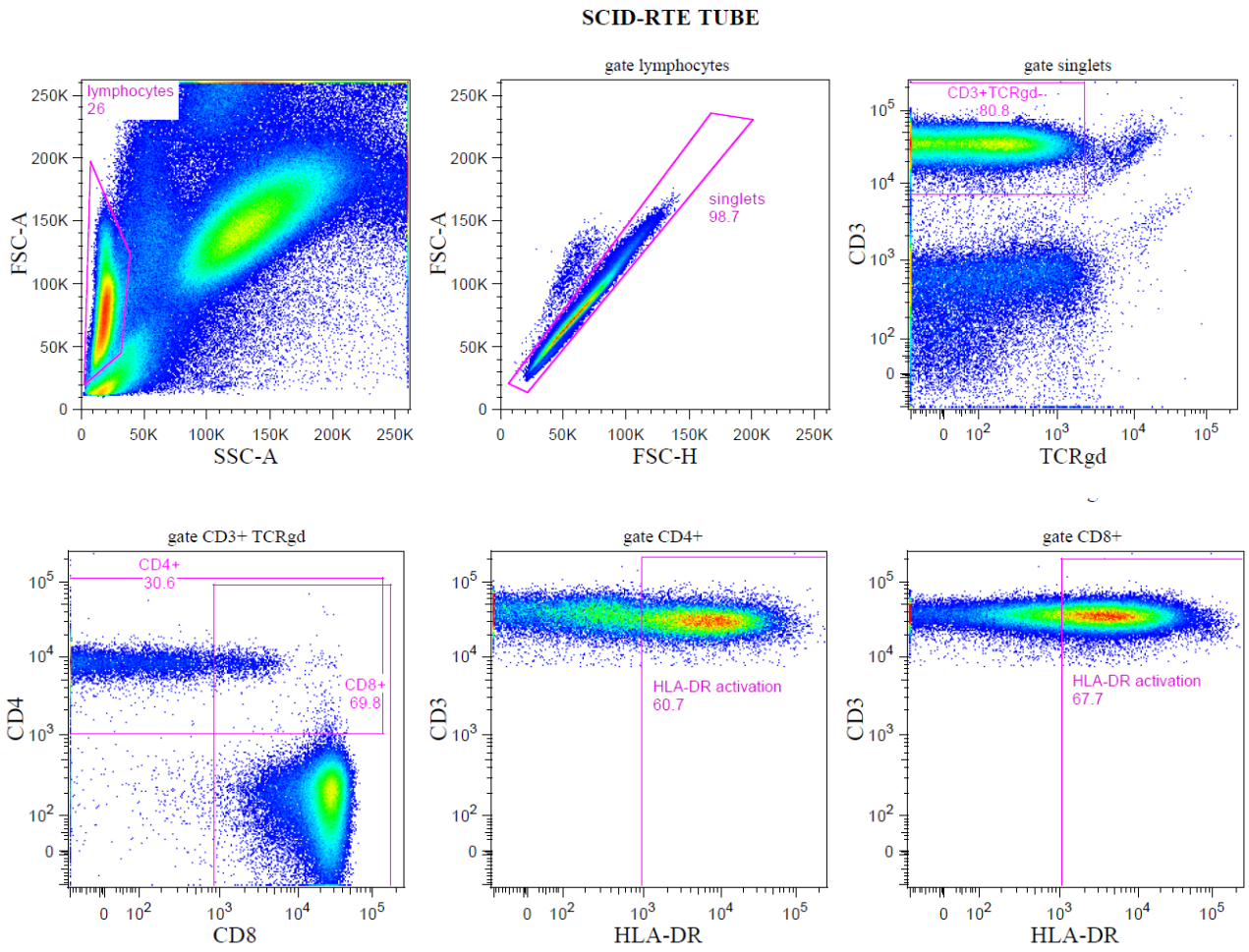

Fig. 23. SCID-RTE tube. CD3+ T-cell activation (HLA-DR+) is shown in patient's peripheral blood.

Table 4. T-cell subpopulations measured by PID panel. A light blue indicates decrease compared to reference values, red indicates increased subpopulations. Reference values were taken from Schatorjé et al., 2012 (*43*).

T-cell subpopulation	Patient	Reference value
naïve from CD4+	14 %	37-97 %
central memory from CD4+	10 %	13-76 %
effector memory from CD4+	70 %	0,5-25 %
naïve from CD8+	3,3 %	20-95 %
central memory from CD8+	1,2 %	0,4-18 %
effector memory from CD8+	72 %	4-100 %
term. differentiated from CD8+	22 %	9-65 %

Table 5. B-cell subpopulations measured by PID panel. A light blue indicates decrease compared to reference values, red indicates increased subpopulations. Reference values were taken from Piatosa et al., 2010 (*44*).

B-cell subpopulation	Patient	Reference value
Naive	93 %	51-82 %
Class-switched	1,8 %	9-26 %
Marginal zone-like	3,8 %	4,6-18 %
Plasmablasts	0,2 %	0,6-6,5 %

7.5.2. Impaired cleavage of caspase-8 and caspase-3 in the patient's cells

Using SDS-PAGE we found a decreased level of procaspase-8 in the patient's cells (Fig. 19, line 1). Moreover, we detected impaired Fas-induced cleavage of caspase-8 and its substrate caspase-3 compared to healthy controls (Fig. 24).

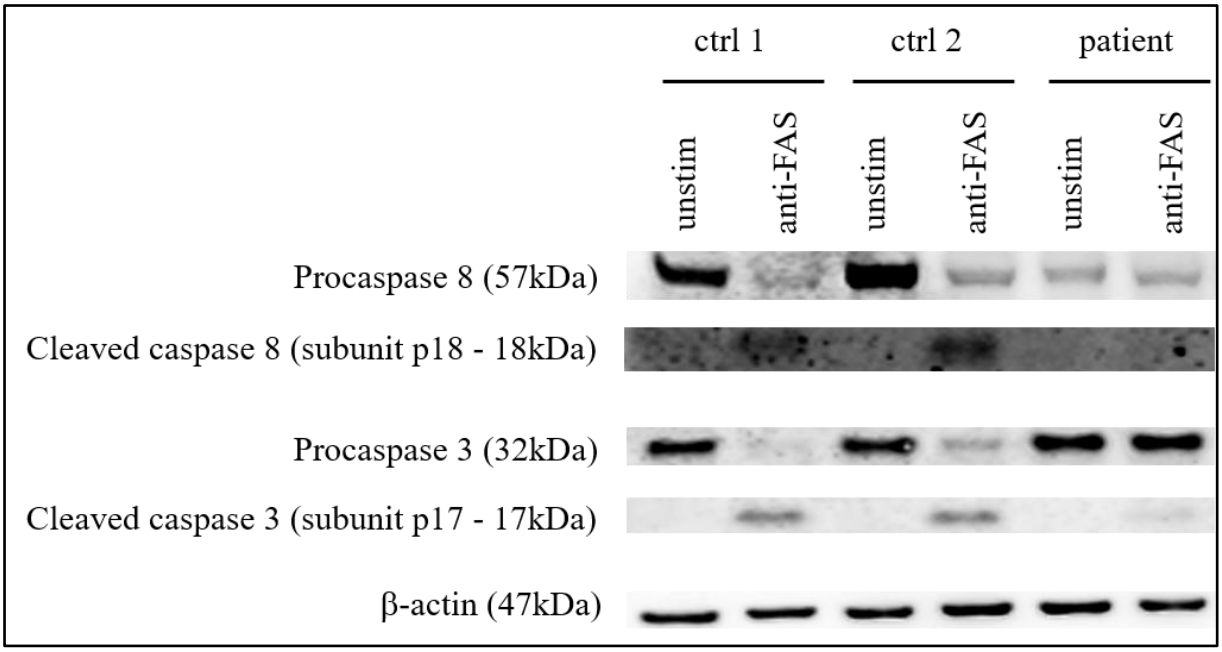

Fig. 24. Procaspases and cleaved caspases 8 and 3. Patient's PBMC presented with decreased level of procaspase-8 as well as decresed Fas-induced cleavage of both procaspase-8 and procaspase-3 compare to healthy controls (ctrl 1, 2). Unstim = 4 h without Fas-stimulation, anti-Fas = 4 h with anti-Fas antibody.

Before successful results from western blot were obtained, we planned to test the cleavage of caspases by flow cytometry. Unfortunately, we failed to find a suitable detection method and suitable fix-perm buffers. Using buffers which were recommended by manufacturer of anti-cleaved caspase antibodies (used antibodies are depicted in Table 6), we did not detect caspase-3 cleavage (Fig. 25).

Table 6. Antibody panel for the detection of cleaved caspase-3 (CASP3).

Fluorochrome	Pacific Blue	Pacific Orange	FITC	PE	PerCP -Cy5.5	PE -Cy7	APC	APC -Cy7
Epitope	cleaved CASP3	CD45	CD45RA	PARP	CD4	CD27	CD3	CD8

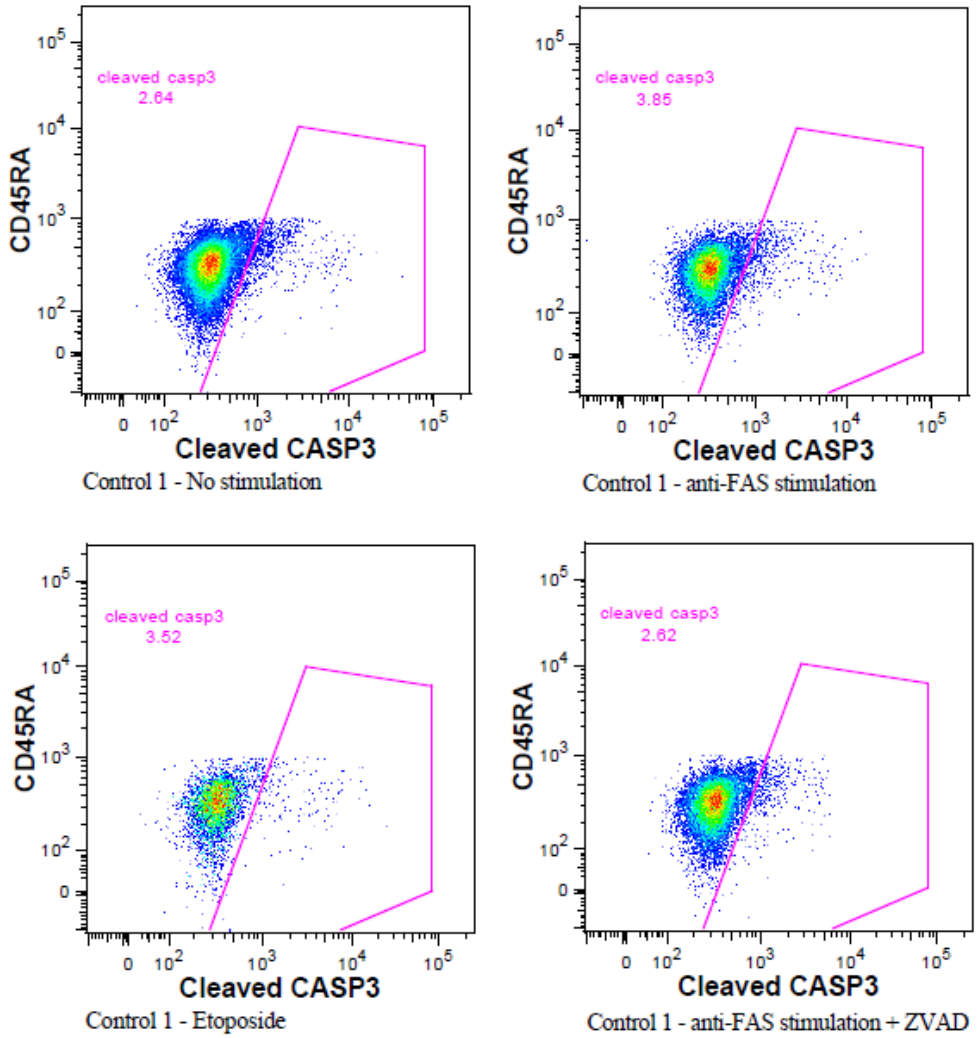

Fig. 25. Flow cytometric detection of cleavage of caspase-3 in a healthy control. Anti-Fas antibody and 5µg/ml etoposide were used to induce apoptosis, 1µg/ml pan-caspase inhibitor Z-VAD-FMK was used to inhibit apoptosis. X-axis indicates fluorescence intensity of cleaved-CASP3-Pacific Blue. Frequency of cells with cleaved CASP3 out of effector memory CD4+CD45RA-CD27-CCR7- T-cells 4 hours upon Fas stimulation is shown. Experiment was not repeated since we obtained clear results using western blot.

7.5.3. Impaired Fas-induced apoptosis in the patient's cells

To validate an impairment in caspase-8 cascade, proliferating PBMCs were stimulated via Fas and effector memory CD45RA-CD27-CCR7- T-cells were stained with Annexin V as described in Lo et al. in 2013. Annexin V binds to phosphatidylserine which appears on the outer layer of the plasma membrane during apoptosis (*112*). Used antibodies are shown in Table 7. The functional apoptotic assay was repeated three times and the final quantification proved impaired Fas-induced apoptosis in the patient's effector memory T-cells (both CD4+ and CD8+) compared to healthy controls (Fig. 26). Fas (CD95) expression on effector memory T-cells was verified before anti-Fas stimulation to avoid false negative results (Fig. 27). In contrast to anti-Fas, etoposide-induced apoptosis in the patient's cells was similar to healthy controls (Fig. 28).

Table 7. Antibody panel for flow cytometric detection of apoptosis.

Dye	**Pacific Orange**	**BV421**	**FITC**	**PE**	**ECD**	**PE-Cy5.5**	**Dy647**	**APC-H7**
Epitope	CD45	CD27	CD45RA	CCR7	CD3	CD4	Annexin V	CD8

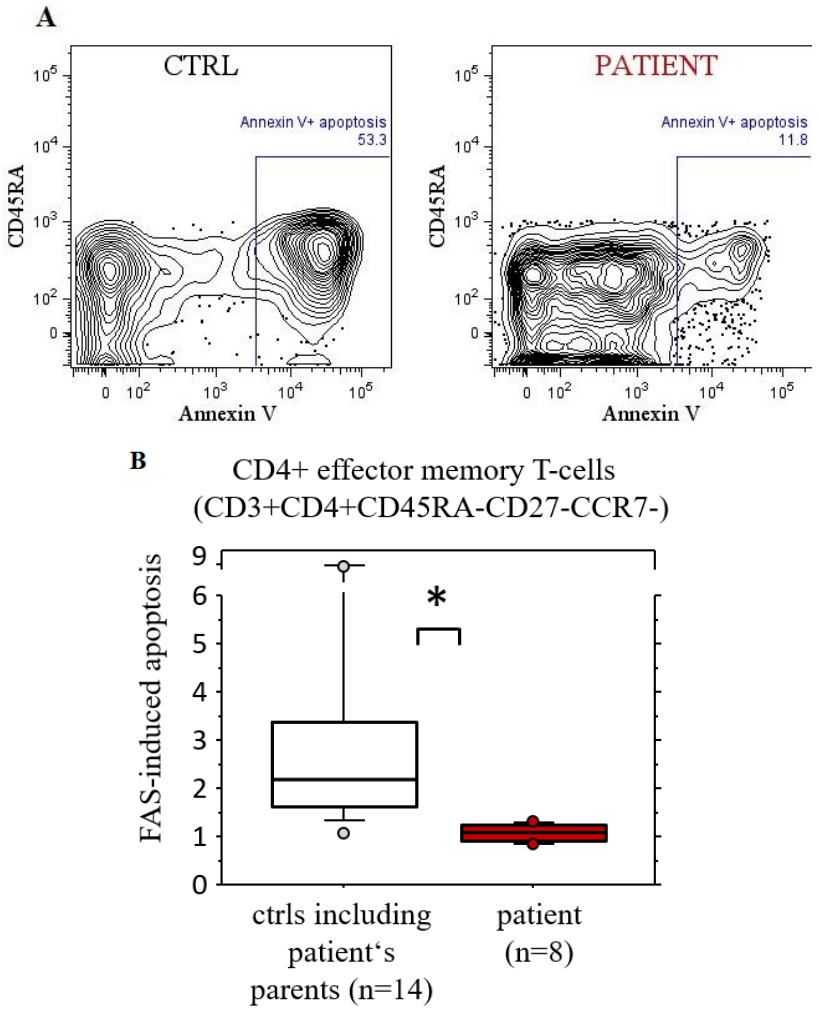

Fig. 26. Apoptosis induced via Fas in CD4+ effector memory T-cells. (A) Contour plots show Annexin V positivity on patient's and healthy controls' effector memory CD4+ T-cells 24 h after anti-Fas stimulation. X-axis indicates fluorescence intensity of Annexin V-Dy647. (B) Patient's effector memory CD4+ T-cells presented with decreased Fas-induced apoptosis compared to healthy controls. Data were obtained from 3 independent experiments, *$p<0.05$ Mann-Whitney U test. Y-axis shows ratio of Annexin V positivity on effector memory CD4+ T-cells with and without anti-Fas stimulation.

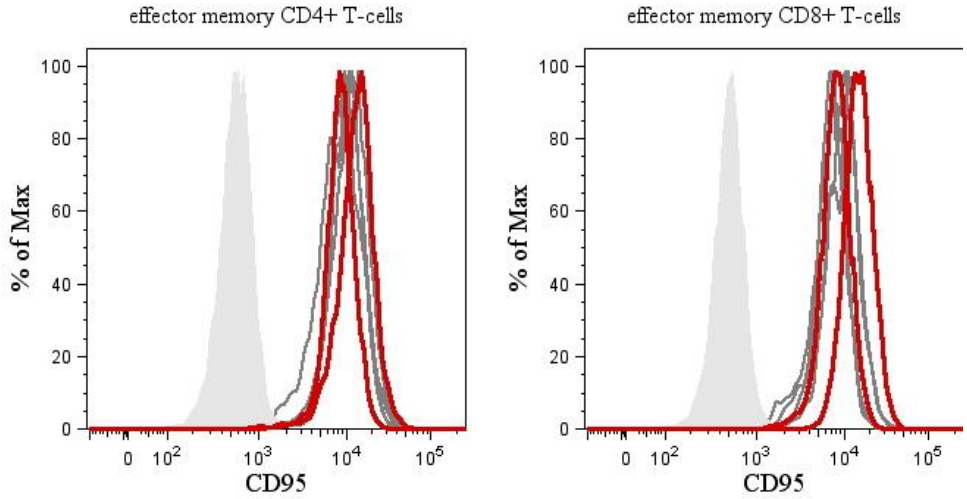

Fig. 27. Expression of Fas (CD95) on CD4+ and CD8+ effector memory T-cells. Patient's cells (red) demonstrated similar expression of Fas as healthy controls (grey) before anti-Fas stimulation. Non-proliferating T-cells are shown in tinted grey. X-axis indicates fluorescence intensity of CD95-APC.

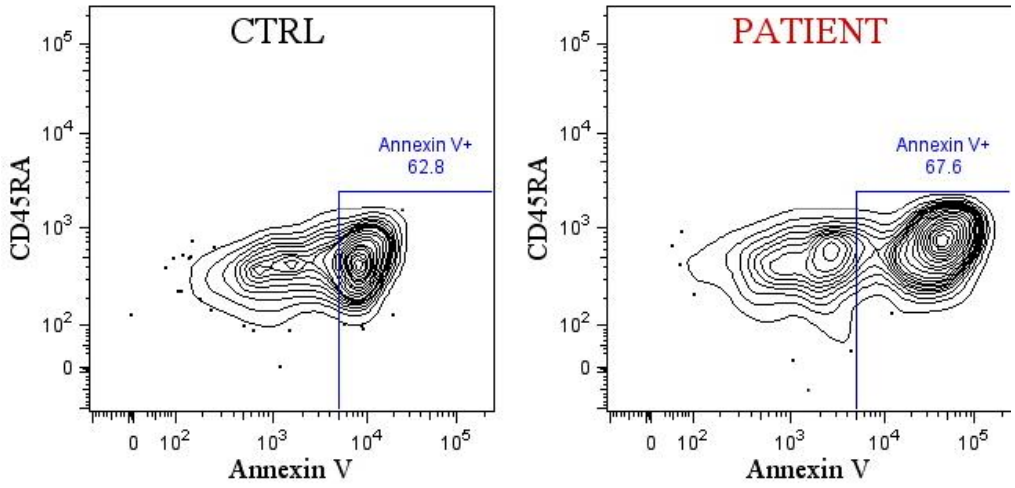

Fig. 28. Apoptosis induced by etoposide measured at the single-cell level using flow cytometry. Patient's effector memory CD4+ T-cells (right) presented with unchanged etoposide-induced apoptosis in comparison to healthy control (left). X-axis indicates fluorescence intensity of Annexin V-Dy647, Y-axis shows negativity of CD45RA.

7.5.4. Impaired non-apoptotic NFκB signaling in the patient's cells

Caspase-8 has been described to be involved in non-apoptotic signaling pathways downstream of TCR or TLRs (*102*). That's why we also tested TCR-mediated signaling in the patient's cells. Upon TCR stimulation, activation of NFκB (measured as phosphorylation of p65 subunit on Ser536) was lowered in the patient's cells compare to healthy control (Fig. 29, 30). To confirm, that decreased NFκB activation is not caused by exhaustion of effector memory compartment, only naïve T-cells were analyzed and similar profile of decreased NFκB activation was obtained (Fig. 31).

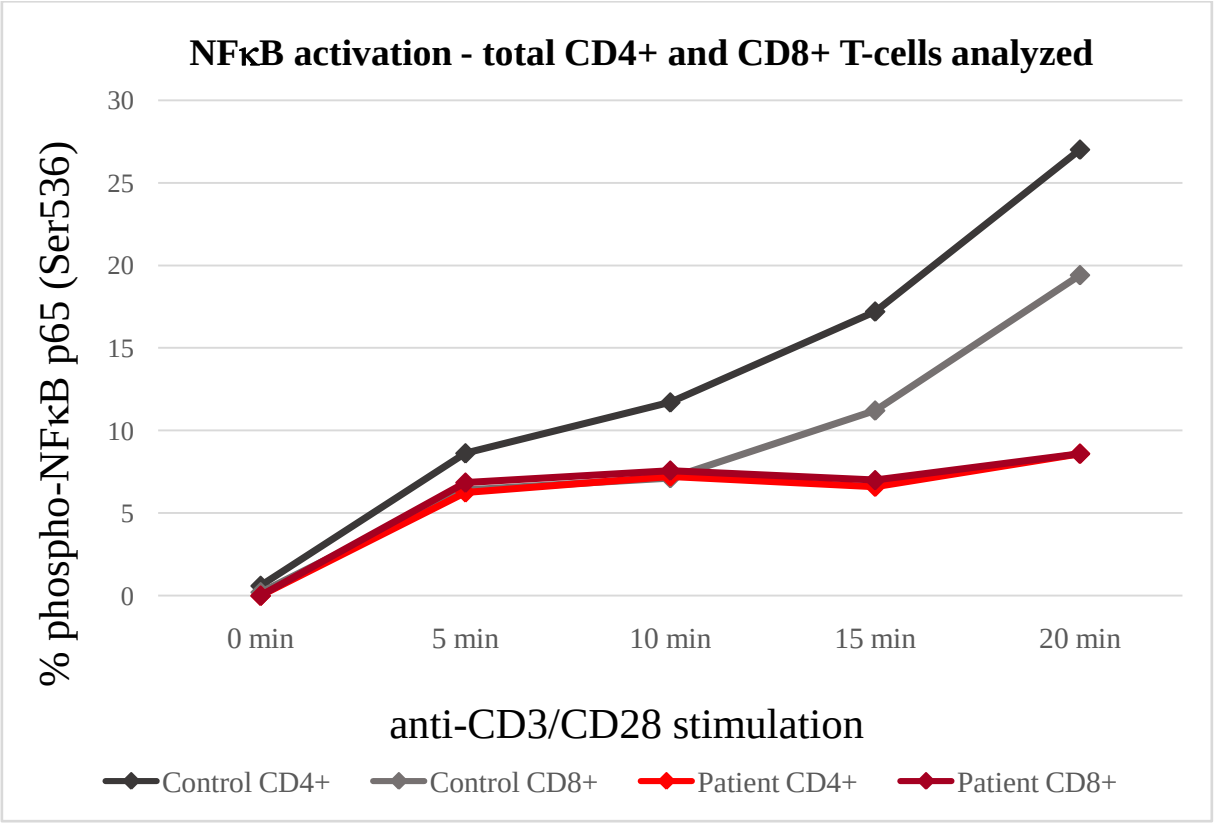

Fig. 29. TCR-induced NFκB activation in total T-cells. Patient's T-cells (both CD4+, light red; and CD8+, dark red) showed decreased NFκB activation compare to healthy control (grey). X-axis shows timepoints of anti-TCR stimulation, Y-axis shows frequency of phospho-NFκB p65 (Ser536) from total CD4+ and CD8+ T-cells.

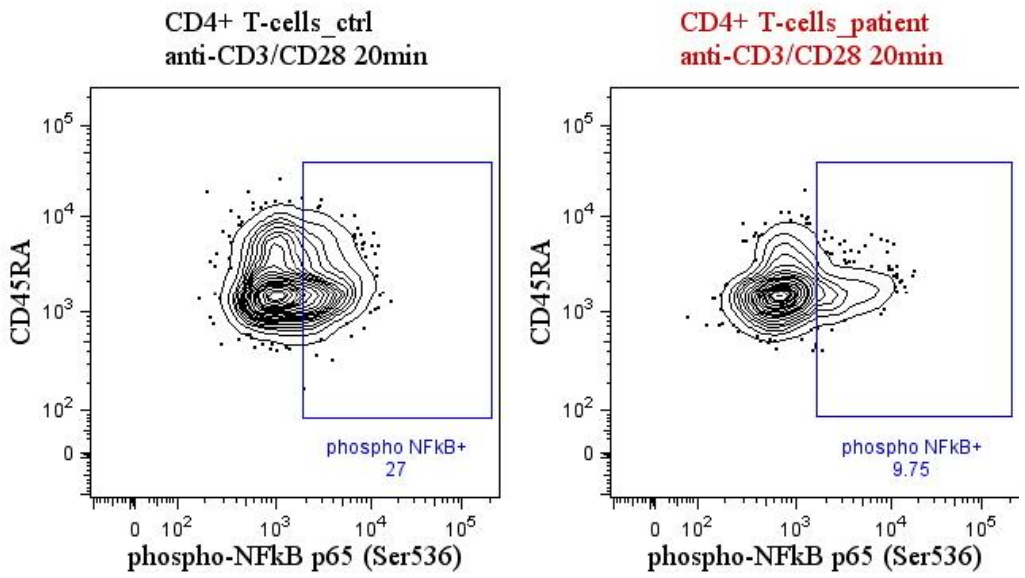

Fig. 30. Frequency of T-cells with activated (phosphorylated) NFκB molecule. Contour plots show timepoint 20 min upon TCR-stimulation in control's and patient's CD4+ T-cells as shown above in Fig. 29. X-axis indicates fluorescence intesity of phospho-NFκB p65 (Ser536) Alexa Fluor 647.

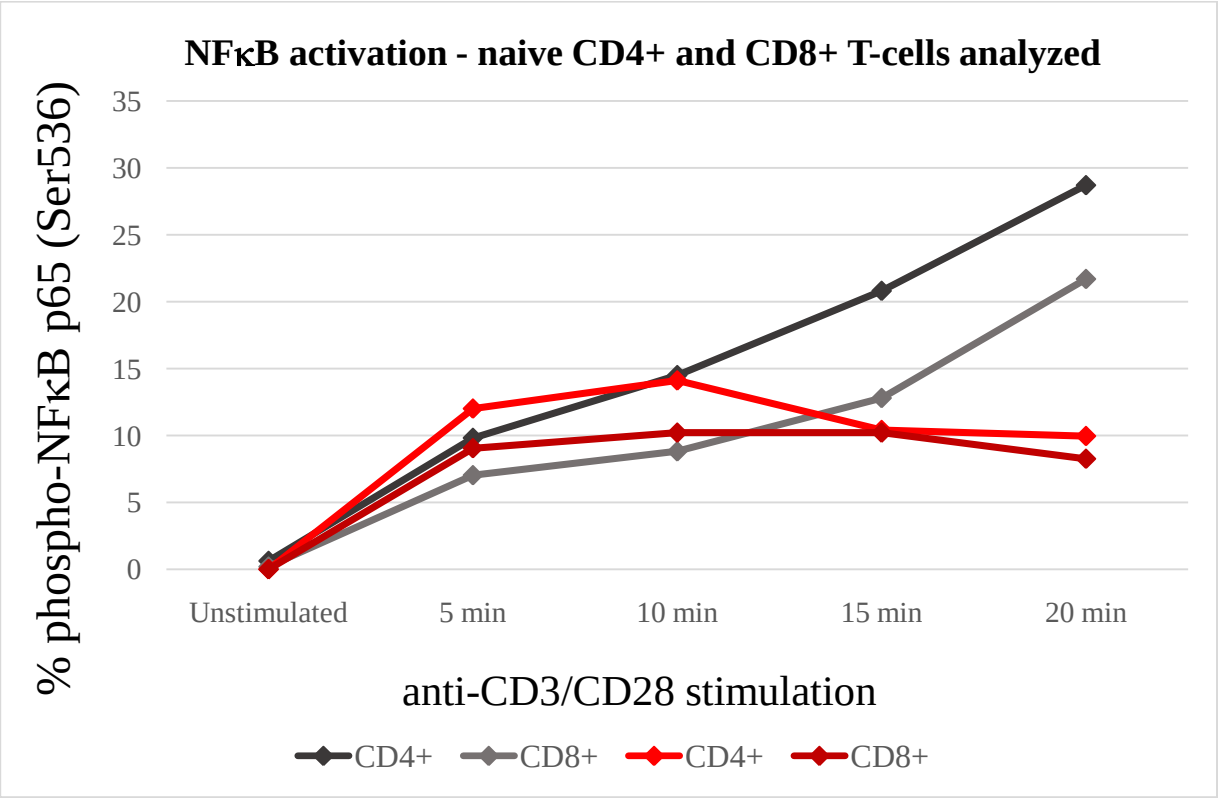

Fig. 31. TCR-induced NFκB activation in naïve CD45RA+ T-cells. Patient's naïve T-cells (both CD4+, light red; and CD8+, dark red) showed decreased NFκB activation compare to healthy control (grey). X-axis shows timepoints of anti-TCR stimulation, y-axis shows frequency of phospho-NFκB p65 (Ser536) from naïve CD4+ and CD8+ T-cells.

7.5.5. Decreased activation and proliferation of the patient's cells

NFkB signaling can lead to cellular proliferation (*113*). We thus tested activation (CD25 and CD69) and proliferation (Ki-67) markers upon TCR-stimulation. The cells were stained using antibody panel shown in Table 8. We revealed decreased activation and proliferation of the patient's cells compared to healthy controls (Fig. 32).

Table 8. Antibody panel for detection of activation and proliferation.

Fluorochrome	**Pacific Blue**	**BV510**	**BV605**	**FITC**	**PE**	**ECD**	**PerCP -Cy5.5**	**PE-Cy7**	**APC**	**Alexa Fluor 700**	**APC -H7**
Epitope	CD25	CD45RA	PD-1	CD57	Ki-67	CD4	CD69	CD19	CCR7	CD8	CD3

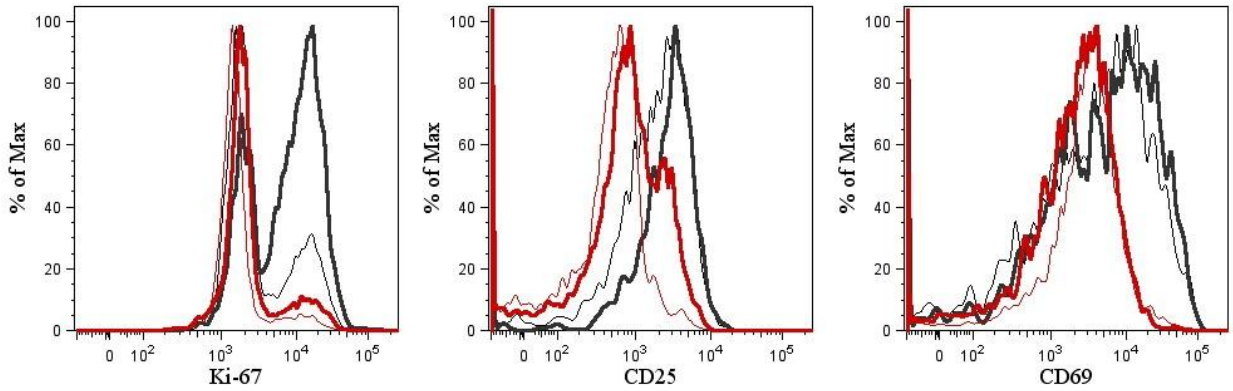

Fig. 32. Proliferation (Ki-67) and activation markers (CD25, CD69) measured 3 days upon TCR-stimulation. Patient's T-cells (red) presented with decreased Ki-67, CD25, and CD69 compared to healthy control's T-cells (grey). IL-2 addition (bold lines) only slightly rescued Ki-67 and CD25 in the patient's cells. X-axes indicates fluorescence intensity of Ki-67-PE, CD25-Pacific Blue, and CD69-PerCP-Cy5.5. The result is representative of three independent tests, CD8+ T-cells are shown.

7.6. Discussion

Here we report a male patient, currently 15-years-old, who carries a homozygous mutation in *CASP8* gene, c.1232C>T, p.P411L. The patient suffers mainly with lymphadenopathy and severe respiratory infections.

When we analyzed immunophenotype of his peripheral blood lymphocytes we found skewed pattern in both T-cells and B-cells. T-cells were activated according to HLA-DR and presented with a differentiation shift toward effector memory cells. Naïve T-cells were decreased. In B-cells, naïve cell prevailed and mature forms (both marginal zone-like, class-switched cells, and plasmablasts) were severely decreased. This was accompanied by low immunoglobulins found in the serum which could explain higher susceptibility to infections.

Caspase-8 has been described as one of the initial molecules of the apoptotic cascade (*114*). Thus, we tested if the discovered mutation affected its apoptotic function. Using a western blot, we observed that patient's procaspase-8 was not cleaved upon Fas-stimulation leading to decreased cleavage of its substrate, caspase-3. Moreover Fas-induced apoptosis tested at the cellular level using flow cytometry was also impaired. Based on the data we suggest that the patient's lymphadenopathy could be caused by Fas-induced apoptosis failure which did not allow to remove effector T-cells from circulation. Indeed, circulating T-cells count was elevated in the patient's peripheral blood.

Interestingly, caspase-8 has been also found in signalosomes downstream of TCR, transmitting the signal to NFκB which subsequently leads to cellular activation and proliferation

(*32*, *113*, *115*). We used flow cytometry to detect mutated CASP8 involvement in these non-apoptotic processes. We found impairment in both NFκB signaling, and activation and proliferation of the patient's cells upon TCR stimulation. To avoid misinterpretation of NFκB signaling results, we analyzed naïve T-cells only because effector memory cells, which were elevated in patient's peripheral blood, may be exhausted and unresponsive (*116*, *117*). NFκB activation was impaired also in naïve T-cell fraction indicating that mutated caspase-8 did not signal properly in the patient's cells.

To date, only four patients with loss-of-function *CASP8* mutation have been described in the literature. In these cases, a mutation was found in p18 subunit of procaspase-8 in position p.R265W (*105*, *106*). Although our mutation was positioned in a linker connecting p18 and p10 subunits of procaspase-8 (*118*), we found similar expression, activation, and functional patterns as those described in the p.R265W mutation.

Interestingly, caspase-8 deficiency in mice was lethal (*107*). When it was restricted only to T-cells, mice survived but had severe symptoms of increased necroptosis and lymphoproliferative disorder (*107*, *119*). We suspect that there may be a residual caspase-8 function which could explain survival and less severe symptoms of described human patients. Moreover, a compensatory role of caspase-10 in caspase-8 deficiencies in human needs to be also addressed (*108*, *119*, *120*).

7.7. Conclusion

To conclude, our data highlighted the dual role of caspase-8 in both apoptosis and non-apoptotic signaling and confirmed a loss-of-function property of the novel *CASP8* mutation, p.P411L. Data presented in my diploma thesis have been included into manuscript "Lymphoproliferation, immunodeficiency and IBD associated with a novel CASP8 mutation" (authors Veronika Kanderova, Hana Grombirikova, Irena Zentsova, Kamila Reblova, Adam Klocperk, Martina Fejtkova, Barbora Ravcukova, Tomas Kalina, Tomas Freiberger, and Anna Sediva) which was submitted to the Journal of Clinical Investigation.

8. Patient no. 3 with heterozygous HCK mutation

8.1. Abstract

Patient no. 3 is a 14-year-old girl suffering with severe lung fibrosis and vasculitis, in whom a novel mutation in hematopoietic cell kinase (*HCK*) was identified using MPS at the

Department of Biology and Medical Genetics in University Hospital Motol. Gene defect was defined as c.1545 C>A p.Tyr515* and it introduced a premature stop codon on C-terminus of *HCK*. The presence of both wild-type and mutated (shortened) HCK protein in the patient's cells was lately confirmed by mass spectrometry in the Protein Structure Characterization by Advanced Mass Spectrometry laboratory in BIOCEV. Similar mutation has not been described in human yet, the closest reference is a mouse model, in which analogous symptoms (pulmonary infiltration and lung fibrosis) were observed (*121*). Using the patient's cells and cell lines with stable expression of mutated HCK we proved activation character of the novel mutation. Mutated HCK was hyperphosphorylated and the cells bearing this mutation presented with higher basal activation, enhanced expression of adhesion molecule and increased production of IL-1β and TNFα cytokines. Prepared cell lines will serve for further testing.

8.2. Introduction to HCK topic

8.2.1. *HCK* gene position

HCK, hematopoietic cell kinase, belongs to Src-kinase family along with e.g. Blk (B-cells), Fgr (B-cells and myeloid cells), Lck (T-cells, NK cells), or Lyn (B-cells, myeloid cells and brain) (*122*). It is localized on chromosome 20 in position is 20q11.21 (Fig. 33). *HCK* has several isoforms with alternative splicing (GeneCards).

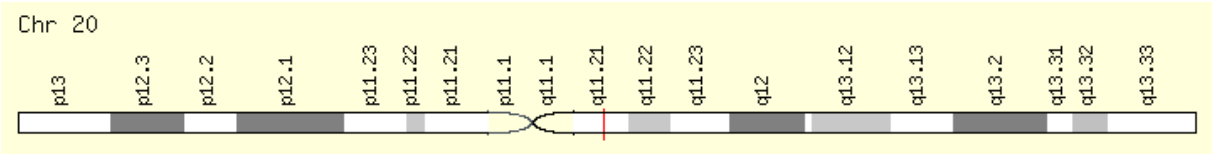

Fig. 33. Position of *HCK* gene. HCK (red) is localized on chromosome 20 in position 11.21. (GeneCards; *genecards.org/cgi-bin/carddisp.pl?gene=HCK*).

8.2.2. Src family protein structure

Src kinases generally consist of three Src homology (SH) domains. Each domain plays a unique role in Src activation/inactivation and in Src-mediated signaling (Fig. 34). N-terminal part of Src kinase is embedded in the plasma membrane, it adjoins the core SH3 domain (pink), connected to SH2 domain (green) which is linked to SH1 catalytic domain (yellow) and C-terminal tail carrying important inhibitory Tyrosine (Y_T). In an active conformation (right) inhibitory Tyrosine (Y_T) in C-terminal tail is dephosphorylated while the activating Tyrosine

(Y_A) on SH1 catalytic domain is phosphorylated. When inactivated (left), the inhibitory Tyrosine (Y_T) in C-terminal tail is phosphorylated and binds to SH2 domain (*123*, *124*).

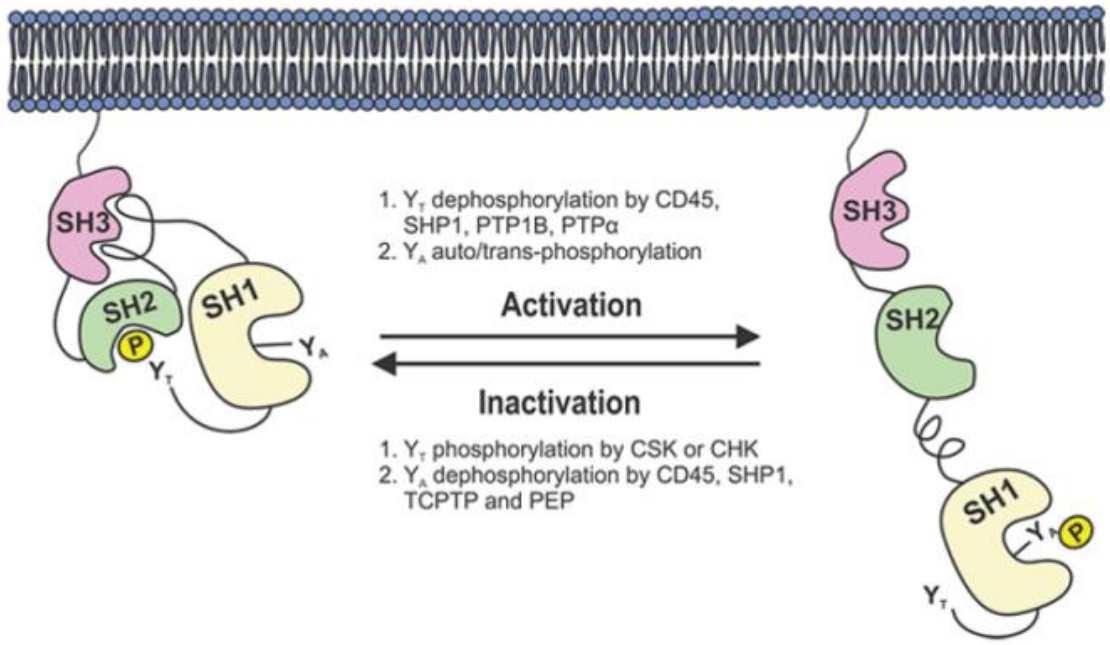

Fig. 34. Src kinase scheme. Inactive (left) and active (right) form of the kinase is shown. SH - Src homology domain (*123*).

8.2.3. HCK protein scheme and a position of a novel mutation

HCK is expressed mainly in hematopoetic system, especially in myeloid lineage and in B-lymphocytes (*125*). It has two major isoforms, p61 and p59 (Fig. 35). p61 HCK associates mainly with lysosomes and p59 HCK associates maily with plasma membrane (*126*). A novel p.Tyr515* mutation was found in C-terminal tail (red arrow) where it introduced a premature stop codon. We hypothesized that a mutated protein, in case of productive translation, lacks 12 amino acids in C-terminal tail including inhibitory Tyrosine (Y_T). This means that a mutated protein could not be inactivated.

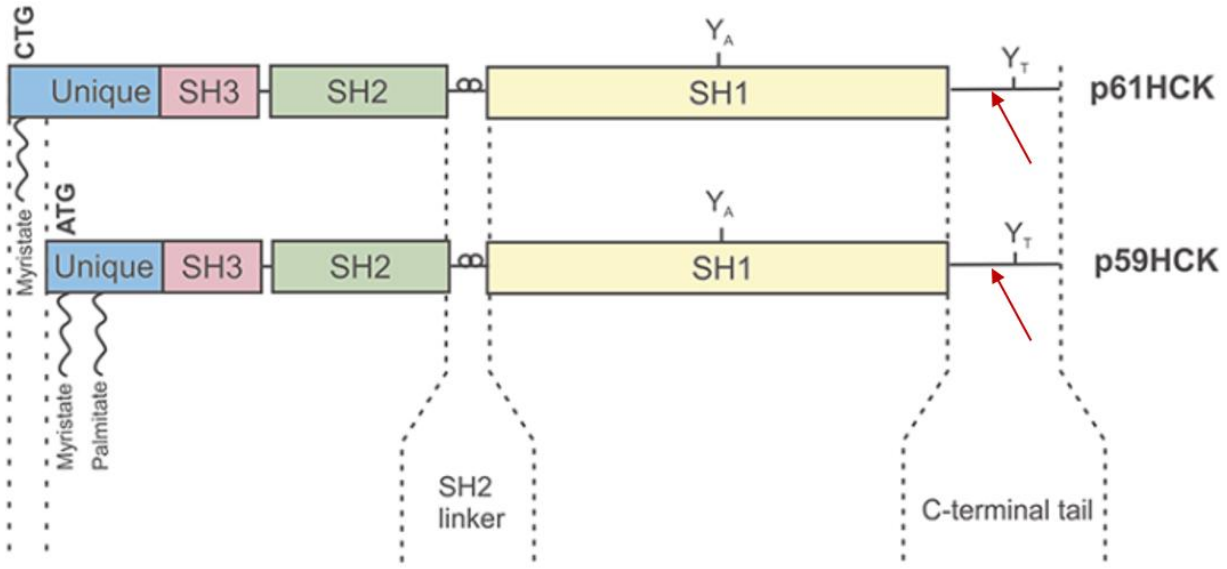

Fig. 35. HCK protein scheme and a position of a novel p.Tyr515* mutation.

N-terminal part of HCK possesses a lipid modification. It is followed by SH3, SH2 and SH1 domain and C-terminal tail. A novel mutation is indicated by red arrow. Y_T - inhibitory Tyrosine, Y_A - activation Tyrosine. (Adapted from Poh et al., 2015 (*123*)).

8.2.4. Src- and HCK-mediated signaling

Src kinases serve as important molecules in several intracellular signaling pathways mediated by cytokine receptors, G protein-coupled receptors (GPCR), or adhesion molecules leading to cell cycle progression or adhesion (Fig. 36) (*127*).

HCK specifically mediates signaling to promote myeloid cell adhesion and migration, proliferation and survival, or inflammatory cytokine production. Membrane-associated activators of HCK include e.g. β2-integrins, CD66 molecules, cytokine and chemokine receptors, Fc-receptors, or TLR4 (*123*). β2-integrins play a key role in myeloid cell adhesion. HCK (along with other Src kinase FGR) were found to be involved in the outside-in β2-integrin signaling to prolong adhesion (*128*). CD66 molecules, surface markers of granulocytes, transmit the signals via HCK to increase cellular adhesion and to promote superoxide production (*129*, *130*). In monocyte and macrophages, HCK activates adaptor protein paxillin to induce podosome formation, it is also important in extracellular matrix proteolysis during transendotelial migration (*131*). Upon TLR4 activation, HCK helps to produce TNFα and IL-6 proinflammatory cytokines (*132*). Downstream of Fc-receptors, HCK influences phagocytosis and respiratory burst of macrophages and neutrophils (*133*).

HCK is also hyperexpressed in various types of leukemia (CML and B-ALL) where it contributes to leukemogenesis through its association with BCR-ABL fusion kinase to enhance cell survival (*134*, *135*).

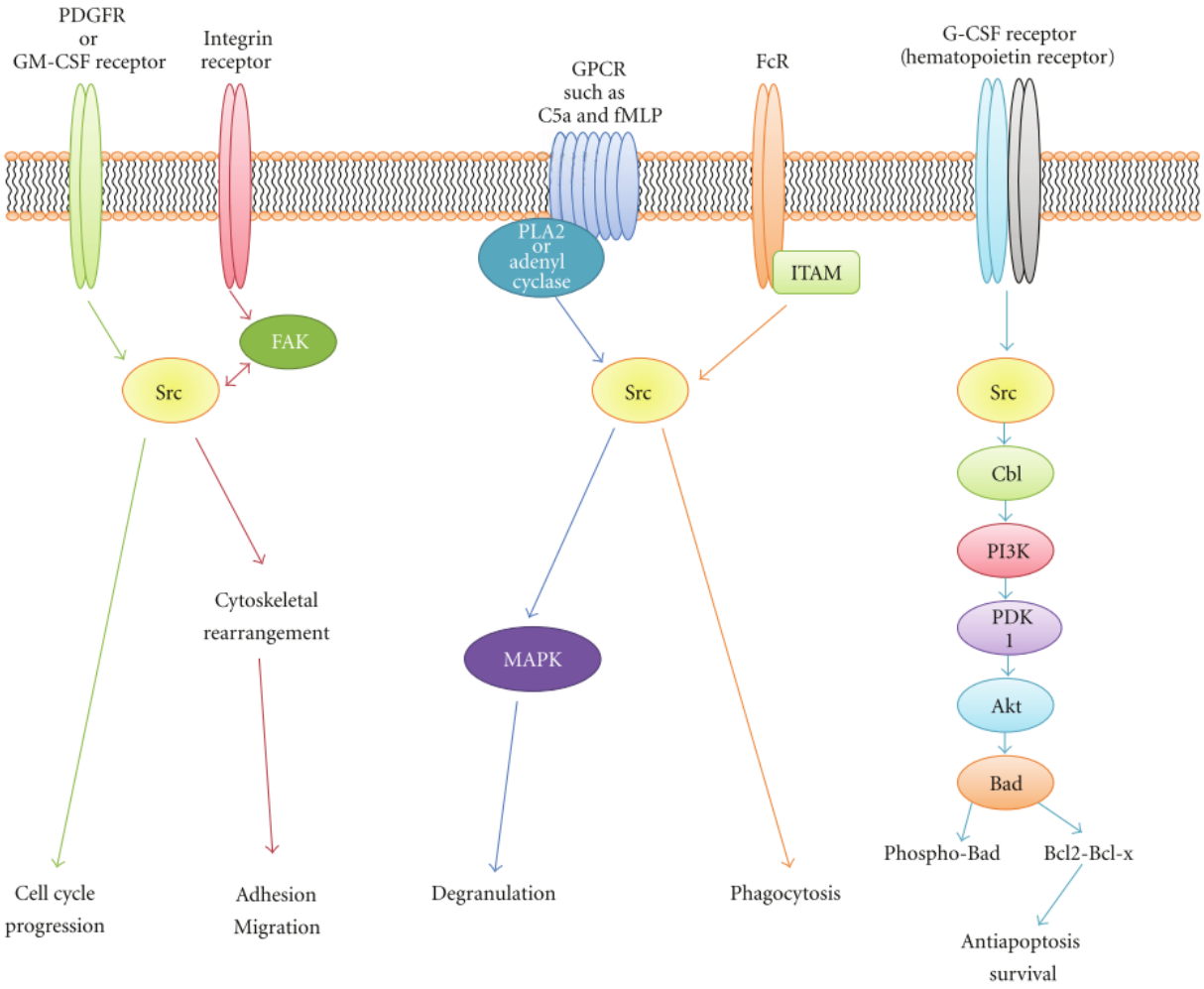

Fig. 36. Src kinases are involved in several signaling pathways in immune response (*127*).

8.2.5. HCK as a target for biological treatment

Src kinases were also found to be involved in cancer progression and transformation so they are tested as targets for biological treatment. Small molecular inhibitors (e.g. dasatinib or bosutinib) which were primarily developed for BCR-ABL fusion kinase inhibition in myeloid leukemias (*136*), are able to inhibit both BCR-ABL and Src-kinase activity (*137*). Bosutinib succesfully inhibited tumor growth in biliary tract cancer cell lines (*138*). Dasatinib was reported as succesfull inhibitor in glioblastoma (*139*) and glioma (*140*).

8.2.6. Reported HCK gain-of-function mutation

In 2002, a team of Matthias Ernst developed knock-in mice ($HCK^{F/F}$), in which an inhibitory Tyrosine 499 was substituted with Phenylalanine in C-terminal tail of the protein. This mutation was similar to the mutation identified in our patient. Clinical presentation of the mice (pulmonary infiltration with mononucler hematopoietic cells and lung fibrosis) also resembled that of our patient. The authors found an increased migration of HCK-mutated cells together with enhanced production of inflammatory cytokines, especially TNFα. When LPS was instilled intranasally a rapid neutrophilic inflammatory response, followed by macrophage invasion into the alveolar spaces of the lungs was seen in the mice (*121*).

8.3. Material and methods

8.3.1. Immunoprecipitation

The lysates were prepared from patient's and controls' peripheral blood cells using tween lysis buffer as previously described in *STAT1* and *CASP8* studies and the protein concentration was adjusted to final concentration 1 mg/ml using BCA kit (Thermo Fisher). Subsequently, anti-HCK antibody (Cell Signaling Technologies) was added to cell lysates in final concentration 1μg/ml and the lysates were kept on carousell for 2 hours at 4°C. Next, G-protein-coupled sepharose beads (GE Healthcare) were added and the samples were incubated on carousell at 4°C overnight. The samples were washed three times in PBS with 0.05% Tween 20 (each centrifugation step run 3 min at 4°C and 1000g). After final wash, supernatants were discarded and the pellets were heated for 5 min at 98°C with sample reducing Laemmli buffer (Sigma Aldrich). Finally, the samples were centrifuged for 5 min at 4°C and 14 000 g and the supernatants were loaded to BOLT 4-12% BisTris plus gels (electrophoresis run for 70 min at 120 V in MOPS buffer, all from Thermo Fisher).

8.3.2. Coomassie Brilliant Blue R-250 staining

The gels were prefixed in solution containing 50 % methanol, 10 % acetic acid (both from Sigma Aldrich), and 40 % distilled water for 30 min at RT and stained in the above solution supplemented with 0.25 % Coomassie Blue R-250 (Thermo Fisher) for 4 hours at RT until the gel was a uniform blue color. Destaining was performed in 5 % methanol, 7.5 % acetic acid, and 87.5% distilled water for 24 hours until background was clear. Coomassie Blue R-250 stained gel was sent to "Protein Structure Characterization by Advanced Mass Spectrometry laboratory" in BIOCEV (RNDr. Petr Novák, Ph.D.) for further analysis.

8.3.3. Western blotting

HCK immunoprecipitates were also transferred to nitrocellulose membranes (Bio-Rad, a tranfer run for 80 min at on 110V). Membranes were blocked in 7.5% low-fat bovine milk in PBS with 0.05% Tween 20 (Sigma Aldrich) at 2-8°C overnight, washed twice in PBS with 0.05% Tween 20 and incubated with primary antibodies anti-HCK and anti-phospho-Src (Tyr416) (both from Cell Signaling Technologies) at 4°C overnight. Peroxidase-conjugated secondary antibodies (Jackson Immunoresearch) (45 min, RT) together with The SuperSignal West Femto Chemiluminescent Substrate (Thermo Fischer) were used for signal detection. Chemiluminiscent detection run on C-DiGit scanner and signal quantification was performed using Image Studio Digits (LI-COR).

8.3.4. Cell line cultivation

THP-1 and Mono-mac-6 cell lines were stably transfected with HCK (both wild-type HCK and mutated HCK) by lentiviral and retroviral vectors by Šimon Borna, MSc. in the "Laboratory of Leukocyte Signalling" in the Institute of Molecular Genetics of the ASCR. Afterwards, the cells were cultivated in RPMI 1640 medium supplemented with L-glutamine, HEPES, penicillin/streptomycin (Lonza), and 10 % heat-inactivated FBS (Thermo Fisher) in optimal concentration 2-5 million cells per 1 ml.

THP-1

THP-1 was purchased from German Collection of Microorganisms and Cell Cultures (DSMZ). It is monocytic suspension cell line derived from human acute monocytic leukemia. It has been used as a model in many leukemic and proteomic studies. THP-1 cells express Fc-receptors, can produce IL-1 and several other cytokines, possess a phagocytic function, and can be differentiated into dendritic cells (*141*). THP-1 cells are CD3-, CD4+, CD13+, CD15+, CD19-, CD34-, cytoplasmic CD68+, and HLA-DR+.

Mono-mac-6

Mono-mac-6 was also purchased from German Collection of Microorganisms and Cell Cultures (DSMZ). It is monocytic suspension cell line derived from human acute monocytic leukemia. It has been used in many immunological studies, for a protein interaction modeling, immunochemistry etc. (*142*). Mono-mac-6 is CD3-, CD4-, CD13+, CD14+, CD15+, CD19-, CD33+, CD34-, and cytoplasmic CD68+.

8.3.5. Adhesion molecules on peripheral blood monocytes

100μl of the whole blood of the patient and healthy controls was stained using antibodies against integrins (CD11b (activation epitope)-PE, CD11a-FITC, CD18-APC (clone MEM-48), CD18-APC (clone MEM-148), all from Exbio), and CD11b-PE and CD11c-PE (BD Biosciences), and against surface markers which define monocytes (CD45-BV510 (Biolegend) and CD14-PB (Exbio)) for 15 min at RT in the dark. Erythrocytes were lysed in the solution containing NH_4Cl (prepared by pharmacy of the University Hospital Motol) for 15 min at RT. After one wash in PBS (centrifugation 5 min, 700g, RT) the samples were measured on LSR II flow cytometer and analyzed using FlowJo software.

8.3.6. Adhesion molecules on the cell lines

100μl of THP-1 (both HCK-wild-type and HCK-mutated) suspension was stained using antibodies against integrins (CD11b (activation epitope)-PE, CD11a-APC, CD18-APC (clone MEM-48), CD18-APC (clone MEM-148), CD11b-PE, and CD11c-PE) and against CD14 marker (CD14-Alexa Fluor 700, Exbio) for 15 min at RT in the dark. After one wash in PBS (centrifugation 5 min, 700g, RT) the samples were measured on LSR II flow cytometer and analyzed using FlowJo software.

8.3.7. Western blotting of the cell lines

The lysates were prepared from cell lines as described above, protein concentration was measured using BCA kit (Thermo Fisher), and the samples were heated for 5 min at 98°C with sample reducing Laemmli buffer (Sigma Aldrich). Proteins were separated on BOLT 4-12% BisTris plus gels (electrophoresis run for 70 min at 120 V in MOPS buffer, all from Thermo Fisher) and then transferred to nitrocellulose membranes (Bio-Rad, a tranfer run for 80 min at on 110 V). Membranes were blocked in 7.5% low-fat bovine milk in PBS with 0.05% Tween 20 (Sigma Aldrich) at 2-8°C overnight, washed twice in PBS with 0.05% Tween 20, and incubated with primary antibodies anti-HCK and anti-phospho-Src (Tyr416, both from Cell Signaling Technologies) at 4°C overnight. Peroxidase-conjugated secondary antibodies (Jackson Immunoresearch) (45 min, RT) together with The SuperSignal West Femto Chemiluminescent Substrate (Thermo Fischer) were used for the signal detection. Chemiluminiscent detection run on MINI HD6 scanner (UVITEC) and the signal quantification was performed using Image Studio Digits (LI-COR).

8.3.8. Cytokine production

Stably transfected THP-1 and Mono-mac-6 cell lines were stimulated with i) 300μg/ml human IgG immunoglobulins (Jackson Immunoresearch) which were heated to 63°C for 30 min to obtain immune complexes (IC) and ii) 1μg/ml Lipopolysaccharide (LPS) for A) 24 hours, B) 6 hours followed by washing in the culture medium and further cultivation (without any stimulation) for additional 42 hours. Finally, the supernatants were harvested and the cytokines (IL-1β, IL-6 and TNFα) were measured using ELISA (RnD Systems)) according to manufacturer's instructions. Briefly, the samples (both our supernatants and standards provided) were incubated with anti-cytokine antibodies on 96-well plates for 2 hours at RT, three times washed using washing buffers, and incubated with conjugated antibodies against detected cytokines for 1-2 hours at RT. After three additional washes the substrates were added to each well and incubated 20 min at RT in the dark. Stop solution was finally added, the absorbance was measured at 450 nm within 30 minutes, and analyzed with VERSAmax Tunable Microplate Reader with appropriate SoftMaxPro software (Molecular Devices).

8.3.9. Fc-receptors on THP-1 and Mono-mac-6 cell lines

100μl of THP-1 and Mono-mac-6 (both HCK-wild-type and HCK-mutated) suspension was stained using antibodies against Fcγ-receptors (CD16-PE (FcγRIII); CD64-PE-Cy7 (FcγRI), and CD32-APC (FcγRII) for 15 min at RT in the dark. After one wash in PBS (5 min, 700g, RT) the samples were measured on LSR II flow cytometer and analyzed using FlowJo software.

8.4. Clinical case

The patient is currently a 14-year old girl who suffers from severe symptoms of leukocytic infiltration of lungs and skin manifested as pulmonary fibrosis and vasculitis. The symptoms occurred within few hours after birth and they have been progressing since. The patient is constantly on corticoid treatment and she currently needs oxygen support (clinical details were kindly provided by MUDr. Tamara Svobodová, CSc.). A novel heterozygous mutation in *HCK* (c.1545 C>A p.Tyr515*) has been identified using MPS in 2016. A presence of both wild-type and mutated mRNA was lately discovered in patient's cells in CLIP-Genomics laboratory. As mentioned above, a new stop codon is incorporated in *HCK* gene causing a transcription of abnormally short mRNA.

8.5. Results

8.5.1. Both wild-type and mutated HCK protein were revealed in the patient's cells

When a novel de-novo heterozygous mutation at position c.1545 C>A in the *HCK* gene was discovered and both wild-type and mutated mRNA were captured, we had to verify whether a translation into protein is productive. We immunoprecipitated HCK protein from the patient's and control's peripheral blood cells, separated proteins by SDS-PAGE, stained the gels with Coomassie Brilliant Blue R-250 and sent them for further isolation and mass spectrometry testing, which was performed in Protein Structure Characterization by Advanced Mass Spectrometry laboratory in BIOCEV (RNDr. Petr Novák, Ph.D.). Fig. 37 shows Coomassie-stained gel and western blot with immunoprecipitated HCK. Mass spectrometry analysis revealed both wild-type and mutated (12 amino acid shorter) HCK proteins present in the patient's cells (the results were kindly provided by RNDr. Petr Novák, Ph.D., Fig. 38).

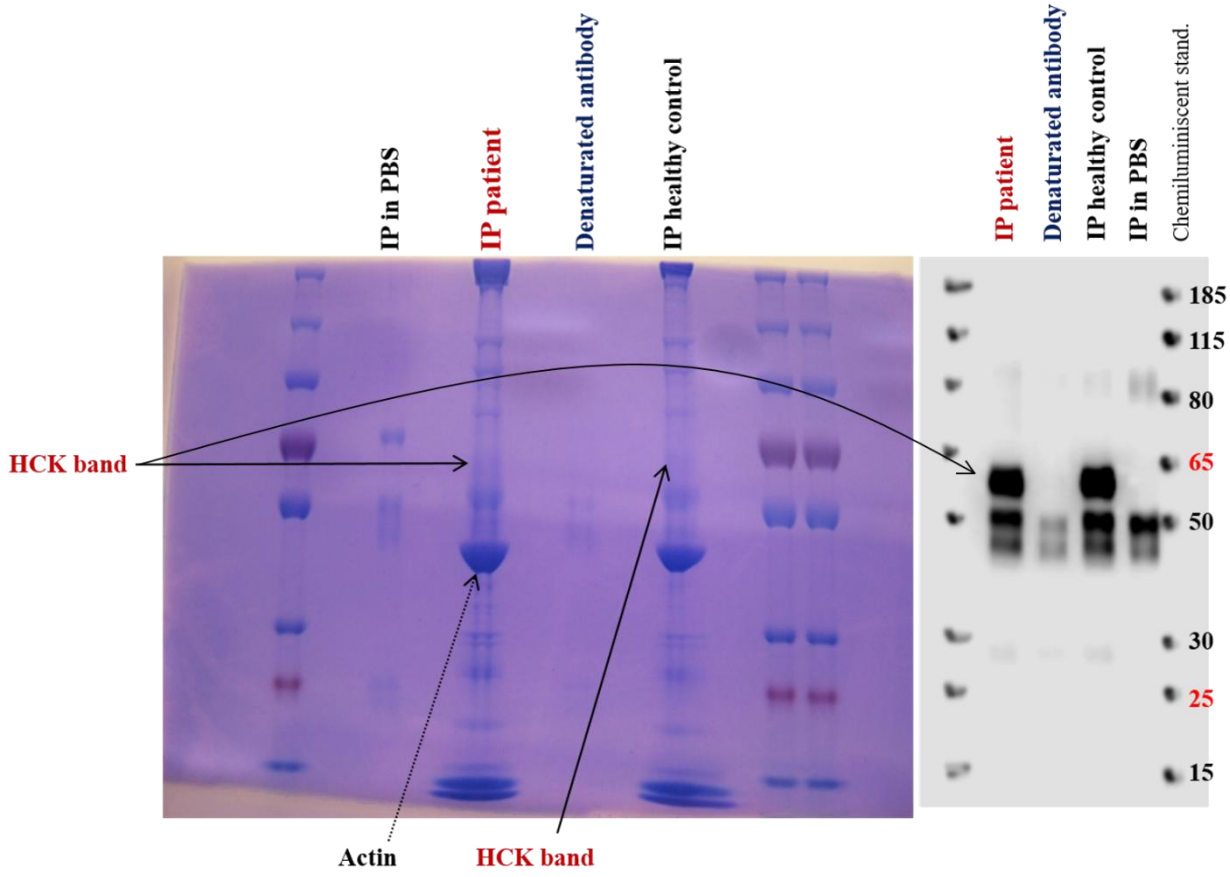

Fig. 37. Immunoprecipitated (IP) HCK stained with Coomassie Brilliant Blue R-250 on SDS-gel (left) and chemiluminiscently detected on nitrocellulose membrane (right). Chemiluminiscent standard shows position of various protein standards (in kDa). HCK position is depicted by arrows. Coomassie-stained gel was used for further analysis by mass spectrometry.

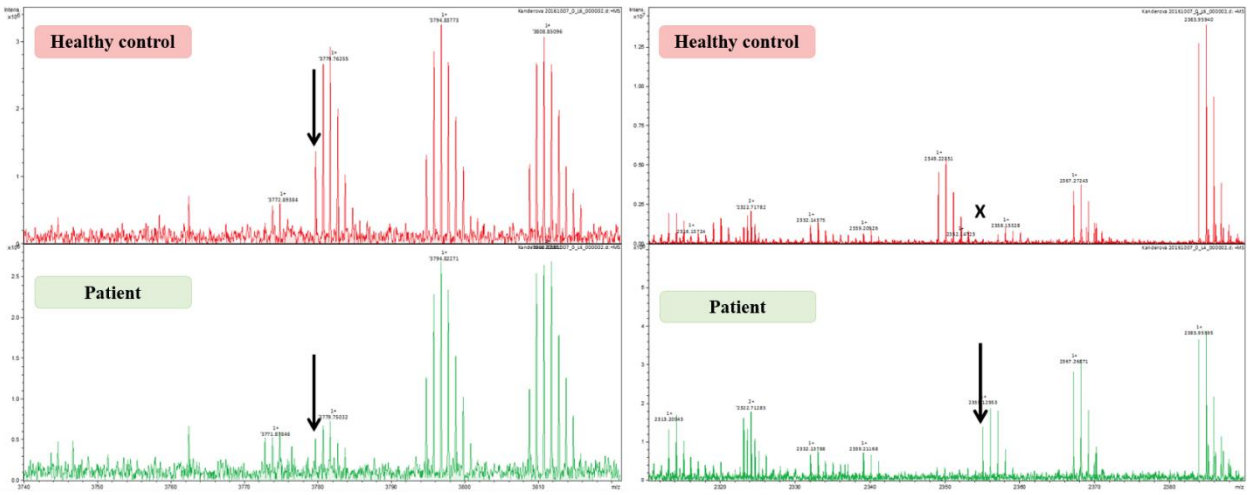

Fig. 38. Mass spectrometry results kindly provided by RNDr. Petr Novák, Ph.D. The arrows on the left graphs show a peptide from the wild-type HCK protein which was present in the healthy control (red) and in the patient's cells (green). The arrow on the right graphs shows a peptide from the shorter mutated HCK protein which was presented only in the patient's cells (red).

8.5.2. Hyperphosphorylation of HCK (Tyr411) in the patients's cells

Activation Tyrosine is located in SH1 domain of Src kinases which is necessary for its enzymatic activity. SH1 has an activation loop with a Tyrosine motif (Y_A). This Tyrosine is responsible for Src kinase autophosphorylation (*124*).

Immunoprecipitated HCK from the patient's and from healthy controls' peripheral blood cells was screened for phosphorylation on this activation Tyrosine (Tyrosine 411 in case of HCK). Patient's HCK presented with higher phosphorylation of HCK on Tyr411 compare to controls (Fig. 39, 40).

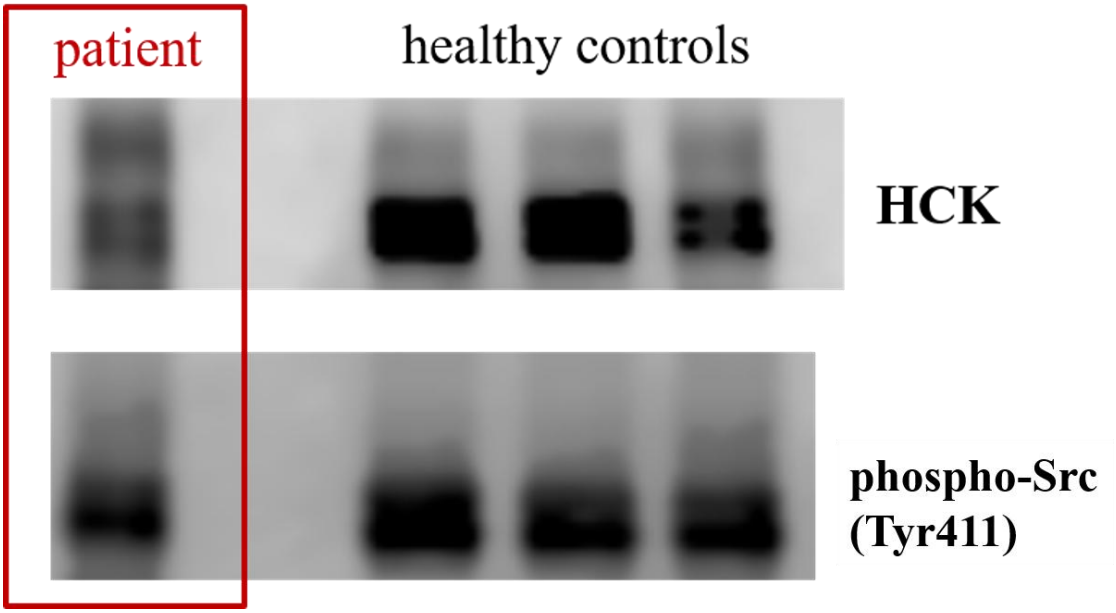

Fig. 39. Western blot of immunoprecipited HCK detected by anti-phosho-Src antibody. The red box depicted HCK level (up) and phospho-Tyr411 level on precipitated HCK (bottom) in the patients' peripheral blood cells. The right side represents 3 unrelated healthy controls.

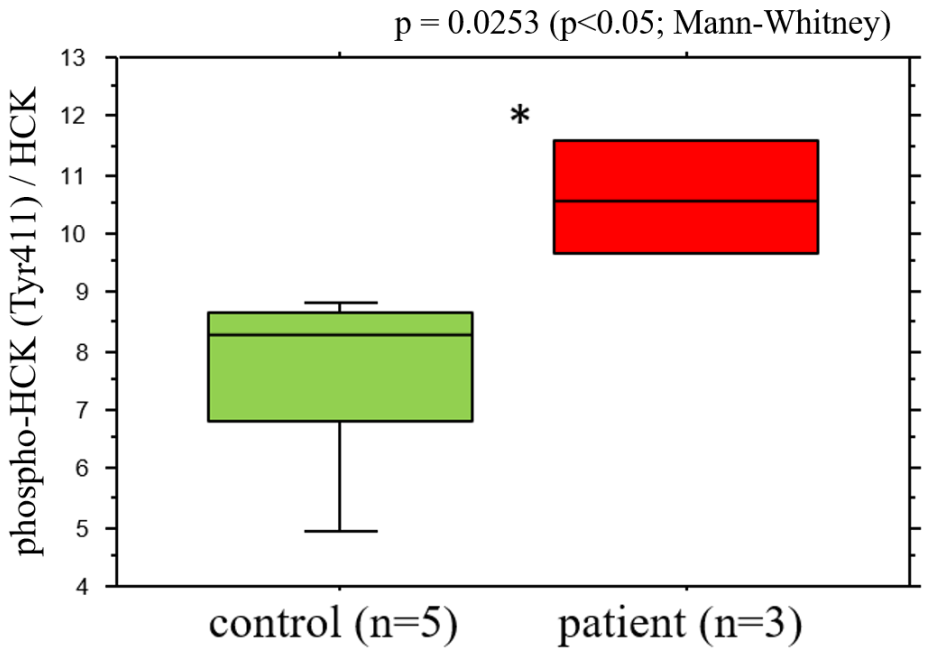

Fig. 40. Quantification of phospho-Tyr411 level on immunoprecipitated HCK. HCK was hyperphosphorylated on activation Tyrosine 411 in the patient's cells (red) compared to healthy controls (green). The data were obtained from western blot above. Asterisk indicates $p<0.05$, Mann-Whitney U test.

8.5.3. Enhanced basal expression of adhesion molecules on patient's monocytes and transformed cell lines

As mentioned in chapter 8.2., HCK mediates various functions including adhesion and migration. Integrins have been discovered as important adhesion molecules involved in these functions and they have been described as influenced by HCK (*143*, *144*). We found higher expression of integrins CD11b and CD18 on patient's monocytes (Fig. 41).

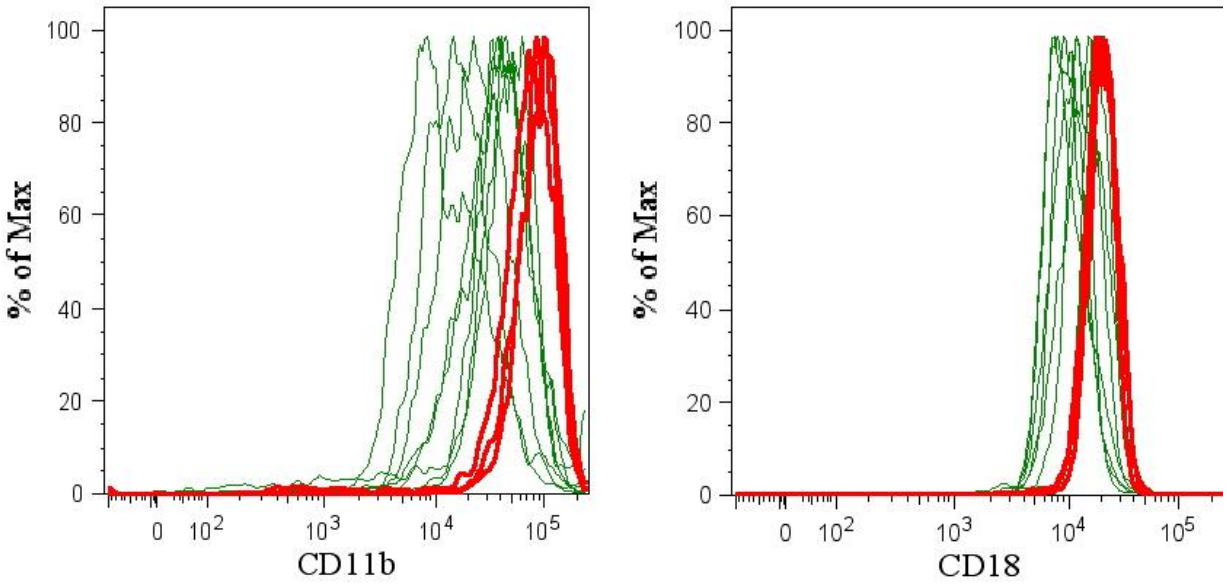

Fig. 41. Basal expression of integrins on patient's and controls' monocytes. n (patient, red) = 3, n (healthy controls) = 8. X-axis shows fluorescent intensity of CD11b-PE and CD18-APC.

Because of a complete novelty of this de-novo *HCK* mutation in humans and limited availability of the patient's peripheral blood, it was necessary to prepare cell line models. We chose THP-1 and Mono-Mac-6 monocytoid cell lines which have been stably transfected with wild-type and mutated form of *HCK* gene plus green fluorescence protein (GFP) as a control of HCK transcription/translation. The cell lines have been prepared by Šimon Borna, MSc. in Laboratory of Leukocyte Signalling in Institute of Molecular Genetics of the ASCR. The methodology of transfection is not a part of my diploma thesis.

8.5.4. Integrins had higher expression on HCK-mutated THP-1 cell line

Expresssion of integrins CD11b and CD18 on the THP-1 cells mimicked their expression on patient's monocytes. Moreover, other integrins (CD11a, CD11c, or activated CD18 (activation epitope which is expressed only in activated CD18 (*145*)) were also elevated on the THP-1 cells which harboured mutated form of HCK (Fig. 42).

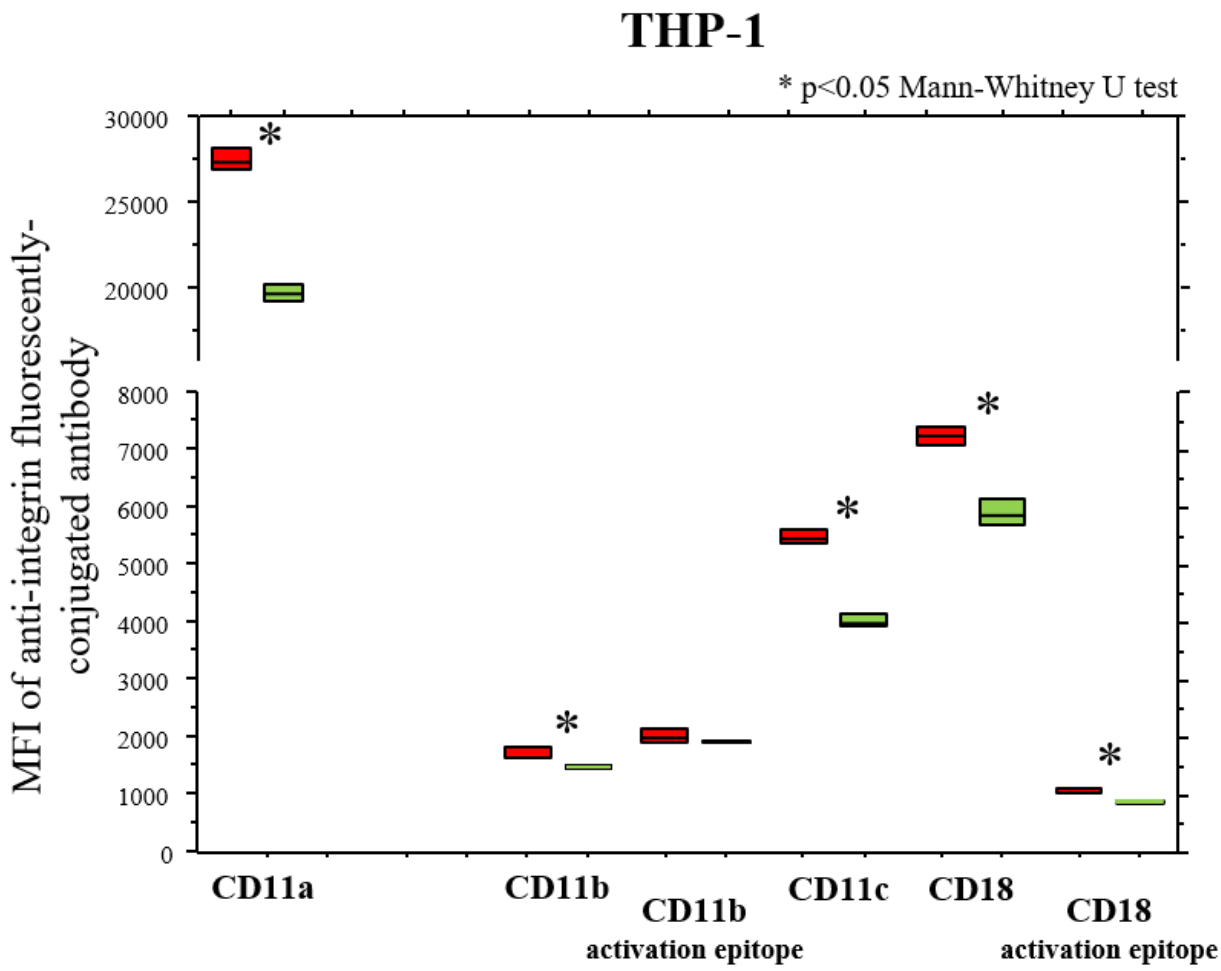

Fig. 42. Basal expression of integrins on THP-1 cells. GFP-positive cells were analyzed within THP-1 cells which harboured wild-type HCK (green) and mutated HCK (red). Y-axis shows MFI of anti-integrin fluorescently-conjugated antibodies. Asterisk indicates $p<0.05$, Mann-Whitney U test. Each measurement was performed in triplicate. (The Mono-mac-6 evaluation is in process).

8.5.5. Enhanced basal Tyrosine phosphorylation of the transformed cell lines

In the murine study of Ernst et al. the authors revealed elevated levels of Tyrosine-phosphorylated proteins in $Hck^{F/F}$ mutant cells (*121*). We also tested total phosphorylation by western blotting and found increased phosphorylation of total Tyrosine and total Src (Tyr416) in the cells which harboured mutated HCK compare to wild-type HCK (Fig. 43).

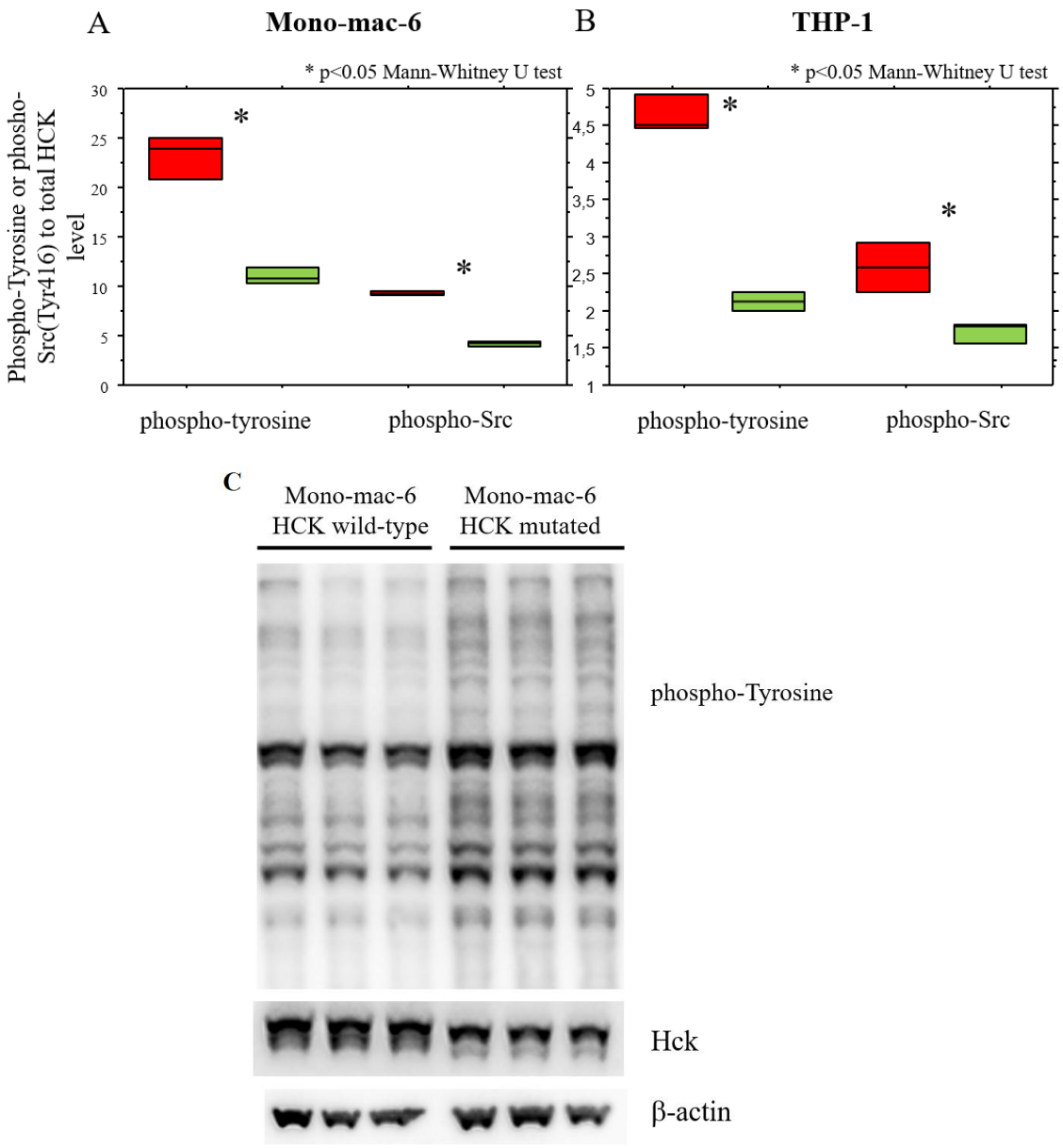

Fig. 43. Basal Tyrosine- and basal Src- phosphorylation (Tyr416) in Mono-mac-6 and THP-1 cells. A, B) Total Tyrosine phosphorylation and total Src phosphorylation (on activating Tyrosine in Src detected with anti-phospho-Src (Tyr416) antibody) in Mono-mac-6 cells and THP-1 cells which harboured wild-type HCK (green) and mutated HCK (red) were analyzed. Y-axis shows ratio of total Tyrosine and total Src (Tyr416) phosphorylation to total HCK level. Asterisk indicates $p<0.05$, Mann-Whitney U test. Each measurement was performed in triplicate. C) Exemplary Western blot shows total phospho-Tyrosine in Mono-mac-6 cell lines.

8.5.6. Enhanced production of inflammatory cytokines by the transformed cell lines

Furthermore, Ernst et al. found abnormal production of inflammatory cytokine TNFα (*121*). We also tested production of IL-1β, IL-6, and TNFα by transformed THP-1 and Mono-mac-6 cell lines using ELISA. The cells were stimulated via TLR4 with LPS and via Fc-receptors with immune complexes (IC). As shown in Fig. 44 the transformed cells were able to produce cytokines and 24 hours upon stimulation with LPS an IC (please see test 1) the production was comparable in the cells harbouring wild-type and mutated HCK. Moreover, when LPS and IC were washed out (test 2), the cells harbouring mutated HCK produced more IL-1β (Mono-mac-6) and TNFα (THP-1) compared to wild-type HCK.

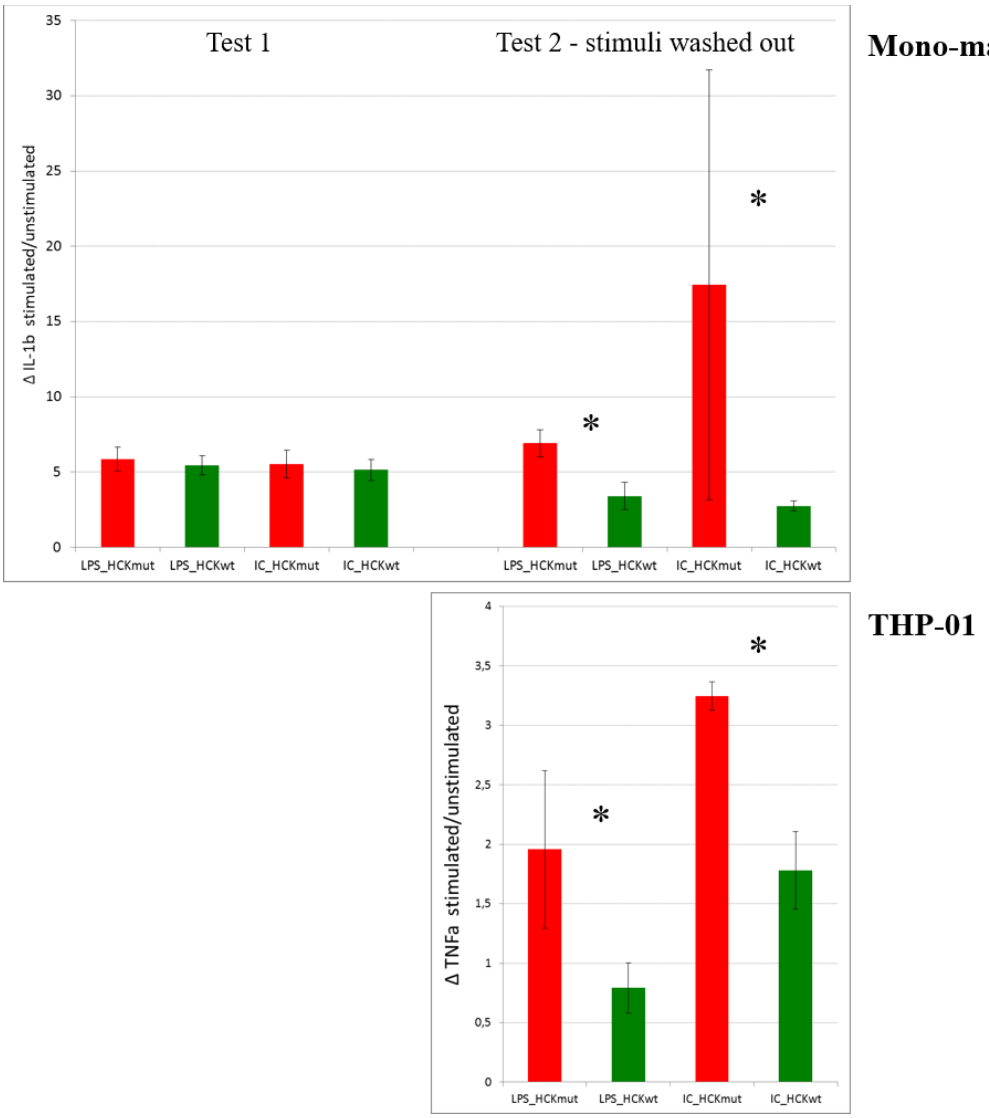

Fig. 44. Production of cytokines. A) Test 1 shows production of IL-1β which was comparable between Mono-mac-6 cells harbouring wild-type HCK (HCKwt, green) and mutated HCK (HCKmut, red) upon 24 hour-stimulation. B) Test 2 shows production of IL-1β which was increased in Mono-mac-6 cells harbouring mutated HCK (HCKmut, red) compare to wild-type HCK (green) when the stimuli were

washed out after 6 hour and the cells were cultured for additional 42 hours without other stimulation. C) Test 2 shows production of TNFα which was increased in THP-1 cells harbouring mutated HCK (HCKmut, red) compared to wild-type HCK (green) when the stimuli were washed out after 6 hour and the cells were cultured for additional 42 hours without other stimulation. Y-axis shows ratio of cytokines produced to culture media upon LPS/IC stimulation and without stimulation. Asterisk indicates $p<0.05$, Mann-Whitney U test. Test 1 was performed in pentaplicates, test 2 in triplicates.

8.5.7. Fc-receptors and GFP tag were equally expressed in the transformed cell lines

Before this final functional test, we analyzed the expression of Fc-receptors CD64, CD32 and CD16, and GFP which were all comparable in the cells with wild-type and mutated HCK (Fig. 45).

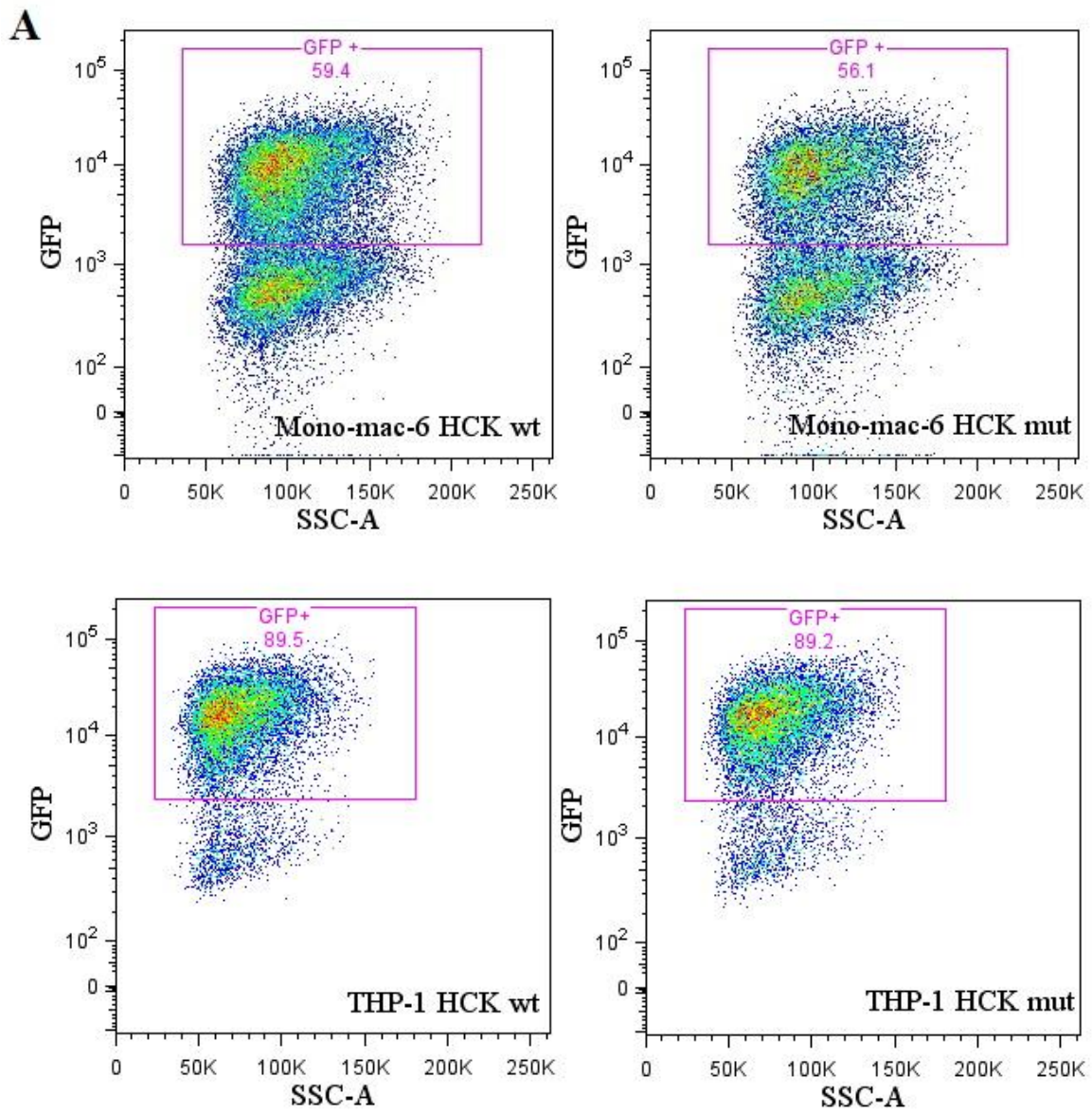

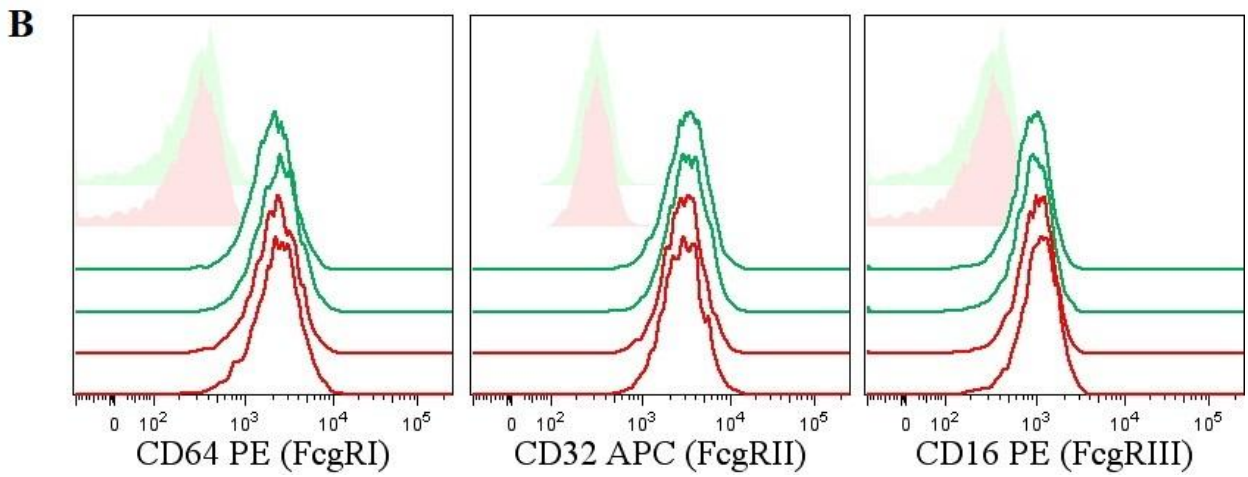

Fig. 45. GFP and Fc-receptor expression.

A) GFP-expression level was similar in cells harbouring wild-type and mutated HCK in both Mono-mac-6 and THP-1 cells. B) Fc-receptors were similarly expressed in the cells harbouring wild-type HCK (green) and mutated HCK (red). Unstained cells in tinted color. Mono-mac-6 cells are shown in duplicates. X-axis shows fluorescent intensity of CD64-PE-Cy7, CD32-APC and CD16-FITC.

8.6. Discussion

Here we report a female patient, currently a 14-year-old girl, who suffers from severe pulmonary leukocyte infiltration, progressive lung fibrosis, and skin lesions. Symptoms started to manifest early after birth, both parents were healthy. After 13 years of treatment with corticosteroids, MPS revealed a novel heterozygous de-novo mutation in Src kinase HCK, c.1545 C>A p.Tyr515*. This mutation introduced a novel stop codon in C-terminal tail of HCK thereby loosing inhibitory Tyrosine (*123*). We found both wild-type and mutated form of HCK protein in the patient's cells. HCK was described to have hematopoetic origin, the only non-hematopoetic cell expressing HCK are squamous epithelial cells of the tonsils. In a hematopoietic system it is expresed mainly in myeloid compartment (Uniprot, *uniprot.org/uniprot/P08631*; Human Protein Atlas, *proteinatlas.org/ENSG00000101336-HCK/cell*). Thus, the information from MPS and Mass Spectrometry revealed the fact that the patient suffers from a novel hematopoietic disease and HSCT could be a possible treatment option. Unfortunately, the patient is not in condition to survive HSCT. To date, only one publication described a similar mutation. Ernst et al. in 2002 created knock-in mice with substituted inhibitory Tyrosine with phenylalanine. This substitution caused defect in dephosphorylation of HCK as well as its hyperactivity expressed as enhanced activation and migration of myeloid cells. The mice suffered with clinical symtoms similar to our patient: leukocyte infiltration and fibrosis of lungs (*121*).

Due to a long-term corticosteroid treatment, we could not precisely evaluate immunophenotype of her peripheral blood cells. We could, however, test phosphorylation of her HCK. Because anti-phospho-HCK(Tyr411) antibody for western blotting or flow cytometry was unavailable, we had to immunoprecipitate HCK from the lysate and stain the immunoprecipitate with anti-phospho-Src (Tyr416) antibody. Thus, we revealed increased phosphorylation of HCK on activation Tyrosine (Tyr411 in case of HCK) in the patient's cells compared to healthy controls suggesting enhanced HCK activity. HCK was described to be functionally associated with integrins to mediate leukocyte adhesion and migration (*123*, *143*, *144*). Indeed, we found increased expression of CD11b and CD18 integrins on patient's monocytes.

Because of the novelty of the mutation in human it was necessary to prepare cell line models to precisely describe a character of the mutation. We chose monocyte lineage cells THP-1 and Mono-mac-6. The incorporated *HCK* gene was marked by GFP tag. The transfected cells harbouring mutated HCK presented with increased expression and activation of integrins, namely CD11a, CD11b, CD18, and CD11c. We assume that the leukocyte infiltration of the lungs may be mediated by hyperactivated HCK since the wild-type HCK was described to be involved in the leukocyte migration during inflammation (*123*, *132*). Further experiments on prepared cell lines concerning leukocyte chemotaxis are in progress. Finally, HCK-mediated activation of myeloid compartment was accompanied by activation of monocytes, macrophages, and neutrophils that led to production of proinflammatory cytokines, especially TNFα (*123*, *146*, *147*). We used ELISA for the detection of IL-1β, IL-6, and TNFα and we found that the HCK-tranformed cells can produce cytokines. Unexpectedly, the production was comparable between wild-type and mutated HCK when the cells were stimulated using LPS and immune complexes for 24 hours. Thus, we also tested another approach; we stimulated the cells for 6 hours, subsequently washed out the stimuli allowing the wild-type HCK activity to be discontinued and we tested the cytokine production after another 42 hours. Surprisingly, we found that the cells, expressing mutated HCK were able to produce more IL-1β and TNFα. This data need to be validated by intracellular cytokine staining assays.

The HCK project is still ongoing and the mice models are also tested by Tomáš Brdička, Ph.D. and his group in Laboratory of Leukocyte Signalling in Institute of Molecular Genetics of the ASCR.

8.7. Conclusion

We present a case report of a 14-year-old female patient with a remarkable mutation in *HCK* gene. The mutation introduced a premature stop codon into DNA sequence and caused a translation of a shortened protein which presented with hyperactivation properties - hyperphosphorylation of HCK on activation Tyrosine, and elevated levels of Tyrosine-phosphorylated proteins, increased expression and activation of integrins, and increased production of IL-1β and TNFα from mutated HCK-bearing cells. The only reference to our study was reported in mice in 2002, further experiments on cell lines and mice are therefore necessary to precisely characterize the functional consequences of the mutation. The experiments are carried out in cooperation with Tomáš Brdička, Ph.D. and his group.

9. Summary

Primary immunodeficiencies (PID) are currently a frequently discussed topic in clinical immunology. The development of massive parallel sequencing has made it possible to discover underlying mutations in several diseases. The discoveries enabled targeted curative or supportive treatment for many patients. However, in many novel mutations the functional consequences are still unknown. Althought we have a lot of diagnostic methods to test a suspicious PID, e.g. TREC testing or immunophenotyping, the functional consequences of novel mutations have to be detected using more sophisticated tools, which cannot be routinely used across diagnostic laboratories. Some of them I used in my diploma thesis, e.g. single-cell phospho-flow cytometry to reveal changes in intracellular signaling pathways, immunoprecipitation and western blotting, and many activation approaches. I used them to functionally characterize novel mutations in *STAT1*, *CASP8*, and *HCK* causing severe dysregulation of the immune system. The described assays (some of them optimized in my thesis) can serve to elucidate other clinical cases.

10. References

1. H. D. Ochs, D. Petroni, From clinical observations and molecular dissection to novel therapeutic strategies for primary immunodeficiency disorders. *Am. J. Med. Genet. Part A*, 1–20 (2017).

2. S. P. Starr, Immunology Update: Primary Immunodeficiency Diseases. *FP Essent.* **450**, 35–53 (2016).

3. N. M. Chase, J. W. Verbsky, J. M. Routes, Newborn screening for SCID: Three years of experience. *Ann. N. Y. Acad. Sci.* **1238**, 99–105 (2011).

4. I. Meyts *et al.*, Exome and genome sequencing for inborn errors of immunity. *J. Allergy Clin. Immunol.* **138**, 957–969 (2016).

5. C. Picard *et al.*, International Union of Immunological Societies: 2017 Primary Immunodeficiency Diseases Committee Report on Inborn Errors of Immunity. *J. Clin. Immunol.* **38**, 96–128 (2018).

6. O. C. BRUTON, Agammaglobulinemia. *Pediatrics*. **9**, 722–728 (1952).

7. J. S. Lin, S. D. Shyur, H. Y. Lin, Severe combined immunodeficiency with B-lymphocytes (T-B+SCID): report of two cases. *Zhonghua Min. Guo. Xiao Er Ke Yi Xue Hui Za Zhi*. **39**, 406–411 (1998).

8. G. P. Yu *et al.*, Genotype, phenotype, and outcomes of nine patients with T-B+NK+ SCID. *Pediatr. Transplant.* **15**, 733–741 (2011).

9. S. Hacein-Bey Abina *et al.*, Outcomes following gene therapy in patients with severe Wiskott-Aldrich syndrome. *JAMA*. **313**, 1550–1563 (2015).

10. F. Hoche *et al.*, Cognitive phenotype in ataxia-telangiectasia. *Pediatr. Neurol.* **51**, 297–310 (2014).

11. B. Zheng, Y. Zhang, Y. Jin, H. Yu, A novel Bruton's tyrosine kinase gene (BTK) missense mutation in a Chinese family with X-linked agammaglobulinemia. *BMC Pediatr.* **14**, 1–5 (2014).

12. O. Lambotte *et al.*, Diagnosis of autoimmune lymphoproliferative syndrome caused by FAS deficiency in adults. *Haematologica*. **98**, 389–392 (2013).

13. P. Bortoletto *et al.*, Chronic Granulomatous Disease. *Pediatr. Infect. Dis. J.* **34**, 1110–1114 (2015).

14. D. B. Kuhns *et al.*, Residual NADPH Oxidase and Survival in Chronic Granulomatous Disease. *N Engl J Med.* **363**, 2600–2610 (2011).

15. X. F. Kong *et al.*, A novel form of human STAT1 deficiency impairing early but not late responses to interferons. *Blood*. **116**, 5896–5906 (2010).

16. N. Dobbs *et al.*, STING activation by translocation from the ER is associated with infection and autoinflammatory disease. *Cell Host Microbe*. **18**, 157–168 (2015).

17. M. M. Gompels *et al.*, C1 inhibitor deficiency: Consensus document. *Clin. Exp. Immunol.* **139**, 379–394 (2005).

18. W. F. Ng *et al.*, Impaired TH17 responses in patients with chronic mucocutaneous candidiasis with and without autoimmune polyendocrinopathy-candidiasis- ectodermal

dystrophy. *J. Allergy Clin. Immunol.* **126**, 1006–1015.e4 (2010).

19. K. Kisand *et al.*, Chronic mucocutaneous candidiasis in APECED or thymoma patients correlates with autoimmunity to Th17-associated cytokines. *J. Exp. Med.* **207**, 299–308 (2010).

20. A. Chapgier *et al.*, A partial form of recessive STAT1 deficiency in humans. *J. Clin. Invest.* **119**, 1502–1514 (2009).

21. S. Baris *et al.*, Severe Early-Onset Combined Immunodeficiency due to Heterozygous Gain-of-Function Mutations in STAT1. *J. Clin. Immunol.*, 1–8 (2016).

22. B. L. Freire *et al.*, Homozygous loss of function BRCA1 variant causing a fanconi-anemia-like phenotype, a clinical report and review of previous patients. *Eur. J. Med. Genet.* (2017), doi:10.1016/j.ejmg.2017.11.003.

23. J. K. Abbott *et al.*, Dominant-negative loss of function arises from a second , more frequent variant within the SAND domain of autoimmune regulator. *J. Autoimmun.* (2017), doi:10.1016/j.jaut.2017.10.010.

24. L. A. Albacker *et al.*, Loss of function JAK1 mutations occur at high frequency in cancers with microsatellite instability and are suggestive of immune evasion. *Plos One*, 1–21 (2017).

25. C. A. Ma *et al.*, Germline hypomorphic CARD11 mutations in severe atopic disease. *Nat. Genet.* **49**, 1192–1201 (2017).

26. J. D. Milner *et al.*, Early-onset lymphoproliferation and autoimmunity caused by germline STAT3 gain-of-function mutations. *Blood*. **125**, 591–599 (2015).

27. S. E. Flanagan *et al.*, Europe PMC Funders Group Activating germline mutations in STAT3 cause early-onset multi- organ autoimmune disease. **46**, 812–814 (2015).

28. S. Mukherjee, A. J. Thrasher, Gene therapy for PIDs: Progress, pitfalls and prospects. *Gene*. **525**, 174–181 (2013).

29. J. W. Leiding *et al.*, Hematopoietic stem cell transplantation in patients with gain-of-function signal transducer and activator of transcription 1 mutations. *J Allergy Clin Immunol.* Feb;141(2):704-717.e5 (2018).

30. M. P. Cicalese *et al.*, Update on the safety and efficacy of retroviral gene therapy for immunodeficiency due to adenosine deaminase deficiency. *Blood*. **128**, 45–54 (2016).

31. S. S. De Ravin *et al.*, *Sci. Transl. Med.*, in press, doi:10.1126/scitranslmed.aad8856.

32. H. C. Su, M. J. Lenardo, Genetic Defects of Apoptosis and Primary Immunodeficiency. *Immunol Allergy Clin North A.* **28**, 329 (2008).

33. A. M. Condliffe, A. Chandra, Respiratory Manifestations of the Activated Phosphoinositide 3-Kinase Delta Syndrome. *Front. Immunol.* **9**, 4–11 (2018).

34. E. Sapey *et al.*, Phosphoinositide 3-kinase inhibition restores neutrophil accuracy in the elderly: toward targeted treatments for immunosenescence. *Blood*. **123**, 239–248 (2014).

35. R. B. Bell *et al.*, OX40 signaling in head and neck squamous cell carcinoma: Overcoming immunosuppression in the tumor microenvironment. *Oral Oncol.* **52**, 1–10 (2015).

36. Y.-B. Hao, S.-Y. Yi, J. Ruan, L. Zhao, K.-J. Nan, New insights into metronomic chemotherapy-induced immunoregulation. *Cancer Lett.* **354**, 220–226 (2014).

37. B. E. Marciano *et al.*, BCG vaccination in SCID patients: complications, risks and vaccination policies. *J. Allergy Clin. Immunol.* **133**, 1134–1141 (2014).

38. G. Preece, G. Murphyt, A. Ager, Metalloproteinase-mediated regulation of L-selectin levels on leucocytes. *J. Biol. Chem.* **271**, 11634–11640 (1996).

39. C. Vermes, J. Kuzsner, T. Bárdos, P. Than, Prospective analysis of human leukocyte functional tests reveals metal sensitivity in patients with hip implant. *J. Orthop. Surg. Res.* **8**, 1–7 (2013).

40. L. Shanmugam *et al.*, Assessment of phagocytic activity of neutrophils in chronic obstructive pulmonary disease. *Lung India*. **32**, 437 (2015).

41. R. Norian, N. Delirezh, A. Azadmehr, Evaluation of proliferation and cytokines production by mitogen-stimulated bovine peripheral blood mononuclear cells. *Vet. Res. Forum*. **6**, 265–271 (2015).

42. K. H. Park *et al.*, Evaluation of NK cell function by flowcytometric measurement and impedance based assay using real-time cell electronic sensing system. *Biomed Res. Int.* **2013** (2013), doi:10.1155/2013/210726.

43. E. J. H. Schatorjé *et al.*, Paediatric Reference Values for the Peripheral T cell Compartment. *Scand. J. Immunol.* **75**, 436–444 (2012).

44. B. Piątosa *et al.*, B cell subsets in healthy children: Reference values for evaluation of B cell maturation process in peripheral blood. *Cytom. Part B - Clin. Cytom.* **78**, 372–381 (2010).

45. D. C. Douek *et al.*, Changes in thymic function with age and during the treatment of HIV infection. *Nature*. **396**, 690–695 (1998).

46. N. M. Chase, J. W. Verbsky, J. M. Routes, Newborn screening for T-cell deficiency. *Curr. Opin. Allergy Clin. Immunol.* **10**, 521–525 (2010).

47. J. E. Darnell, STATs and gene regulation. *Science* **277**, 1630–1635 (1997).

48. E. A. Bach, M. Aguet, R. D. Schreiber, The IFN gamma receptor: a paradigm for cytokine receptor signaling. *Annu. Rev. Immunol.* **15**, 563–591 (1997).

49. M. Sakatsume *et al.*, The Jak kinases differentially associate with the alpha and beta (accessory factor) chains of the interferon gamma receptor to form a functional receptor unit capable of activating STAT transcription factors. *J. Biol. Chem.* **270**, 17528–17534 (1995).

50. C. D. Krause, W. He, S. Kotenko, S. Pestka, Modulation of the activation of Stat1 by the interferon-gamma receptor complex. *Cell Res.* **16**, 113–123 (2006).

51. D. Ma, H. Huang, Z. Huang, STAT1 signaling is required for optimal Th1 cell differentiation in mice. *Chinese Sci. Bull.* **55**, 1032–1040 (2010).

52. L. Hibbert, S. Pflanz, R. De Waal Malefyt, R. A. Kastelein, IL-27 and IFN-alpha signal via Stat1 and Stat3 and induce T-Bet and IL-12Rbeta2 in naive T cells. *J. Interferon Cytokine Res.* **23**, 513–522 (2003).

53. H. A. Bluyssen, D. E. Levy, Stat2 is a transcriptional activator that requires sequence-specific contacts provided by stat1 and p48 for stable interaction with DNA. *J. Biol. Chem.* **272**, 4600–4605 (1997).

54. M. Martinez-Moczygemba, M. J. Gutch, D. L. French, N. C. Reich, Distinct STAT

structure promotes interaction of STAT2 with the p48 subunit of the interferon-alpha-stimulated transcription factor ISGF3. *J. Biol. Chem.* **272**, 20070–20076 (1997).

55. C. M. Horvath, G. R. Stark, I. M. Kerr, J. E. Darnell, Interactions between STAT and non-STAT proteins in the interferon-stimulated gene factor 3 transcription complex. *Mol. Cell. Biol.* **16** (1996), pp. 6957–6964.

56. S. Hambleton *et al.*, STAT2 deficiency and susceptibility to viral illness in humans. *Proc. Natl. Acad. Sci. U. S. A.* **110**, 3053–3058 (2013).

57. K. TAKEDA *et al.*, Targeted disruption of the mouse Stat 3 gene leads to early embryonic lethality. **94**, 3801–3804 (1997).

58. X. O. Yang *et al.*, STAT3 regulates cytokine-mediated generation of inflammatory helper T cells. *J. Biol. Chem.* **282**, 9358–9363 (2007).

59. M. H. Kaplan, STAT4: A critical regulator of inflammation in vivo. *Immunol. Res.* **31**, 231–241 (2005).

60. C. M. Bacon *et al.*, Interleukin 12 induces tyrosine phosphorylation and activation of STAT4 in human lymphocytes. *Proc. Natl. Acad. Sci. U. S. A.* **92** (1995), pp. 7307–7311.

61. T. Nosaka *et al.*, STAT5 as a molecular regulator of proliferation, differentiation and apoptosis in hematopoietic cells. *EMBO J.* **18** (1999), pp. 4754–4765.

62. S. A. Mahmud, L. S. Manlove, M. A. Farrar, Interleukin-2 and STAT5 in regulatory T cell development and function. *JAK-STAT*. **2**, e23154 (2013).

63. V. Hwa, STAT5B deficiency: Impacts on human growth and immunity. *Growth Horm. IGF Res.* **28**, 16–20 (2016).

64. A. a. Cumaraswamy, A. Todic, D. Resetca, M. D. Minden, P. T. Gunning, Inhibitors of Stat5 protein signalling. *Med. Chem. Commun.* **3**, 22–27 (2012).

65. K. Shimoda *et al.*, Lack of IL-4-induced Th2 response and IgE class switching in mice with disrupted Stat6 gene. *Nature*. **380**, 630–633 (1996).

66. E. Maier, A. Duschl, J. Horejs-Hoeck, STAT6-dependent and -independent mechanisms in Th2 polarization. *Eur. J. Immunol.* **42**, 2827–2833 (2012).

67. X. Chen *et al.*, A reinterpretation of the dimerization interface of the N-terminal domains of STATs. *Protein Sci.* **12**, 361–365 (2003).

68. A. Begitt, T. Meyer, M. van Rossum, U. Vinkemeier, Nucleocytoplasmic translocation of Stat1 is regulated by a leucine-rich export signal in the coiled-coil domain. *Proc. Natl. Acad. Sci.* **97**, 10418–10423 (2000).

69. X. Chen *et al.*, Crystal structure of a tyrosine phosphorylated STAT-1 dimer bound to DNA. *Cell*. **93**, 827–839 (1998).

70. E. Yang, Z. Wen, R. L. Haspel, J. J. Zhang, J. E. Darnell, The linker domain of Stat1 is required for gamma interferon-driven transcription. *Mol. Cell. Biol.* **19**, 5106–5112 (1999).

71. K. Mowen, M. David, Role of the STAT1-SH2 domain and STAT2 in the activation and nuclear translocation of STAT1. *J. Biol. Chem.* **273**, 30073–30076 (1998).

72. K. ching Liang, Y. Suzuki, Y. Kumagai, K. Nakai, Analysis of changes in transcription start site distribution by a classification approach. *Gene*. **537**, 29–40 (2014).

73. A. Pilz *et al.*, Dendritic Cells Require STAT-1 Phosphorylated at Its Transactivating Domain for the Induction of Peptide-Specific CTL. *J. Immunol.* **183**, 2286–2293 (2009).

74. T. Kawata, STAT signaling in Dictyostelium development. *Dev. Growth Differ.* **53**, 548–557 (2011).

75. M. Depner *et al.*, The Extended Clinical Phenotype of 26 Patients with Chronic Mucocutaneous Candidiasis due to Gain-of-Function Mutations in STAT1. *J. Clin. Immunol.* **36**, 73–84 (2016).

76. C. Semper *et al.*, STAT1beta is not dominant negative and is capable of contributing to gamma interferon-dependent innate immunity. *Mol. Cell. Biol.* **34**, 2235–2248 (2014).

77. E. Voigt, B. Inankur, A. Baltes, J. Yin, A quantitative infection assay for human type I, II, and III interferon antiviral activities. *Virol. J.* **10**, 1–10 (2013).

78. S. Dupuis *et al.*, Impaired response to interferon-α/β and lethal viral disease in human STAT1 deficiency. *Nat. Genet.* **33**, 388–391 (2003).

79. A. Chapgier *et al.*, Human complete Stat-1 deficiency is associated with defective type I and II IFN responses in vitro but immunity to some low virulence viruses in vivo. *J. Immunol.* **176**, 5078–83 (2006).

80. J. Toubiana *et al.*, Heterozygous STAT1 gain-of-function mutations underlie an unexpectedly broad clinical phenotype. *Blood*. **127**, 3154–3164 (2016).

81. L. Liu *et al.*, Gain-of-function human *STAT1* mutations impair IL-17 immunity and underlie chronic mucocutaneous candidiasis. *J. Exp. Med.* **208**, 1635–1648 (2011).

82. B. Soltész *et al.*, New and recurrent gain-of-function STAT1 mutations in patients with chronic mucocutaneous candidiasis from Eastern and Central Europe. *J. Med. Genet.* **50**, 567–578 (2013).

83. X. Wang, F. L. van de Veerdonk, When the Fight against Fungi Goes Wrong. *PLoS Pathog.* **12**, e1005400 (2016).

84. A. K. Alves de Medeiros *et al.*, Chronic and Invasive Fungal Infections in a Family with CARD9 Deficiency. *J. Clin. Immunol.* **36**, 204–209 (2016).

85. S. P. Smeekens *et al.*, Skin microbiome imbalance in patients with STAT1/STAT3 defects impairs innate host defense responses. *J. Innate Immun.* **6**, 253–262 (2014).

86. Y. Ling, A. Puel, IL-17 and infections. *Actas Dermosifiliogr.* **105 Suppl**, 34–40 (2014).

87. A. R. Khosravi, H. Shokri, S. Darvishi, Altered immune responses in patients with chronic mucocutaneous candidiasis. *J. Mycol. Med.* **24**, 135–140 (2014).

88. E. Higgins *et al.*, Use of ruxolitinib to successfully treat chronic mucocutaneous candidiasis caused by gain-of-function signal transducer and activator of transcription 1 (STAT1) mutation. *J. Allergy Clin. Immunol.* **135**, 551–553 (2015).

89. G. Stoehr, C. Schaab, J. Graumann, M. Mann, A SILAC-based Approach Identifies Substrates of Caspase-dependent Cleavage upon TRAIL-induced Apoptosis. *Mol. Cell. Proteomics*. **12**, 1436–1450 (2013).

90. V. Kanderova *et al.*, High-resolution Antibody Array Analysis of Childhood Acute Leukemia Cells. *Mol. Cell. Proteomics*. **15**, 1246–1261 (2016).

91. J. ten Hoeve *et al.*, Identification of a nuclear Stat1 protein tyrosine phosphatase. *Mol.*

Cell. Biol. **22**, 5662–5668 (2002).

92. S. Verstovsek *et al.*, Safety and Efficacy of INCB018424, a JAK1 and JAK2 Inhibitor, in Myelofibrosis. *N Engl J Med.* **363**, 1922–2013 (2010).

93. R. Davies, P. Vogelsang, R. Jonsson, S. Appel, An optimized multiplex flow cytometry protocol for the analysis of intracellular signaling in peripheral blood mononuclear cells. *J. Immunol. Methods*. **436**, 58–63 (2016).

94. S. Chow *et al.*, Whole blood fixation and permeabilization protocol with red blood cell lysis for flow cytometry of intracellular phosphorylated epitopes in leukocyte subpopulations. *Cytom. Part A.* **67**, 4–17 (2005).

95. A. Tefferi, A. Pardanani, Serious adverse events during ruxolitinib treatment discontinuation in patients with myelofibrosis. *Mayo Clin. Proc.* **86**, 1188–1191 (2011).

96. J. Jones-Carson *et al.*, Gamma delta T cell-induced nitric oxide production enhances resistance to mucosal candidiasis. *Nat. Med.* **1**, 552–557 (1995).

97. S. Cheuk *et al.*, CD49a Expression Defines Tissue-Resident CD8+ T Cells Poised for Cytotoxic Function in Human Skin. *Immunity*. **46**, 287–300 (2017).

98. A. C. Cohen *et al.*, Cutting edge: Decreased accumulation and regulatory function of CD4+ CD25(high) T cells in human STAT5b deficiency. *J. Immunol.* **177**, 2770–2774 (2006).

99. M. Baik, J. H. Yu, L. Hennighausen, Growth hormone-STAT5 regulation of growth, hepatocellular carcinoma, and liver metabolism. *Ann. N. Y. Acad. Sci.* **1229**, 29–37 (2011).

100. I. Lavrik, P. H Krammer, Life and Death Decisions in the CD95 System: Main Pro-and Anti-Apoptotic Modulators, *Acta Naturae* Apr; 1(1): 80–83 (2009).

101. B. Tummers, D. R. Green, Caspase-8: regulating life and death. *Immunol. Rev.* **277**, 76–89 (2017).

102. H. Su *et al.*, Requirement for caspase-8 in NF-κB activation by antigen receptor. *Science* **307**, 1465–1468 (2005).

103. S. Gupta, A. Agrawal, S. Agrawal, H. Su, S. Gollapudi, A paradox of immunodeficiency and inflammation in human aging: Lessons learned from apoptosis. *Immun. Ageing*. **3**, 1–8 (2006).

104. N. H. Philip *et al.*, Activity of Uncleaved Caspase-8 Controls Anti-bacterial Immune Defense and TLR-Induced Cytokine Production Independent of Cell Death. *PLoS Pathog.* **12**, 1–30 (2016).

105. H. J. Chun *et al.*, Pleiotropic defects in lymphocyte activation caused by caspase-8 mutations lead to human immunodeficiency. *Nature*. **419**, 395–399 (2002).

106. J. Niemela *et al.*, Caspase-8 deficiency presenting as late-onset multi-organ lymphocytic infiltration with granulomas in two adult siblings. *J. Clin. Immunol.* **35**, 348–355 (2015).

107. E. E. Varfolomeev *et al.*, Targeted disruption of the mouse Caspase 8 gene ablates cell death induction by the TNF receptors, Fas/Apo1, and DR3 and is lethal prenatally. *Immunity*. **9**, 267–276 (1998).

108. F. C. Kischkel *et al.*, Death Receptor Recruitment of Endogenous Caspase-10 and Apoptosis Initiation in the Absence of Caspase-8. *J. Biol. Chem.* **276**, 46639–46646 (2001).

109. I. Ben-Mustapha, N. Agrebi, M.-R. Barbouche, Novel insights into FAS defects underlying autoimmune lymphoproliferative syndrome revealed by studies in consanguineous patients. *J. Leukoc. Biol.*, 1–8 (2017).

110. A. Nocerino, E. Valencic, C. Loganes, G. Pelos, A. Tommasini, Low-dose sirolimus in two cousins with autoimmune lymphoproliferative syndrome-associated infection. *Pediatr. Int.*, 1–3 (2018).

111. B. Lo *et al.*, A rapid ex vivo clinical diagnostic assay for Fas receptor-induced T lymphocyte apoptosis. *J. Clin. Immunol.* **33**, 479–488 (2013).

112. J. F. R. Kerr, A. H. Wyllie, A. R. Currie, Apoptosis: a Basic Biological Phenomenon With Wide- Ranging Implications in Tissue Kinetics. *J. Intern. Med.* **258**, 479–517 (1972).

113. W. Li *et al.*, An essential role for the Id1/PI3K/Akt/NFkB/survivin signalling pathway in promoting the proliferation of endothelial progenitor cells in vitro. *Mol. Cell. Biochem.* **363**, 135–145 (2012).

114. J. Beaudouin, C. Liesche, S. Aschenbrenner, M. Hörner, R. Eils, Caspase-8 cleaves its substrates from the plasma membrane upon CD95-induced apoptosis. *Cell Death Differ.* **20**, 599–610 (2013).

115. N. J. Kennedy, T. Kataoka, J. Tschopp, R. C. Budd, Caspase activation is required for T cell proliferation. *J. Exp. Med.* **190**, 1891–1896 (1999).

116. S. M. Kahan, E. J. Wherry, A. J. Zajac, T cell exhaustion during persistent viral infections. *Virology*. **479**–**480**, 180–193 (2015).

117. K. Sumida *et al.*, Characteristics of splenic CD8+ T cell exhaustion in patients with hepatitis C. *Clin. Exp. Immunol.* **174**, 172–178 (2013).

118. N. Keller, J. Mareš, O. Zerbe, M. G. Grütter, Structural and Biochemical Studies on Procaspase-8: New Insights on Initiator Caspase Activation. *Structure*. **17**, 438–448 (2009).

119. L. Salmena, R. Hakem, Caspase-8 deficiency in T cells leads to a lethal lymphoinfiltrative immune disorder. *J. Exp. Med.* **202**, 727–732 (2005).

120. D. R. Beisner, I. L. Ch'en, R. V Kolla, A. Hoffmann, S. M. Hedrick, Cutting edge: innate immunity conferred by B cells is regulated by caspase-8. *J. Immunol.* **175**, 3469–3473 (2005).

121. M. Ernst *et al.*, Constitutive Activation of the Src Family Kinase Hck Results in Spontaneous Pulmonary Inflammation and an Enhanced Innate Immune Response. *J. Exp. Med.* **196**, 589–604 (2002).

122. S. J. Parsons, J. T. Parsons, Src family kinases, key regulators of signal transduction. *Oncogene*. **23**, 7906–7909 (2004).

123. A. R. Poh, R. J. J. O'Donoghue, M. Ernst, Hematopoietic cell kinase (HCK) as a therapeutic target in immune and cancer cells. *Oncotarget*. **6**, 15752–15771 (2015).

124. R. Guiet *et al.*, Hematopoietic cell kinase (Hck) isoforms and phagocyte duties - From signaling and actin reorganization to migration and phagocytosis. *Eur. J. Cell Biol.* **87**, 527–542 (2008).

125. K. Podar *et al.*, Critical role for hematopoietic cell kinase (Hck)-mediated phosphorylation of Gab1 and Gab2 docking proteins in interleukin 6-induced proliferation and survival of multiple myeloma cells. *J. Biol. Chem.* **279**, 21658–21665 (2004).

126. S. Carreno, M. E. Gouze, S. Schaak, L. J. Emorine, I. Maridonneau-Parini, Lack of palmitoylation redirects p59(Hck) from the plasma membrane to p61(Hck)-positive lysosomes. *J. Biol. Chem.* **275**, 36223–36229 (2000).

127. S. E. Byeon *et al.*, The role of Src kinase in macrophage-mediated inflammatory responses. *Mediators Inflamm.* **2012** (2012), doi:10.1155/2012/512926.

128. C. Giagulli *et al.*, The Src Family Kinases Hck and Fgr Are Dispensable for Inside-Out, Chemoattractant-Induced Signaling Regulating beta-2 Integrin Affinity and Valency in Neutrophils, but Are Required for beta-2 Integrin-Mediated Outside-In Signaling Involved in Sustained A. *J. Immunol.* **177**, 604–611 (2006).

129. M. C. Bosco *et al.*, IL-2 Signaling in Human Monocytes Involves the Phosphorylation and Activation of p59hck 1. *J. Immunol.* **164**, 4575–4585 (2000).

130. J. Yoon, A. Terada, H. Kita, CD66b Regulates Adhesion and Activation of Human Eosinophils. *J. Immunol.* **179**, 8454–8462 (2007).

131. C. Cougoule *et al.*, Three-dimensional migration of macrophages requires Hck for podosome organization and extracellular matrix proteolysis. *Blood*. **115**, 1444–1452 (2010).

132. P. Mazzi, E. Caveggion, J. A. Lapinet-Vera, C. A. Lowell, G. Berton, The Src-Family Kinases Hck and Fgr Regulate Early Lipopolysaccharide-Induced Myeloid Cell Recruitment into the Lung and Their Ability To Secrete Chemokines. *J. Immunol.* **195**, 2383–2395 (2015).

133. A. Baruzzi, E. Caveggion, G. Berton, Regulation of phagocyte migration and recruitment by Src-family kinases. *Cell. Mol. Life Sci.* **65**, 2175–2190 (2008).

134. Y. Hu *et al.*, Requirement of Src kinases Lyn, Hck and Fgr for BCR-ABL1-induced B-lymphoblastic leukemia but not chronic myeloid leukemia. *Nat. Genet.* **36**, 453–461 (2004).

135. S. Li, Src kinases as targets for B cell acute lymphoblastic leukaemia therapy. *Expert Opin Ther Targets*. **9**, 329–341 (2005).

136. H. Sakamaki *et al.*, Phase 1/2 clinical study of dasatinib in Japanese patients with chronic myeloid leukemia or Philadelphia chromosome-positive acute lymphoblastic leukemia. *Int. J. Hematol.* **89**, 332–341 (2009).

137. J. Xiao *et al.*, Dasatinib enhances antitumor activity of paclitaxel in ovarian cancer through Src signaling. *Mol. Med. Rep.* **12**, 3249–3256 (2015).

138. A.-R. Nam *et al.*, Src as a Therapeutic Target in Biliary Tract Cancer. *Am. Assoc. Cancer Res.* **15**, 1515–1524 (2016).

139. A. Calgani *et al.*, Suppression of SRC Signaling Is Effective in Reducing Synergy between Glioblastoma and Stromal Cells. *Am. Assoc. Cancer Res.* **15**, 1535–1544 (2016).

140. L. J. Lewis-Tuffin *et al.*, Src family kinases differentially influence glioma growth and motility. *Mol. Oncol.* **9**, 1783–1798 (2015).

141. W. Chanput, J. J. Mes, H. J. Wichers, THP-1 cell line: An in vitro cell model for immune modulation approach. *Int. Immunopharmacol.* **23**, 37–45 (2014).

142. H. W. L. Ziegler- Heitbroc *et al.*, Establishment of a human cell line (mono mac 6) with characteristics of mature monocytes. *Int. J. Cancer*. **41**, 456–461 (1988).

143. C. A. Lowell, G. Berton, Integrin signal transduction in myeloid leukocytes. *J. Leukoc. Biol.* **65**, 313–320 (1999).

144. F. Meng, C. A. Lowell, A β1 integrin signaling pathway involving Src-family kinases, Cbl and PI-3 kinase is required for macrophage spreading and migration. *EMBO J.* **17**, 4391–4403 (1998).

145. K. Drbal, P. Angelisová, J. Černý, I. Hilgert, V. Hořejší, A novel anti-CD18 mAb recognizes an activation-related epitope and induces a high-affinity conformation in leukocyte integrins. *Immunobiology*. **203**, 687–698 (2001).

146. M. Kovács *et al.*, The Src family kinases Hck, Fgr, and Lyn are critical for the generation of the in vivo inflammatory environment without a direct role in leukocyte recruitment. *J. Exp. Med.* **211**, 1993–2011 (2014).

147. A. Achuthan, C. Elsegood, P. Masendycz, J. A. Hamilton, G. M. Scholz, CpG DNA enhances macrophage cell spreading by promoting the Src-family kinase-mediated phosphorylation of paxillin. *Cell. Signal.* **18**, 2252–2261 (2006).